Wheel and Rail Contact Simulation Using a Twin Disc Tester

Ezequiel Alberto Gallardo Hernandez

Thesis Submitted for the Degree of Doctor of Philosophy

**Department of Mechanical Engineering
The University of Sheffield**

September 2008

Wheel and Rail Contact Simulation Using a Twin Disc Tester

Ezequiel Alberto Gallardo Hernandez

Summary

The contact between wheel and rail has been studied for many years in the field and using different test approaches. The wheel/rail contact in this work was simulated by a rolling-sliding twin disc contact machine. Currently this approach is widely accepted as a technique for studying different aspects of the wheel/rail contact such as; wear, rolling contact fatigue (RCF) crack propagation and issues concerning wheel/rail isolation.

In this thesis, one of the studies consisted of measuring temperatures in the twin disc contact. Experiments carried out with a thermal camera were compared with analytical solutions to measure temperature developed by Lewis & Dywer-Joyce (2004) and two methods proposed by Olver (1991). The thermal camera gave a full validation for these solutions.

This work also looks to fill some gaps on the study of wheel and rail contact. The twin disc methodology has not been used to evaluate temperature using a thermal imaging camera, nor has the application of some contaminants and isolation in terms of signalling using commercial friction modifiers.

Another study was carried out on adhesion. Poor adhesion in braking is a critical safety issue. Tests were run with water, oil and leaves in dry conditions and with water. Results showed that water and oil reduce the adhesion coefficient and wet leaves reduce adhesion even lower. The same behaviour was seen with dry leaves. Sand applied with the leaves, was shown to mitigate the effect of low adhesion. Oil and water mixtures were evaluated in terms of adhesion. Whatever the amount of the water present the traction coefficient stayed at the oil level. Test also showed that very low amount of oil gave a sustainable low traction coefficient; spraying water onto this low oil amount made little difference; drying a wet contact reduced traction. Roughness increases were shown to raise traction coefficient as well as reducing contact pressure.

A solid friction modifier (HPF) was also studied in dynamic and static conditions for a simulated 8Hz electrical circuit. The results have proved that the interfacial film by the friction modifier no affect the impedance either in dynamic or static conditions and the variation seen in voltage are related to some other issues as roughness, disc creep level, surface profile and interfacial film thickness (presence of debris).

Contents

Nomenclature

Symbol	Description	Units
A	Contact area	(m^2)
A_d	Area of a disc dissipating radiation energy	(m^2)
a	Disc contact half width	(m)
b	Disc contact width	(m)
C_p	Specific heat capacity of air	(1 kJ/kg/K)
C_{ps}	Specific heat capacity of the wheel/rail steel	(kJ/kg K)
E	Young's modulus	(MPa)
E^*	Contact modulus	(MPa)
F_n	Normal Force	(N)
G	Conductance	(Ω^{-1})
h	Convective heat transfer coefficient	(W/K m^2)
I	Current	(A)
k	Wear coefficient	
k_a	Thermal conductivity of air	(0.025 W/m/K)
k_s	Thermal conductivity of the wheel steel	(W/m/K)
K_{lc}	The material of fracture toughness	(MPa$\sqrt{m}$)
L	Track width	(m)
l	Length of the resistance	(m)
L	Peclet number	(given by $Ua/2\chi$)
L_1	The stub shaft length	(m)
L_2	The stub shaft length	(m)
L_d	Disc circumference	(m)
L_s	Shaft length	(m)
M	Thermal responsivity of the disc surface	(°C/W)
P_0	Maximum contact pressure	(MPa)
p	Load applied	(N)
Q	Heat generated	($\mu F_n u_s$)
$\dot{Q}_1$	Heat loss due to convection	(W)

$\dot{Q}_2$	Heat loss due to conduction	(W)
$\dot{Q}_3$	Heat loss due to radiation	(W)
q	Traction distribution	(N)
R_l	Radius of curvature of rail disc	(m)
R_2	Radius of curvature of wheel disc	(m)
R'	Reduced radius of curvature	(m)
R	Resistance across the disc contact	(Ω)
r	Disc radius at any point within the disc	(m)
r_0	Disc outer radius	(m)
r_i	Disc inner radius	(m)
r_s	Shaft diameter	(m)
T	Tractive force ($\mu \times p$)	(N)
T	Tangential force	(N)
T_a	Ambient air temperature	(°C)
T_b	Disc body temperature	(°C)
T_f	Flash temperature in disc contact	(°C)
T_i	Disc inner temperature	(°C)
$\overline{T}_f$	Average flash temperature in disc contact	(°C)
$\hat{T}_f$	Maximum flash temperature in disc contact	(°C)
T_{fA}	True flash temperature in the body A	(°C)
T_{fB}	True temperature in the body B	(°C)
$\overline{T}_{fc}$	Maximum flash temperature	(°C)
$\overline{T}_{fA}$	Average flash for a line contact in body A	(°C)
$\overline{T}_{fB}$	Average flash for a line contact in body B	(°C)
$\hat{T}_{fC}$	Maximum flash temperature	(°C)
$\hat{T}_{fA}$	Maximum flash temperature in body A	(°C)

$\hat{T}_{fB}$	Maximum flash temperature in body B	(°C)
T_{tot}	Total surface temperature	(°C)
T_B	Body Temperature	(°C)
T_C	Contact Temperature	(°C)
T_A	Ambient temperature	(°C)
u_s	Disc sliding speed	(m/s)
u_r	Air velocity relative to the disc	(m/s)
U	Velocity of contacting solid	(m/s)
V	Voltage	(V)
W	Load applied	(N)
Y	Constant depending on the crack geometry	
Z	Location of the maximum shear stress	(m)
α	Proportion of heat entering disc 1	
γ	Slip (percentage in disc surface speeds)	
ε	Emissivity	
η_a	Dynamic viscosity of air	$(2\times10^{-5}\ \text{kg/m/s})$
μ	Coefficient of friction	
v	Possion's ratio	
ρ	Resistivity	(Ω-m)
ρ_a	Density of air	$(1.2\ \text{kg/m}^3)$
ρ	The density of the wheel/rail	$(8000\ \text{kg/m}^3)$
σ	Stefan-Boltzmann constant	$(5.6\times10^{-8}\text{W/m}^2\text{/K})$
σ	The stress surrounding the particle	(MPa)
σ_x	Thermal compressive stresses	(MPa)
σ_y	Thermal compressive stresses	(MPa)
τ_{max}	Maximum shear stress	(MPa)
χ	Thermal diffusivity	$(\text{m}^2\text{/s})$
υ	Vehicle speed	(m/s)

Acknowledgements

The author would like to thank Dr. Roger Lewis for his great support, guidance and friendship throughout all these years.

The author would also like to thank, Professor R. S. Dwyer-Joyce for his support and Dr. Mike Frolish for the technical assistance during the testing process with the SUROS machine.

Dedication

I dedicate this work to my parents Ofelia Hernandez Campos and Nicolas Gallardo Ojeda that with their emotional and guidance made all this possible. Thank you very much. I love you!

To my sister and brother, Dulce Maria Gallardo Hernandez and Jose de Jesus Gallardo Hernandez.

I also dedicate this work to my wife Magdalena Diaz Fernandez. I love you!

Acknowledgements

Dedication

I dedicate this work to my parents Ofelia Hernandez Campos and Nicolas Gallardo Ojeda that with their emotional and guidance made all this possible. Thank you very much. I love you!

To my sister and brother, Dulce Maria Gallardo Hernandez and Jose de Jesus Gallardo Hernandez.

I also dedicate this work to my wife Magdalena Diaz Fernandez. I love you!

Chapter 1. Introduction

1.1 Statement of the Problem

Railway systems involve vehicles that receive support and lateral guidance from a track structure. The vehicle reacts to the topology of the track due to the rail-bounds. The rail crown provides vertical support and lateral guidance for the wheel of the vehicle. The vehicles are designed to support very high loads over their axles however a bad design could rapidly jeopardize the operation of railway systems. In order to illustrate a railway vehicle a picture of a Diesel Locomotive F-10 #1114 on the Cape Cod Railroad in USA is shown in the Figure 1.1. The locomotive was built by General Motors Electromotive Division in 1946.

Figure 1.1 Diesel Locomotive F-10 #111. Catnip website, (1996-2007), Track pictures (online), Available: www.catnip.co.uk (Accessed 03 September 2007).

Railway vehicles are complex and consist of many sub-systems, such as; bogies, wheel sets, suspensions, body shells, couplers, power collectors, doors, lights, ventilation, communication systems, water provision and waste management. Wheel-sets contain

elements as; axles, suspension, springs and wheels. In particular, wheels are in close relationship with the railway tracks (Schmid, 2003). Rail tracks support and guide the wheels of the vehicle. Figure 1.2 illustrates the wheel shape. The wheel and rail profiles have been the object of continuous improvement.
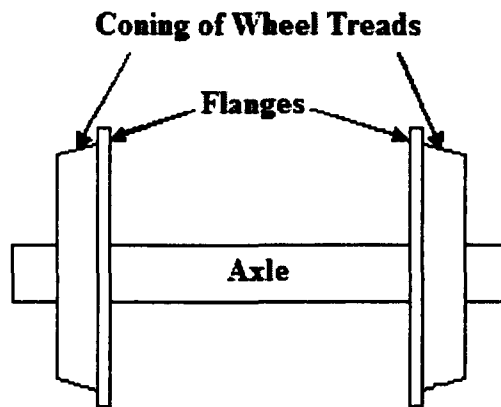
Figure 1.2 Wheel Shape and wheel-rail contact (Railway-Technical Web Pages 1998 – 2007, Wheels and Bogies (online), Available: www.railway-technical.com/whlbog.shtml (Accessed 03 September 2007)).

Currently, of the first rail profiles, the only one surviving is the grooved rail, which is presently used along tracks where the rail top and the pavement surface are at the same level. The double headed or bull-head rail was widely used in the last century, it is still in use in some railways and metros in the UK. The flat bottom rail, or Vignole-type rail, consists of a head, web and base. This rail cross-section was formulated on the basis of the need to join rail lengths together. In Figure 1.3 illustrates some shapes of rails previously mentioned.

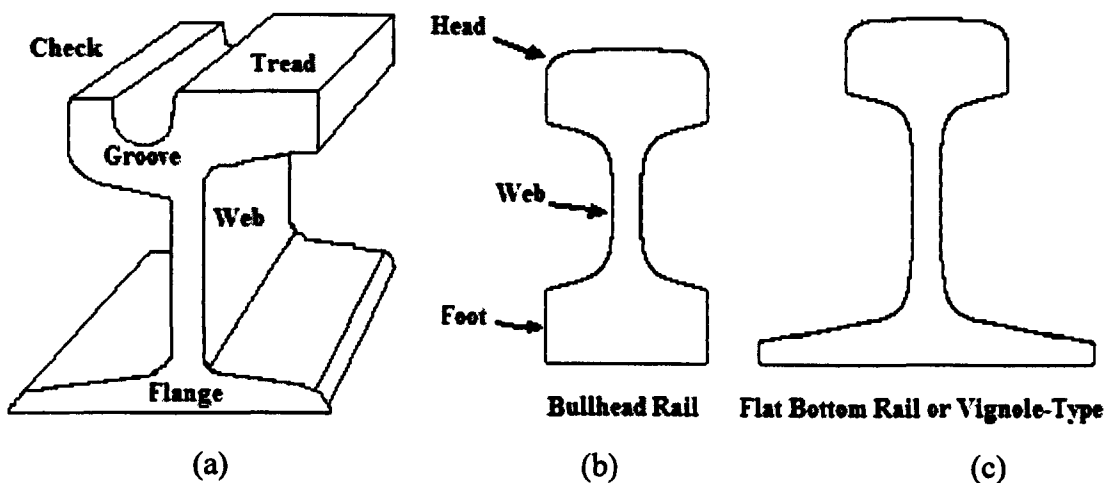Figure 1.3 a) Grooved (www.tmsv.org.au), b) Bull head and c) Flat or Vignole-Type rails. (Railway-Technical Web Pages 1998 – 2007, Track (online), Available: www.railway-technical.com/whlbog.shtml (Accessed 03 September 2007)).

There is a tiny contact area between wheel and rail which is very similar in size to a 20p coin (of 13 mm diameter) (Williams et al., 2001). On straight track the wheel tread is in contact with the rail head, but in curves the wheel flange may be in contact with the gauge corner of the high rail (Nilsson, 2003). The wheel load is transmitted to the rail through the contact under high stress. The developed stresses on the rail are; stresses resulting from rail bending on the ballast, stresses resulting from bending of the rail head on the web, stresses resulting from thermal effects, plastic stresses remaining on the rail after the removal of external loads and Hertz stresses (at the wheel-rail contact) (Profillidis, 1995). Therefore the wheel-rail contact can be a source of many phenomena which could put at risk the performance of the railway during every journey. There are some related to damage, such as; rolling contact fatigue (RCF), wear and crack propagation, etc. loss of adhesion, etc. and some related to performance, such as adhesion and wheel and rail isolation in terms of train detection. All of these are affected by a number of variables, load, speed, temperature, material, etc. Adhesion and isolation are also influenced by contaminants formed on the rail head such as leaves, water, oil, etc.

Wheel and rail contact performance is key to having a safe and reliable railway network. Damage resulting from RCF and wear driven by the wheel and rail contact can lead to rail breakages and consequently accidents can occur. Adhesion loss results in reduced performance (train delays) or safety problems as in braking. Isolation of the wheel/rail contact can cause train detection to be lost. As it is so important a large body of research has been carried out looking at, in particular, rolling contact fatigue and wear. Less has been carried out on adhesion and isolation, however.

1.2 Aims

The objective of the project is, through the use of experimental and analytical simulation to study temperatures, adhesion and isolation in the wheel and rail contact.

1. Temperature evaluation

The aim of this part of the project was to carry out experimental temperature measurement of a twin disc wheel/rail contact simulation using a thermal camera and to compare these with a range of analytical calculations methods.

2. Adhesion

A number of contaminants are found in the wheel/rail contact; water, oil, leaves, etc. The aim here was to establish their effect on adhesion experimentally, and compare measurements with other measurements techniques and field measurement and also to test methods for mitigating the problem.

3. Isolation

The aim of this part of the project was to establish the effect of friction modifiers on wheel/rail isolation, again using a twin disc technique.

1.3 Benefits of the Work

The benefits of the work are obtained below;

1. Greater knowledge of the temperature in the contact will help understanding of the wear mechanism and transitions seen in a rolling/sliding contact as contact parameters are varied.

2. Understanding the effects of contamination has on adhesion will help with mitigation of adhesion problems on the actual rail network or in deciding whether mitigation the wheel and rail well work, or in decaling whether mitigation is actually required.

3. Establishing the effect on conductance of friction modifiers will help determine whether there are any safety issues concerning their use.

1.4 Thesis Layout

The thesis presents a description of the nature of the wheel/rail contact for train systems in chapter 2 as well as some of the factors that affect the performance of the contact. Some information has been focused on solutions to improve the contact in terms of efficiency.

Temperatures for the twin disc contact were studied in analysis described in chapter 3. Experiments carried out using a thermal camera to measure disc body and contact temperatures were obtained. These results are then compared with a number of analytical calculation methods.

In chapter 4, experiments are described that were carried out to asses the effect of contaminants on adhesion. Contaminants such water, oil, wet leaves and dry leaves were tested. Sand, which is used widely to improve the adhesion between wheel and rail contact was also evaluated.

Experiments are outlined in chapter 5 that were carried out to assess wheel/ rail isolation when using a friction modifier in the wheel/rail contact. The friction modifier was applied to the wheel disc to simulate a train measured application.

The last part of the thesis, chapter 6, focused on adhesion in a wheel/rail disc contact and oil-water mixtures. The testing consisted of evaluating water and oil together at different percentages to see which had the overriding effect. The last set of tests in this chapter was focused on observing the remaining effect on the adhesion coefficient of some oil dropped on top disc. Also experiments were carried out to observe the effect of water dropping on the top disc and some remaining oil in terms of adhesion coefficient.

Chapter 2. The Wheel and Rail Contact

2.1 Introduction

This chapter describes some of the current knowledge of wheel/rail contact issues. As mentioned earlier the contact is small, around the size of a 20p coin (Nilsson, 2003) and transmits high loads.

The resulting contact stresses along with the slip inherent in the system lead to wear, RCF etc. occurring. As it is an open system there are many factors that can influence what happens in the contact.

Contaminants can lead to low friction where it is undesirable. Further contaminants are applied to remedy this, such as sand or sandite. Other products, such as grease, are applied to reduce friction on curves, for example. All these contaminants can also affect wear and RCF. It is clearly a complex system.

2.2 The Wheel / Rail Contact

Several factors affect the performance of the wheel/rail contact. Each influences to a different degree and in different mode. Figure 2.1 shows five categories for the wheel/rail contact. These are wheel and rail materials, wheel dynamics, contact mechanics, friction management and damage modes (Kalousec et al., 1997).
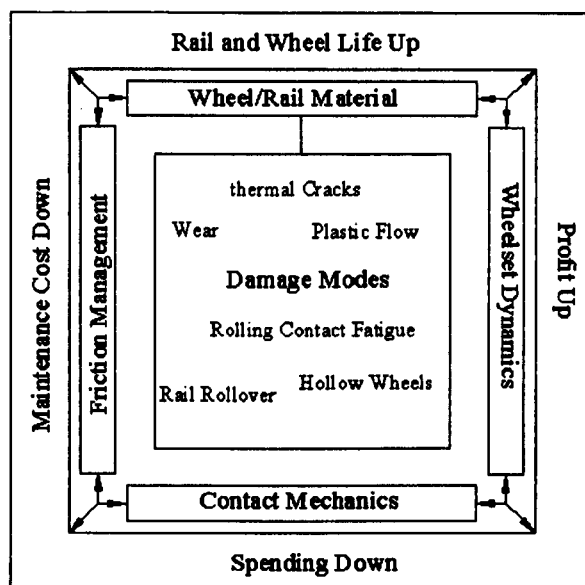

Figure 2.1 Categories of study in rail/wheel contact (Kalousec et al., 1997).

The wheel/rail contact is approximately $1cm^2$ in size. The contact is illustrated in Figure 2.2, along with the forces acting (Sinclair, 2004).
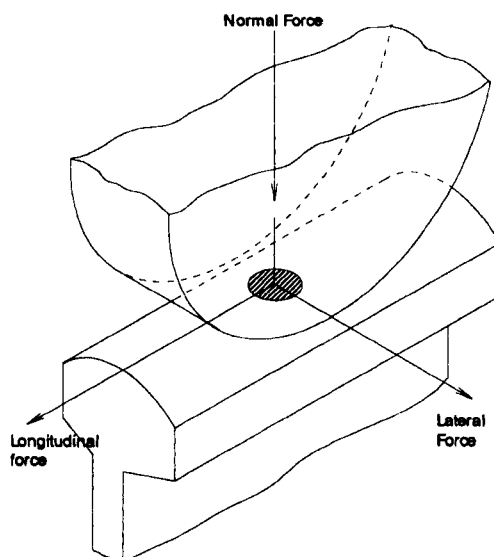

Figure 2.2 Forces acting in the interaction between wheel and rail (Sinclair, 2004).

Wheel/rail contact mechanics involve the study of the geometry of the contact and also the levels of stress and creepage. These vary with dynamics of the vehicle/track characteristics and directly affect wear and RCF of the wheel and rails. Figure 2.3 shows how dynamics and wear are related and the influencing parameters. Coordinates, velocities, forces and moments acting from rails on wheelsets are known from the dynamics of vehicle/track interaction, the magnitude and distribution of normal and tangential stresses, relative slippage (creepage) and friction on the contact patch can be found. Possibly a third body can affect the contact producing a change in the friction and causing abrasion on the wheel and rail surfaces (Kalker, 1990).
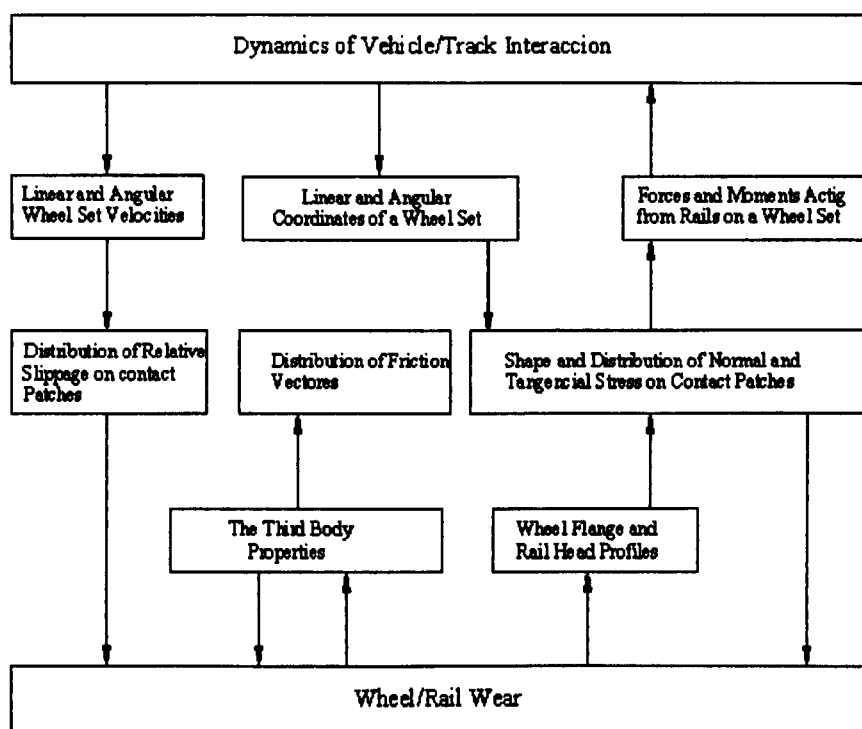
Figure 2.3 Vehicle track interaction (Zakharov et al., 2001).

There are three possible regions of wheel/rail contact. These regions are shown in Figure 2.4. Due to the difference of levels of force and slip in each region different wear rates are seen in each (Tourney, 2001). The three regions are:

1. Region A is the contact between the central region of the rail crown and wheel tread. Contact is made most often in this region and occurs when the vehicle

negotiates tangent track, mild curves and on straight track. The contact stress is low and lateral and longitudinal creepages and forces are lower.

2. Region B. Contact between the gauge corner of the rail and the flange. The contact patch in that region is smaller than that region A and is often much more severe. There are high wear rates and high contact stresses. Some times two parts of contact can occur simultaneously in region A and B.

3. Region C is the contact between the field sides of both rail and wheel. Contact is least likely to occur here and if it does, high contact stress is generated it produces wear features causing incorrect steering of the wheelset.
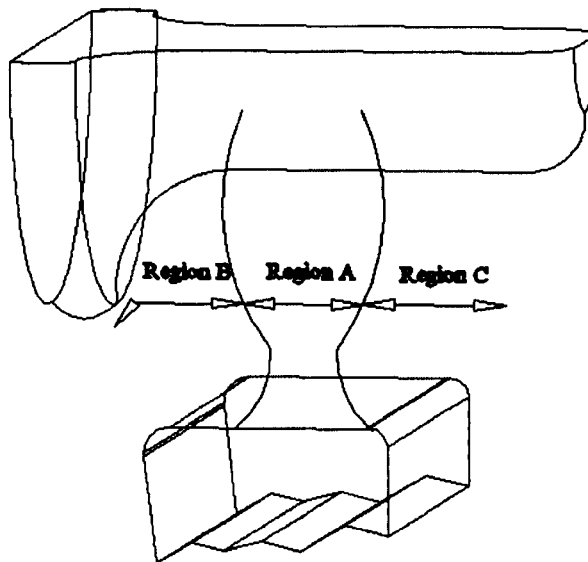
Figure 2.4 Three regions of contact in wheel and rail (Tourney, 2001).

2.3 Loads

Loads vary for each type of railway vehicle. For passenger and lightweight vehicles axles support loads in a range from 90 kN to 300 kN on main lines for example, (for a fully occupied vehicle) while a lightweight passenger coach of mass 36 t supports a single wheel static load between 45 kN to 150 kN. However, dynamic forces grow as a function of v^2(speed) by the energy stored in the linearly moving and rotating masses of wheels, axles, bogies and vehicles bodies (Schmid, 2003).

Typically, there is a wheel-rail contact stress of around 3000 MPa between a flange and the gauge corner of the rail which occurs on curves (Region B, Figure 2.4). The wear of rail and wheel in this sort of contact causes the contact patch to change its configurations. The contact patch size decreases and shifts to the field side of the high rail resulting in growth of the contact pressure which results in a railhead plastic flow. Typically tread wheel runs over the central region in the crown rail is 1300 MPa and 1700 MPa (Region A Figure 2.4).

2.4 Wear in the Wheel/Rail Contact

Wear is the continuous loss of material between two surfaces in motion, that are loaded. Wear leads to the degradation of the material and it losing its functionality (Seireg, 1998). In the wheel and rail contact there are two main areas where wear occurs. The first one is the top of rail wheel/tread contact. The second one is the gauge face and wheel flange, mainly seen in curves. Wear is determined by the slippage and stress in the contact. In turn, the relative slippage and stress depend on dynamic parameters of wheel and rail interaction. The top of rail is subject to contact stresses of about 1300-1700 MPa, depending on the axle load and relative slippage. The flange contact is subjected to wear especially when the vehicle takes the curves or in changes of tracks.

When the wear has been generated particles become detached from the surface and are mixed with various environmental contaminants that compose a third body layer on the top of the rail. In this case the mild wear mode of oxidative origin is predominant. Abrasive particles resulting from sanding to increase adhesion or from other sources can also affect the wear rate and may increase it by two or three times (Kalousek et al., 1999; Lewis et al., 2004; Ghonem et al., 1982). Figure 2.5 shows the result of wear on the tread, which can cause a hollow profile to form. The rail crown causes the wheel tread become hollow due to the wear. The hollow is generated when tread wear is high, and the wheel forms a false flange at the end of treads areas Figure 2.5a. Figure 2.5b show the damaged generated by high contact stress in wheel tread, which could rise until 6000 MPa for 2 mm hollow worn wheel (Williams et al., 2001). Also shown in the Figure 2.5c is a rail with wear and deformation.
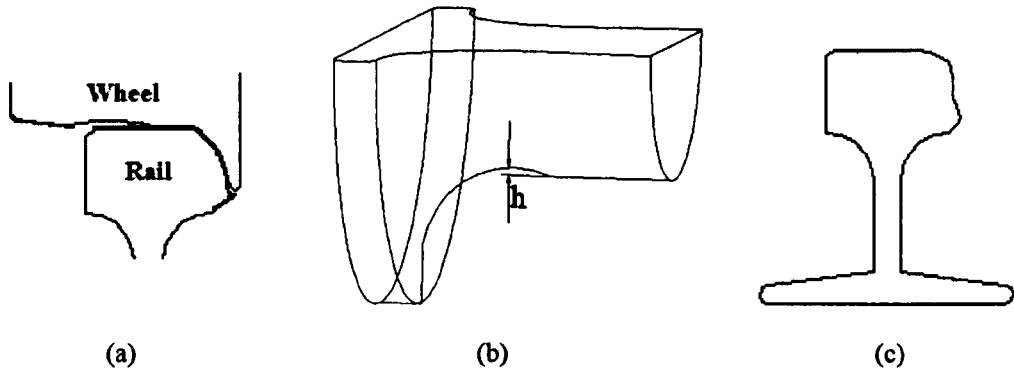
| (a) | (b) | (c) |

Figure 2.5 Hollow worn wheel profile (h is depth of hollow) and rail with wear and deformation (Ghonem et al., 1982).

Wheel hollowing causes changes in the effective contact, below there are some results of these changes;

- Increased car rolling resistance and fuel consumption.
- Creation of a false flange, which causes surface damage of rails, switches, frogs, and crossings.
- Increased lateral forces on rails in curved track, increasing track deterioration and the risk of derailment.
- Increased shear stress acting toward the field side of the low rail and the incidence of flaking damage.

Railhead gauge face and wheel flange wear usually takes place in curves, although it may occur on straight track. In sharp curves under dry conditions, catastrophic wear can occur resulting in a large amount of wear particles deposited on the track, sometimes the particles are captured into the contact causing a modification of the friction and abrasive wear. Wear is highly dependent on the third body properties, which are strongly influenced by lubrication, environment conditions (humidity, rain and snow), and the presence of sand (Adrievsky, 1961).

Experiments by Lewis et al. (2004), have shown that three wear regimes exist for wheel steels; mild, severe and catastrophic. These have been defined in terms of wear rate and wear debris and recent work has been carried out to explain the cause of the transitions between the regimes.

Figure 2.6 shows the results of twin discs wear testing between R8T wheel steel and UIC60 900A rail steel. An energy approach is used to plot the wear data. It is assumed that wear rate is related to work done at the interface. (Wear rate= $kT\gamma/A$, where T is tractive force and γ is slip at the interface, k is a wear coefficient and A the contact area). Figure 2.6 clearly shows the three regimes of wear due to the severity of the contact (Lewis et al., 2004).
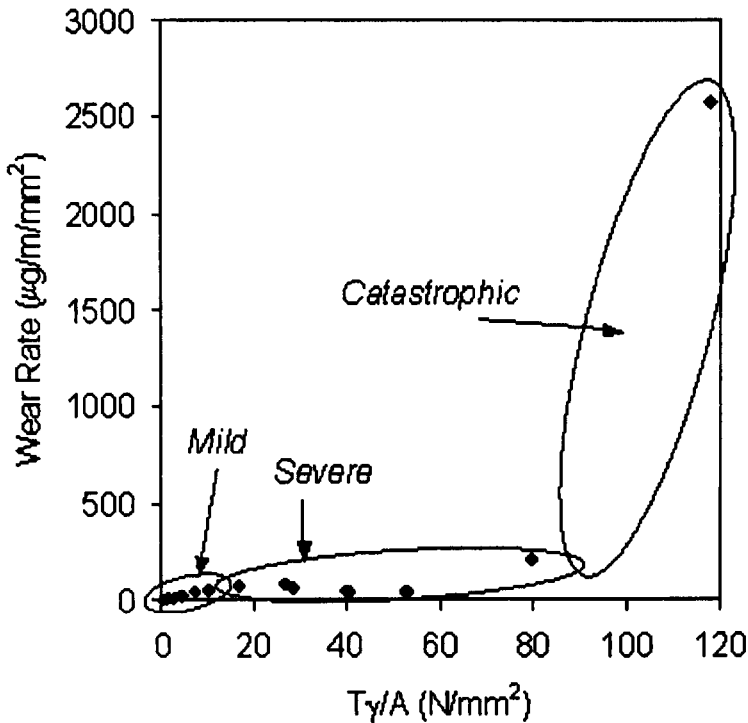
Figure 2.6 Wheel steels wear transitions (Lewis et al., 2004).

At mild contact conditions the wear is dominated by surface oxidation as exhibited by a brown colouration on the surface, with some abrasive scoring. At more severe contact conditions the wear is dominated by presence of cracking on the surface, and mass loss by spalling. Wheel tread wear is mainly in the mild regime with flange wear in the severe to catastrophic regimes.

It is proposed that the first transition (mild-severe) is associated with the onset of full sliding in the contact and the second is result of excessive surface temperature.

For twin-disc testing at the point of transition from partial slip to full slip a wear transition occurs. After the full slip condition has been reached, increasing the magnitude of slip has no affect on friction or wear in the contact.

As slip is increased the traction distribution, q, in the contact increases (whilst $q < \mu p$). The shear stress at the surface increases, which results in increasing wear with slip. Once limiting friction has been reached ($q < \mu p$ everywhere in the contact region) then the surface shear stress remains constant with increasing slip. The wear is largely independent of the sliding velocity. This is an interesting observation. In this regime the wear is controlled by constant stress alone. If the wear mechanism had been by abrasion, (for example caused by asperities or hard particles abrading the surface) increasing the sliding velocity would result in proportionally more abrasive ploughing wear (Lewis et al., 2004).

At the second wear transition (where the wear data breaks from pattern of the friction measurements) another mechanism must be initiated, leading to the much higher wear rate observed (Lewis et al., 2004). As shown in Figure 2.7, the second wear transition occurs at around 200-250°C, which coincides with the point at which the properties of the wheel steel such as hardness and yield stress decrease.
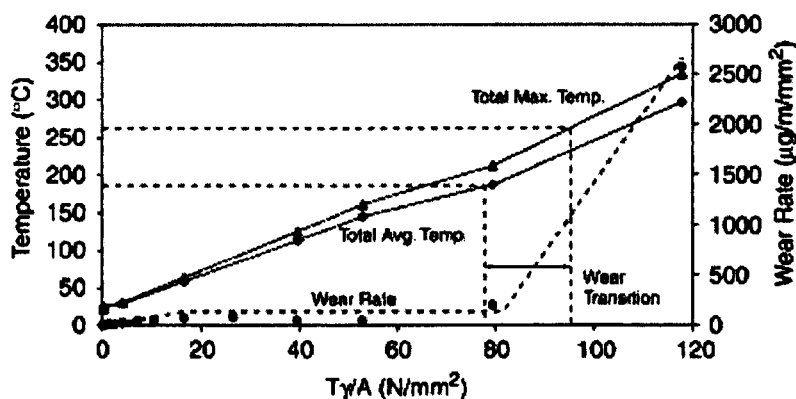

Figure 2.7 Twin disc contact temperatures and wear coefficients for UIC60 900A rail material versus R8T wheel material (Lewis et al., 2004).

2.5 Heat Generation in the Wheel/Rail Contact

While railway wheels are heated by friction in the contact patch, there is also heat loss due to conduction through the contact patch into the rail (Ertz et al., 2002). High temperatures and thermal stress in wheels are also caused by non-uniform heating, which results from tread braking.

The bulk temperature of the wheel increases with time due to the continuous frictional heating on its surface. Therefore, the temperatures of wheel and rail are very different. This gives rise to a considerable heat flow from the wheel into the cold rail due to conduction through the contact patch (Ertz et al., 2002).

A surface temperature change of 200°C would result in thermal compressive stresses σ_x = σ_y ≈ -700 MPa. This may cause plastic deformation, residual stresses and work hardening at the surfaces of wheel and rail. While the contact temperatures are confined to a very thin surface layer, the bulk temperature of the wheel also increases with time by continuous frictional heating. It can be shown that the wheel temperature for constant operating conditions cannot be more than twice the average temperature for the first contact of the cold wheel. This limit is due to the heat conduction from the hot wheel into the cool rail. It corresponds to the usual assumption that the wheel is an insulator and all the frictional heating flows into the rail (Ertz et al., 2002).

Temperature calculations have been developed using analytical models developed by Lewis et al. (2004). The models equate frictional heat generated in the contact with heat dissipation due to conduction convection and radiation. Using the models temperatures were calculated in the body and contact for a number of contact conditions using a twin disc sliding rolling machine. Temperatures were compared to wear rates as shown in figure 2.7 and helped identify the cause of the severe to catastrophic wear regimes.

2.6 Adhesion

Friction is defined by Williams (1994) and Seireg (1998), as the resistance encountered to the motion of a body respect to another when are in contact. Adhesion is also defined by Ohyama (1991) and Eadie et al. (2000) as the maximum traction coefficient reached. The relative slip is a non dimensional value, which for the wheel tread contact is calculated as the ratio of the velocity of relative movement of the surfaces to the linear velocity of the surface. The relative velocity depends on wheel and rail profiles, the angle of attack and such dynamic parameters as the position of a wheel-set and its instantaneous axle of rotation.

Three types of creepage occur in wheel/rail contact, lateral, longitudinal and spin. The degree of creepage depends on the normal load and friction in the contact. The level of slip increases until a full slip, condition is reached, as shown in Figure 2.8.
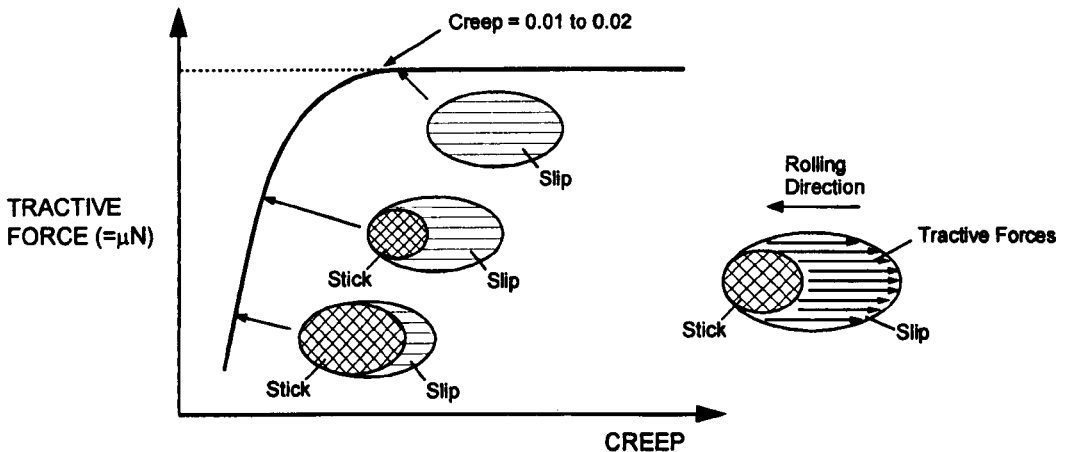
Figure 2.8 Transition from partial to full slip between traction and creepage (Tourney, 2001).

Wheel/rail adhesion is the term used to describe as the limiting friction which can be exerted between wheel and rail (Broster et al., 1974). Poor or high adhesion causes difficulties of operation in railway systems. Poor adhesion leads to loss of traction that can cause delays or braking problems that affect safety. High adhesion can lead to an increase in wear, RCF or noise generation.

In the wheel and rail contact, friction determines the vehicle dynamic behaviour because the forces are a product of the friction or creepages characteristics. For instant, a high friction coefficient is required to climb slopes or for braking or leaving stations, and high

friction coefficients are not required for cars running in curves with small radius. It brings an increase in lateral forces resulting in noise and rail corrugations due to the motion of the wheel along of the rail (Tomeoka et al., 2002).

If good adhesion is achieved a lot of troubles would disappear (Broster et al., 1974). Adhesion has a direct influence on the cost of rail maintenance and the surface damage on wheels treads and rails. Common damage is wheel flats, skidding marks. Wheel/rail adhesion is commonly affected by contaminants, such, leaves, wear, debris, dust, oils, water and snow.

Water and oil show low values of friction. In experiments carried out between wheel and rail using water, friction coefficients of less than 0.3 were observed. Water mixes with solid debris or rust to form a paste with similar properties to oil reducing friction even more to around 0.03. Nevertheless, in steady rain when water removes most of the particles higher values of adhesion were observed (Ohyama, 1991).

Experiments carried out in a rolling contact machine by Ohyama (1991) and using a wheel-set mounted on rail rollers rig (Zhang et al., 2002), have been used to demonstrate that in presence of water, adhesion can be affected and increasing the speed up to 250 km/hr and 270 km/hr, adhesion coefficient can be reduced to around 0.03 and 0.05 respectively. Rough surfaces influence adhesion coefficients. Smooth surfaces present lower values of adhesion compared with more rough surfaces.

Nevertheless, under a perfect lubricant film it was found that the adhesion coefficient increases when the contact pressure rises, but the influence of speed was slight (Ohyama et al., 1991). Zhang et al. (2002) carried out experiments with a wheel-set mounted over two rollers in order to simulate the rail track. It was demonstrated that no matter what contaminants are introduced, the adhesion coefficients decreases with an increase in axle-load, independent of speed.

During autumn, leaves on the track affect adhesion quite dramatically. In normal conditions some leaves are wiped away, but some can be dragged into the contact

accumulating and crushing to form a permanent film. Oxide and iron debris mixed with the leaves generates a black hard and glazed film over the rails (Rail Safety and Standards Board, 2004).

In some cases, it is necessary to fell problem trees. However to protect the environment, these are replaced with smaller leaves trees such as hazel, cherry and holly. Network Rail's tree surgeons take advice from conservation specialists to minimise the impact tree management can have on wildlife. For example, no work is planned during the main nesting season (Arriva Trains Wales, 2006).

Studies carried out by Olofsson & Sundvall (2004), showed how friction coefficient decreases due to the increases in the relative humidity and decreases when leaves are present. Tests were carried out in a pin on-disc-rig. The friction coefficient for a non-lubricated system varied between 0.5 and 0.6, while for lubricated the range was between 0.2 and 0.4. For elm leaf lubrication, the friction coefficient was around 0.1 with some variation due to increasing humidity.

Adhesion and factors influencing have mainly been investigated using experimental techniques, although some attempts have been made to model so called third body layers in the wheel/rail contact (Iordanoff at al., 2002; Hou et al., 1997). Chen et al. (2002) have produced theoretical models to investigate the effect of water in a contact.

2.7 Friction Modifiers

Three methods have been developed to improve the adhesion for wheels on the rails, such as;

1. Mechanical, scouring, branding and sanding on the rail.
2. Chemical, using additives on the rail surface (Friction Modifiers).
3. Electrical, sparking discharge by an electrode between wheel and rail (Fichaux et al., 1968).

Fleets of trains are also fitted with sophisticated sanding equipment to improve traction on slippery rails – the equivalent of ABS on a car. The driver can apply the sand when

wheel spin occurs during acceleration. In Japan to improve wheel-rail adhesion under such conditions, a ceramic particle jetting system was developed which uses compressed air to spray fine ceramic particles (about 10μm diameter) between the wheel tread and rail. The ceramic particles act as tiny wedges, increasing adhesion. This system is used on the Series 500 Nozomi Shinkansen and on conventional rolling stock operating on steep gradients.

Network Rail has a fleet of special 'sandite' trains, which spread a gritty paste on the rails to give trains improved adhesion. Known problem areas such as deep cuttings and steep inclines are targeted in order to minimise delays. There are also static machines to apply sandite at known trouble spots and mobile applicators, which can be used by track workers. High pressure water jets are also used to remove crushed leaves before they form a hard coating (Arriva Trains Wales, 2006).

The application of sand/ceramic particles to the wheel/rail contact from train mounted systems is commonly used to increase adhesion. This has a number of disadvantages as rail and wheel damage can result and build up of sand can cause problems to the rail infrastructure (Kumar et al., 1986; Lewis at al., 2006; William, 2001). Alternatively, rail or wheel mounted systems are also used to apply other types of friction modifiers in either solid or liquid form, these can be designed to increase or decrease friction.

Friction modifiers are substances capable of manage the friction to obtain desirable characteristics. These substances are materials that are added as a layer into the wheel and rail contact. There are three categories of friction modifiers (Kalousek et al., 1999):

1. Low coefficient (LCF), with coefficient of friction 0.2 or less. Approximately the layer thickness is 10-30 microns for solid lubricant whilst 5 microns greases.

2. High friction modifiers in the range of friction coefficient (from 0.2 to 0.4, HPF).

3. Very high friction modifiers or friction enhancers are applied to increase locomotive adhesion and improving braking effort in railway systems (VHPF).

Figure 2.9 shows how the friction modifiers can be classified according to the behaviour after creepage saturation. If the traction decreases after saturation then the modifier has a negative friction. If the traction increases after point of saturation so the modifier has positive friction. The friction modifiers categories are; high positive friction (VHF) and very high positive friction modifier (VHPF) (Eadie et al., 2000).
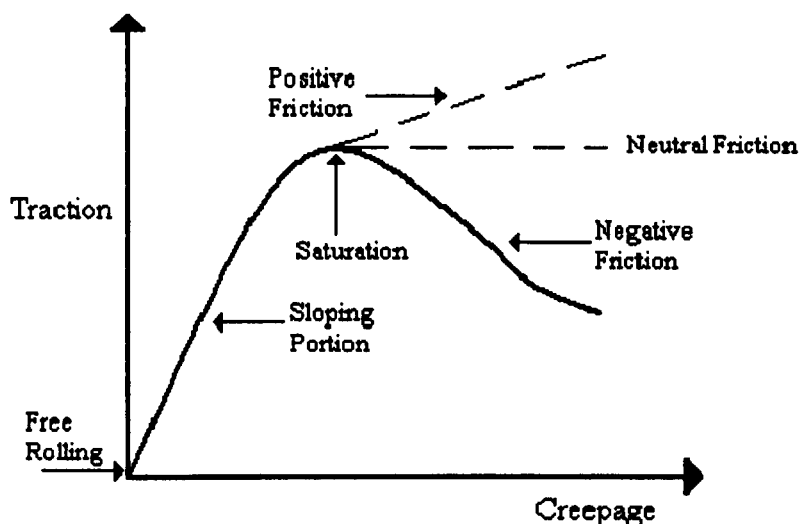
Figure 2.9 Traction force against creepage (Eadie et al., 2000).

2.8 Rolling Contact Fatigue

Wheels and rails suffer damage due to wear and crack growth due to rolling contact fatigue (RCF). In some cases one of the mechanisms can dominate to the extent than the other may be neglected. In other cases both processes are of almost equal importance in determining component life making their interaction critical (Kapoor et al., 2003).

One critical influence on crack growth is crack length. However, wear is completely independent of crack length. In practice it is most likely that wear and fatigue occur simultaneously under contact loading, for which the crack growth rate has a more complex relationship to crack length.

There are three critical stages in wear and rolling contact fatigue as shown in Figure 2.10:

(1) Material subject to rolling contact may separate as wear debris.

(2) Small crack may develop.

(3) Early propagation of cracks will be in the near surface plastically deformed material.

(4) Later propagation will be driven by contact stress and the fluid pressurisation of the crack in deeper, elastic, material.

(5) As the crack extends it may branch and driven by rail bending stress.

(6) Eventual rail fatigue occurs by fast fracture after a critical crack length is reached (Kapoor et al., 2003).
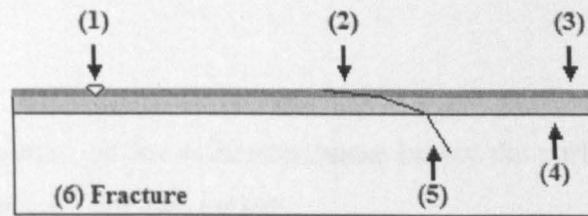

Figure 2.10. Critical stages in wear and rolling contact fatigue (Kapoor et al., 2003).

To estimate the life of the material element at the rail surface is necessary to use either the operating conditions (maximum contact pressure, friction coefficient) or material properties (shear stress at yield, strain hardening properties, critical strain to failure) (Kapoor et al., 2003).

Three modes of crack propagation exist. Mode I refers to crack propagation when the applied load pulls open the crack faces. This mode is not possible without water entering into the crack, propagation is due to the cracks being pressurized by the passing wheel contact. The hydraulic pressure gets transmitted to the crack tip and propagates the crack growth. Mode II and III refer to the situation when the faces are sheared backwards and forwards, and sideways respectively. For this mode water can also reduce friction between the crack faces increasing the mode II stress intensity factor, and hence the crack propagation rate.

Fatigue is considered a form of wear. Subsurface and surface fatigue is observed during constant rolling and sliding load applied. The repeated loading and unloading induces the formation of subsurface and surface cracks. Eventually after a critical number of cycles the surface breaks-up. This effect leads to formation of wear fragments and pits on the contact surface, known as pitting. It can occur after hundreds, thousands or may be millions of cycles. For fatigue, life is more relevant and useful rather than the amount

of material removed from the surface material. Life must be defined in terms of number of revolutions or time before fatigue failure occurs. To calculate the maximum shear stress in sub-surfaces the following equation can be used;

$$\tau_{max} \approx 0.4 \sqrt[3]{\frac{P}{R^{'2}} E^{*2}} \tag{2.1}$$

$$Z \approx 0.56 \sqrt[3]{W \frac{R^{'}}{E^{*}}} \tag{2.2}$$

Where, (*Z*) is the location of the maximum shear below the surface (m), *W* is the load applied (N), and *R'* and *E***, are defined by;

$$R^{'} = \frac{1}{\frac{1}{R_1} + \frac{1}{R_2}} \; ; \text{It is the effective radius.} \tag{2.3}$$

$$E^{*} = \frac{1}{\frac{1}{E_1} + \frac{1}{E_2}} \; ; \text{It is the effective modulus of elasticity.} \tag{2.4}$$

The cyclic loading of steels in the rolling/sliding contact takes four different forms. Figure 2.11 illustrates the response of material to repeated loading;

(1) Perfectly elastic behaviour if the load not exceeds the elastic limit during any load cycle.

(2) Elastic Shakedown, where plastic deformation takes place during the early cycles but due to the development of residual stress and the strain hardening of steel. The steady state behaviour is perfectly elastic.

(3) Plastic shakedown is experienced in the steady state is a closed elastic-plastic loop with no net accumulation of plastic deformation. This behaviour is sometimes referred to as cyclic plastic. In here the load limit is called the ratchetting (or sometimes the plastic shakedown limit).

(4) Above the ratchetting threshold, this steady state consists of open elastic-plastic loops ratchetting; Bower and Johnson, (1989) have shown that ratchetting is a function of both the operating and the shakedown loads.

Ratchetting is sometimes referred to as incremental collapse. Results showed that ratchetting of the surface of the surface layer during the dry phase of a dry-wet rolling process can cause significant deterioration in RCF life of the driven (rail disc).
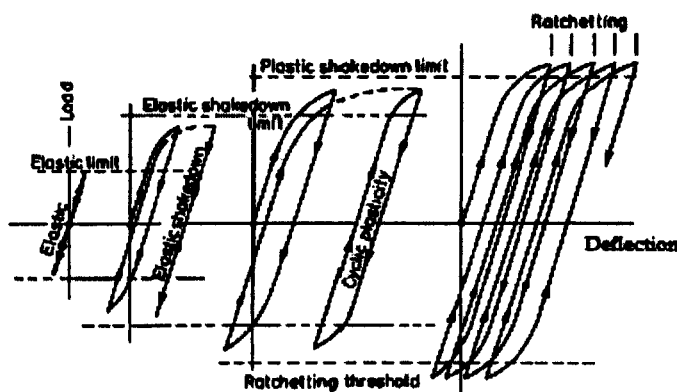
Figure 2.11 Response of material the repeated loading (Kapoor, 1995).

The effect on life of the materials response is shown in Figure 2.12 Clearly the two important factors are load or contact pressure and friction (influenced by lubrication applied). The other main factors are thickness of the hardened layer at the material's surface; residual stress and the size of the contact.
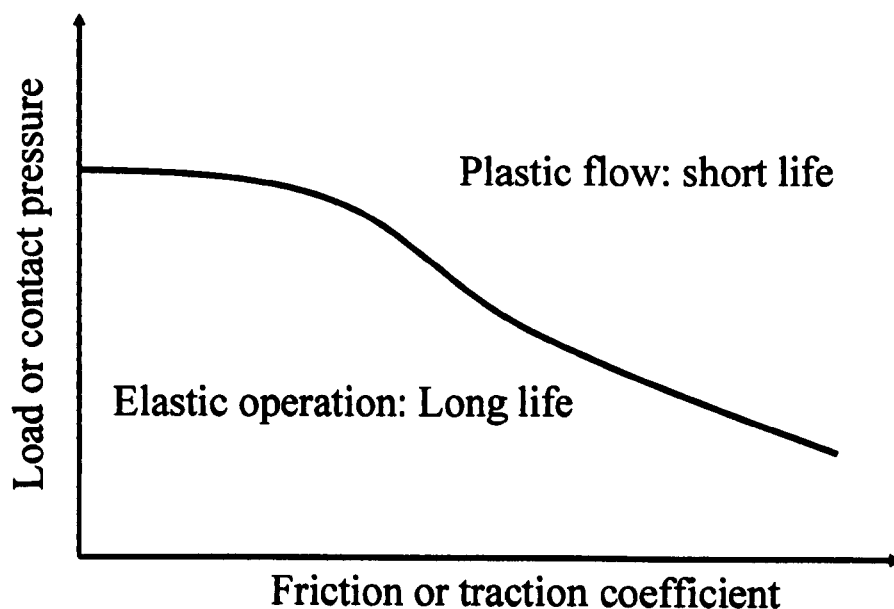
Figure 2.12 Typical shakedown plot (Kapoor, 1995).

Analysis has shown that a rail surface fails by both wear and rolling contact fatigue (RCF) (Figure 2.13). Below the horizontal line is the optimum life. The line intersects the life curve at two points, A and B. Point A represents failure by Rolling Contact Fatigue and point B failure by wear. It can be seen schematically in the figure 2.13. This analysis has shown an interesting observation that for the same life a higher material removal rate leads to a safer operation. This higher material removal rate can achieved through use of a softer rail material or through grinding (Kapoor et al., 2003).

Below the horizontal line is the optimum life. The curves in figure 2.10 represent the control of rail life by wear and fatigue for a given wear rate (thick lines).
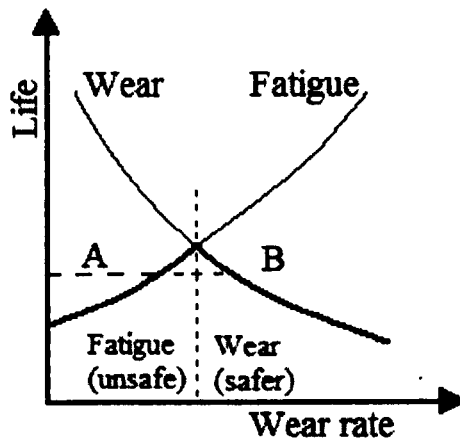

Figure 2.13 Rolling contact fatigue (Kapoor et al., 2003).

Operation at the maximum life point (dotted line) is difficult because of variability in operating conditions. For a reduce life (dashed line) operation could be at point A or B, but B is inherently safer (Kapoor et al., 2003).

Some possible sources of error can be considered during the test process, such as; dimension of the disc (diameter and disc width track), line up of the discs, variation of the load (overshooting), and bearing torque. Taken in account all these issues, the next expression can be presented:

$\Delta T = \Delta D + \Delta T_1 + \Delta L + \Delta N + \Delta B$; ΔT=Total error, ΔD=Error due to diameter of the discs, ΔT_1=Error due to disc width track, ΔL=Error due to line up, ΔN=Error due to overshooting, B=Error due to torque bearing.

2.9 Testing

To investigate the behaviour of wheel/rail materials under different circumstances work has been carried out using different equipment configurations, such as: full scale, wheel and plate, pin-on-disc and twin disc rigs. For full scale experiments were performed by Ahlstrom et al. (1999). To evaluate the mechanical and thermal effects in zones under railway flats, wheel flats are formed when a wheelset is locked and skids along the rail. Experiments were performed in 1996 on a regular line in Stockholm, a whole train which consisted of a locomotive and three carriages. The carriages were equipped with instrumentation and loaded with some weight. The last axle was equipped with a separate braking system which was controlled from a measurements carriage. This was locked to generate the wheel flats. With the data collected, such a train speed, test axle rotation and the force in the brakes, the friction coefficient could be calculated. Multiplying the friction coefficient by the train speed and the axle load, the total power generated in the contact surface can be computed.

Some other testing has been carried out in order to understand of the influence of leaves on adhesion, but this has been using a pin-on-disc set-up using full sliding conditions, rather than the rolling-sliding found in an actual wheel/rail contact (Olofsson et al., 2004). Also Lewis and Olofsson (2004), have investigated the wear producing in wheel and rail material in a pin-on-disc tester. The results have been displayed as wear maps to understand more about wear. In the pin-on-disc tester a hundred percent of slip is reached. This apparatus consists of a rotating disc against a pin which is loaded. Other investigation in this equipment by Olofsson et al. (2004), was to find out the influence of wet leaves in the wear/adhesion of wheel and rail materials.

The rig described by Beagley et al. (1975), consisted of a wheel and one plate simulating the rail. This work was carried out to shows the effect of oily fluids on adhesion. The slipping effect was produced by a spring balance until the slip desired was achieved. Another rig is that used by Broster (1974), in work carried out to investigate the effect of rail contamination, on adhesion which consists in a powered trolley running along one rail of 60 ft length. This rig was mounted on the tracks. Furthermore work by Fichaux & Moore (1968), used a wheelset vehicle over rollers which is mounted on a rail. It was developed to do some work to improve adhesion by spark discharge.

Two roller/sliding testing machines have been developed. They are used to study wear, isolation, RCF and adhesion. With such rigs is possible to evaluate the creep characteristics of various contact conditions of wheel and rail steels. In these measurements are able to select accurate values of slip, speed and load. Tomeakoa et al., 2002, used this type of tester to evaluate the friction between wheel and rail in lubricated conditions. Lewis and Dwyer-Joyce (2004), analyzed the contact in wheel/rail materials to study the wear characteristics in order to establish the wear regimens. Works as those done by Ohyama (1991) and Bugarcic (1986), to explain the friction performing under different circumstances, such as; high speeds and contaminants, using two discs against each other.

2.10 Isolation

Train detection on many railway networks is facilitated by track circuits. These are devices designed to continuously detect the absence of a train from a particular section of track. Their failure mode is to indicate the presence of a train and therefore they cannot be used to detect whether a train is present.

A track section is electrically defined by insulated joints, which is shown in Figure 2.14. An electrical energy source (transmitter) is connected, via a series impedance, across one end of the track circuit. At the other end is a detector. If there is no train within the boundaries of a track circuit the detector picks-up the electrical energy from the transmitter. It in turn energies a repeater circuit, which tells the signalling system the section of track is clear.
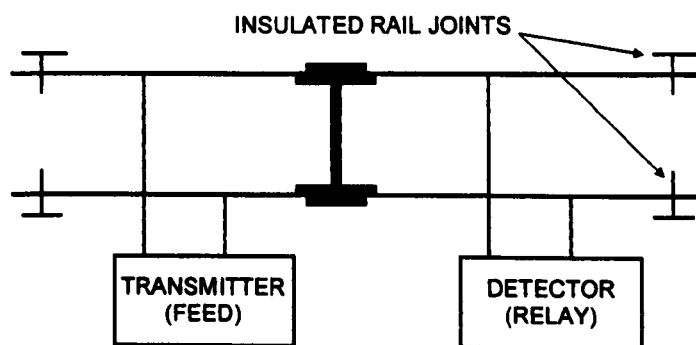

Figure 2.14 Track Circuit Schematic (Lewis et al., 2006).

If a train is present on the track section the rails will be short-circuited and the detector will no longer be able to sense the electrical energy from the transmitter. It therefore changes state and the signalling system is informed that the section of track is occupied.

It can be seen that any short-circuit, caused by a train or otherwise, or a break in the circuit will fail the track circuit and inform the signalling system that the track is occupied, so a good degree of *fail-safe* is incorporated. The system, however, relies on good wheel/rail electrical contact to work (Lewis et al., 2006).

Third bodies present on the rail head or wheel tread surface, whether they be natural (rust, leaves, ballast fragments) or deliberately applied (friction modifiers, sand, lubricants etc.) could compromise the wheel/rail electrical contact and lead to loss of train detection (Lewis et al., 2006).

As was mentioned before, sand, is applied into the wheel and rail interface to increase adhesion in braking and traction and contaminants such as leaves fall naturally over the tracks affecting the wheel/rail adhesion. Studies have been carried out to identify the effect of sanding and contaminants on electrical isolation for signalling purposes. Sand and/or contaminants (third body) entering into the contact between wheel and rail can compromise the contact, inhibiting train identification. Lewis et al, (2003) have done some work using a twin disc machine to simulate isolation. The contact discs were isolated from the rest of the twin disc machine to pass electric current through the discs contact. A simulated TI21 track circuit was used which is applied widely in the UK in railway networks (Figure 2.15). The circuit used consist of a 2 kHz AC Voltage source, V_0, connected in series with a resistor. Another 10 Ω resistor was connected in parallel with the disc contact. The resistor was used as a replication of transmitter and receiver resistances from the TI21 track circuit. RMS (root mean square) voltage, V, was logged using data-capture apparatus with samples taken at 0.1s intervals. The aim of the tests was to establish the minimum amount of sand required for sand and contaminants to asses the effect of them over the isolation.
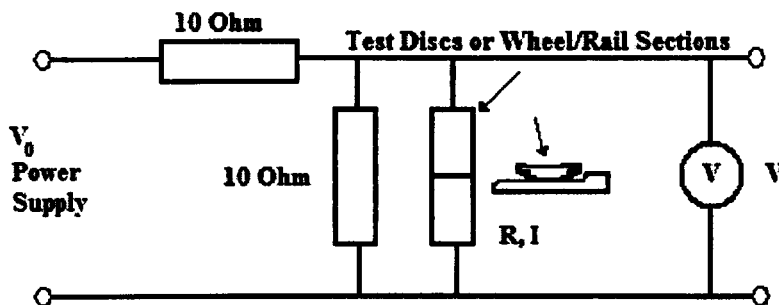
Figure 2.15 Electrical circuit used for determining voltage across the wheel/rail section and twin disc.

The work related the resistance of the contact to the sand flow-rate. This was to help asses the likelihood of isolation occurring for all different types of track circuit. The resistance, R, across the disc can be calculated by:

$$R = \frac{10}{V_0/V - 2} \tag{2.5}$$

This makes assigning an average value for contact resistance for a given sand flow-rate. In order to overcome this, the conductance, G, was considered rather than resistance (where $G=1/R$).

Results showed that for sand flow rates 0.5 kg/min and above the voltage is apparently continues above the closed circuit-value. With sand flow-rates of 0.5 Kg/min and lower the voltage change intermittently but tend toward its closed-circuit values.

Adding water and the same 0.5 Kg/min, the voltage was above of the closed-circuit value observing complete isolation.

Varying the voltage in wet from $5 - 2$ V, 1500 MPa at 10 % of slip and nominal sand flow rate of 0.38 kg/min occurring the same phenomena than those where water and different sand flow rates were applied.

The conductance for two experiments with two different values of sand flow rate which are 0.68 and 0.20 kg/min respectively. At the higher sand rate, where voltages remained at open-circuit value, the conductance remains very low. At the lower sand flow-rate, where closed-circuit values for voltage and current were seen, conductance is several orders of magnitude higher.

Another interesting observation was that the isolation times are of the same order of magnitude for 0.40 kg/min sand flow-rate in wet and dry conditions. The tests were carried out at 2 mile/h and 5 mile/h. better conductance was observed at 5 mile/h than at 2 mile/h. It suggested that sand entrainment was grater at the higher speed.

The contact resistance for the situation where the two discs are separated by a thin layer of sand can be modelled using:

$$R = \frac{\rho l}{A} \tag{2.6}$$

Where ρ is the resistivity of the sand layer, l is the length of the resistance (the thickness of the sand layer and A is the area of the disc contact.

The size of crushed sand fragment will be dictated and the size of any flaws in the material. The minimum fragment size after crushing in the disc can be obtained from the stress surrounding the particle, σ, and the size of any flaw, a', in the material of fracture toughness K_c:

$$K_{Ic} = Y\sigma\sqrt{\pi a'} \tag{2.7}$$

where Y is a constant depending on the crack geometry and σ is the maximum stress. Here it is equal to the hardness of the disc material and a, can be estimated for the smallest possible surviving sand fragment as $0.1 - 0.2\ \mu$m.

2.11 Summary

Clearly a large amount of knowledge has been accumulated on wheel/rail contact issues, but some gaps exist. The aim of this thesis is to try and fill some of these gaps relating to wheel/rail temperature and wear transmission; adhesion testing with different contaminants and isolation issues.

Chapter 3. Thermal Analysis

3.1 Introduction`

The aim of the work described in this chapter was to measure temperatures in a twin disc simulation of the wheel/rail contact. These data are then compared with analytical calculations of temperature.

Temperature can have a large influence on material properties and affect damage mechanisms, so a good understanding of its magnitude at typical operating conditions is important. The thermal experiments results are compared with the analytical calculations using the method developed by Lewis & Dywer-Joyce (2004). This model compares calculations of the heat generated by friction in the contact with heat loss due to conduction, convection and radiation. Further comparisons were made with two methods proposed by Olver (1991), to calculate temperatures in twin disc contacts.

3.2 Thermal Camera Measurements

3.2.1 Twin Disc Test Apparatus

The thermal camera tests were carried out using a twin-disc machine test; a schematic view can be seen in Figure 3.1. In this machine it is possible to simulate typical wheel/rail contact conditions by varying the slip and load between the discs. The machine has two independently driven shafts that permit control of the speed to attain the desired slip values. The machine is based upon a standard Colchester Mascot 1600 lathe. It uses the lathe motor to drive the top "braking" disc. A 4 kW a-c motor drives the bottom "driving" disc via a separate Fenner interchangeable gear box, flexible drive shaft and a pivoting bearing housing. In effect, the 7.5 kW lathe a-c induction motor acts as a "generating brake" on the system, thus creating a slippage at the disc contact (Garnham, 1991 and Fletcher, 2000). The test discs are hydraulically loaded together.
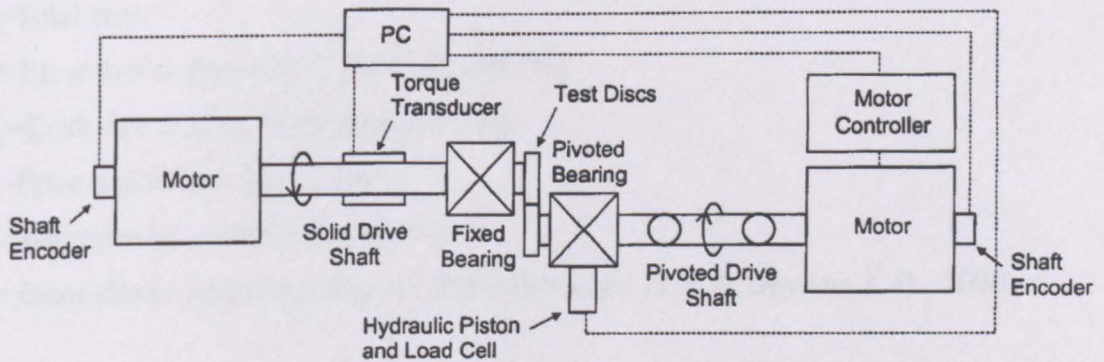
Figure 3.1 Schematic diagram of the twin-disc test machine.

3.2.2 Specimens and Test Conditions

The discs tested were cut from R8T wheel rims and UIC60 900A rail and machined to a diameter of 47 mm and the contact track width was 10 mm. The discs are shown in Figure 3.2. The wheel disc was the driving disc and the rail disc the brake. A nominal disc rotational speed of 400 rpm was used and a contact pressure of 1500 MPa which is typical of the actual wheel/rail contact. Tests were carried out at slip values of 0.5%, 1%, 2%, 3% and 5%. Tests were run until steady state friction and temperatures were achieved (2000-2800 cycles).

(a) Rail

(b) Wheel

Figure 3.2 Rail and wheel disc specimens.

Some possible sources of error can be considered during the test process, such as; dimension of the disc (diameter and disc width track), line up of the discs, variation of the load (overshooting), and bearing torque. Taken in account all these issues, the next expression can be presented:

$$\Delta T = \Delta D + \Delta T_1 + \Delta L + \Delta N + \Delta B$$

ΔT=Total error

ΔD=Error due to diameter of the discs (±0.1%)

ΔT_l=Error due to disc width track (±0.5%)

ΔL=Error due to line up (±2.5%)

ΔN=Error due to overshooting (1.3%)

ΔB=Error due to torque bearing (±1.25%) (Fletcher, D. I. & Beynon, J. H., 2000)

3.2.3 Thermal Camera

In taking the temperature measurements the thermal camera was placed in front of the twin disc machine as shown in the Figure 3.3. Disc "body" temperatures were recorded at spots 5 and 6 and "contact" temperature at spots 1-4.
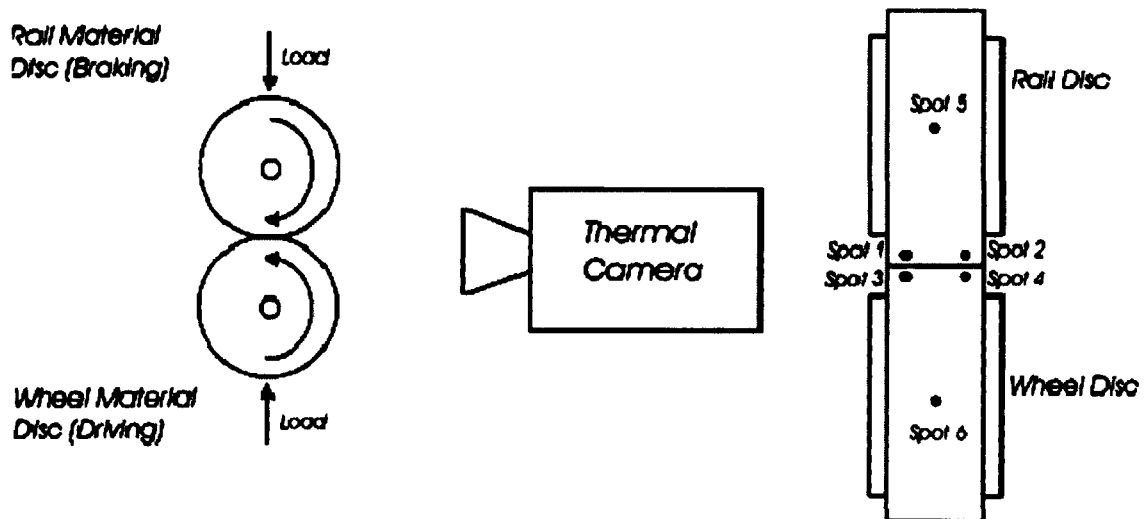
Figure 3.3 Temperature measurement spots near to the contact and on the disc bodies and view of the camera set up.

The camera used was a long wave infrared type from FLIR Systmems. The images recorded during the test were analyzed and films were analyzed using the software package to determine temperatures provide for FLIR Systems. For the camera the spatial resolution is a fundamental property, and directly determines the spatial scale of the resultant information. The spatial resolution for the camera used during the testing (IFOV The instantaneous field-of-view) was 1.1 mrad, IFOV is a combination of geometric, mechanical and electronic properties of the imaging system.

3.2.4 Calibration Measurements

During the testing the emissivity was set to a nominal value of 0.9. This could be changed post test using the previously mentioned software.

After the temperature measurements were completed, the next step was to find the actual emissivity in the contact and on the disc surfaces. The worn discs were placed in an oven with a small piece of black tape on the surfaces for a couple of hours until they reached a steady temperature. After that, the discs had to be moved quickly from the oven and put in front of the camera, avoiding a temperature drop, to obtain the emissivities. The black tape on the surface was used as a reference with emissivity of 0.9. Emissivities were calculated by comparing points on the tape surface with points on the metallic disc surface. Figures 3.4 and 3.5 show the camera images of the discs with tape on.
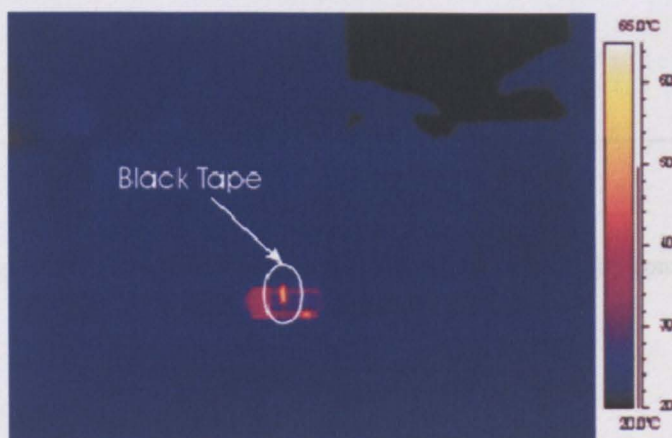

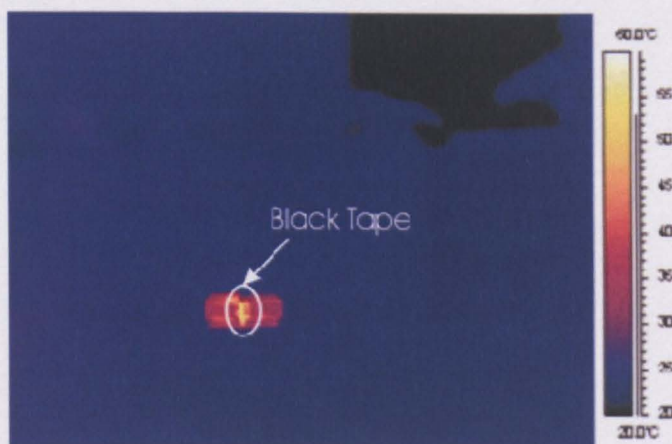Figure 3.4 Black tape on rail disc surface.

Figure 3.5 Black tape on the wheel disc surface.

Figure 3.6 shows the temperature data collected during the test run at 3% slip. The values of emissivity determined during the calibration tests were used to recalculate temperatures post-test ($\varepsilon=0.67$ for the wheel and $\varepsilon=0.22$ for the rail). As can be seen, using these values the wheel and rail body temperatures are approximately equal as would be expected.
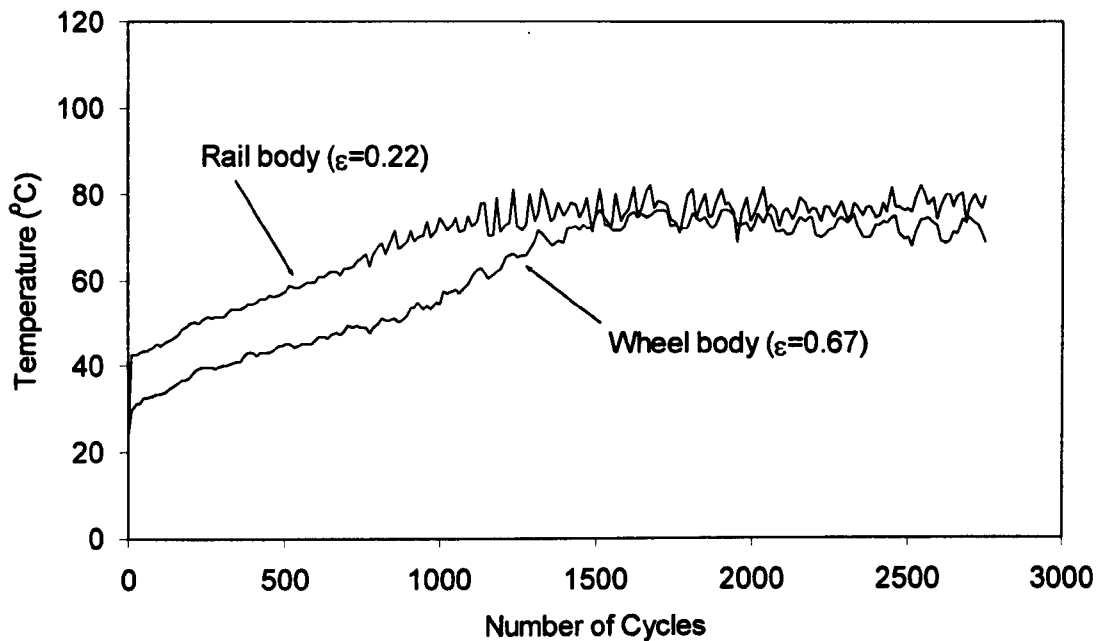

Figure 3.6 Temperature behaviour at 3% slip for a twin-disc contact.

3.2.5 Results

The results of the friction measurement are shown in the Figures 3.7 for the five values of slip selected. Also the resulting creep curve is presented Figure 3.8.
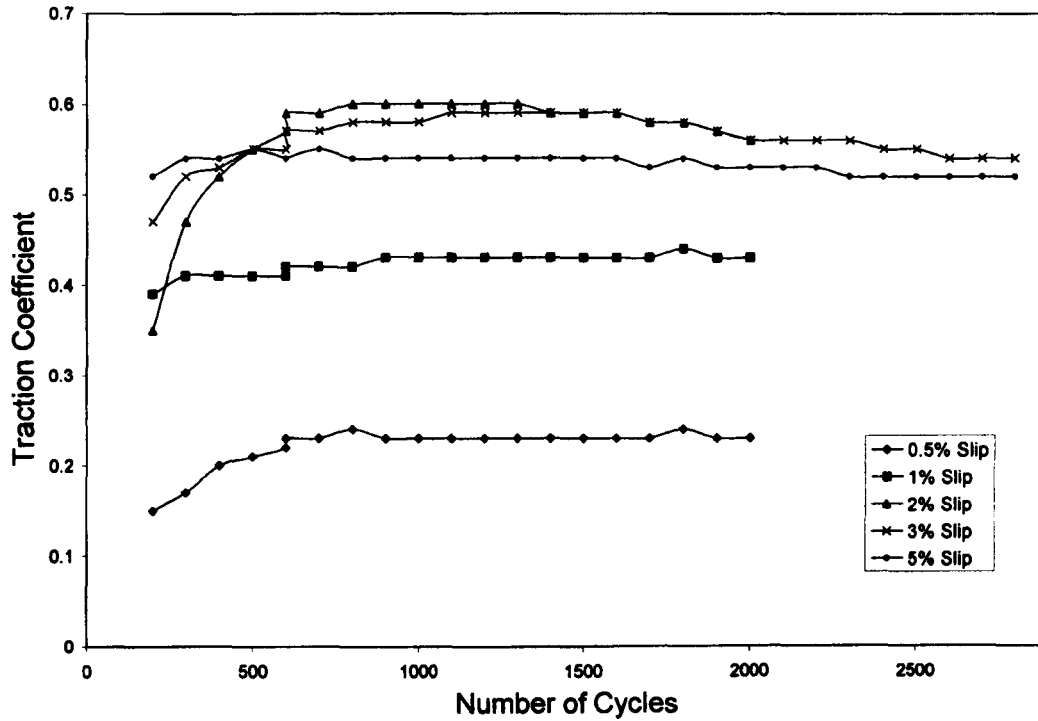

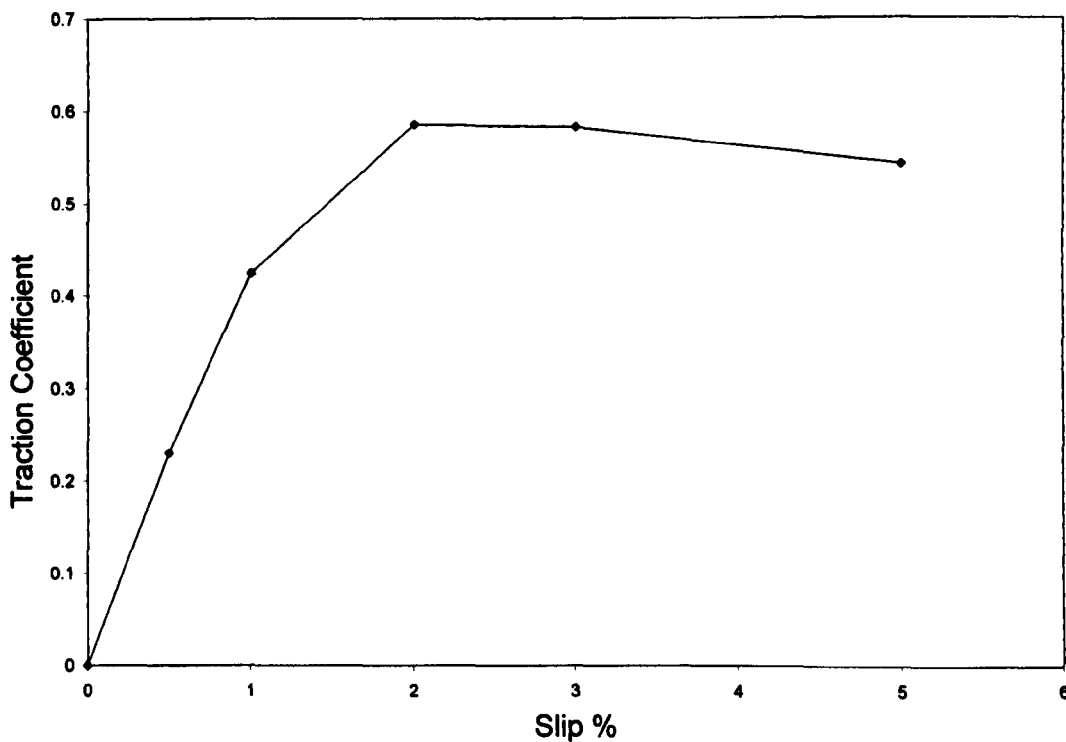Figure 3.7 Traction coefficient evolution during the test.

Figure 3.8 Creep curve showing the steady state traction coefficient measurements variation with slip.

Figures from 3.9 to 3.13 show the pictures taken using the camera. The images were taken every 2 seconds during each experiment. The pictures shown were for 0.5%, 1%, 2% 3% and 5% slip. The images were taken every two seconds with an emissivity of 0.9. This means that the temperature data as shown is not accurate, but can be used as a guide in comparing the different cases. Clearly at 5% slip temperatures are much higher and the temperature increase is much more rapid than the 0.5% case, for example.
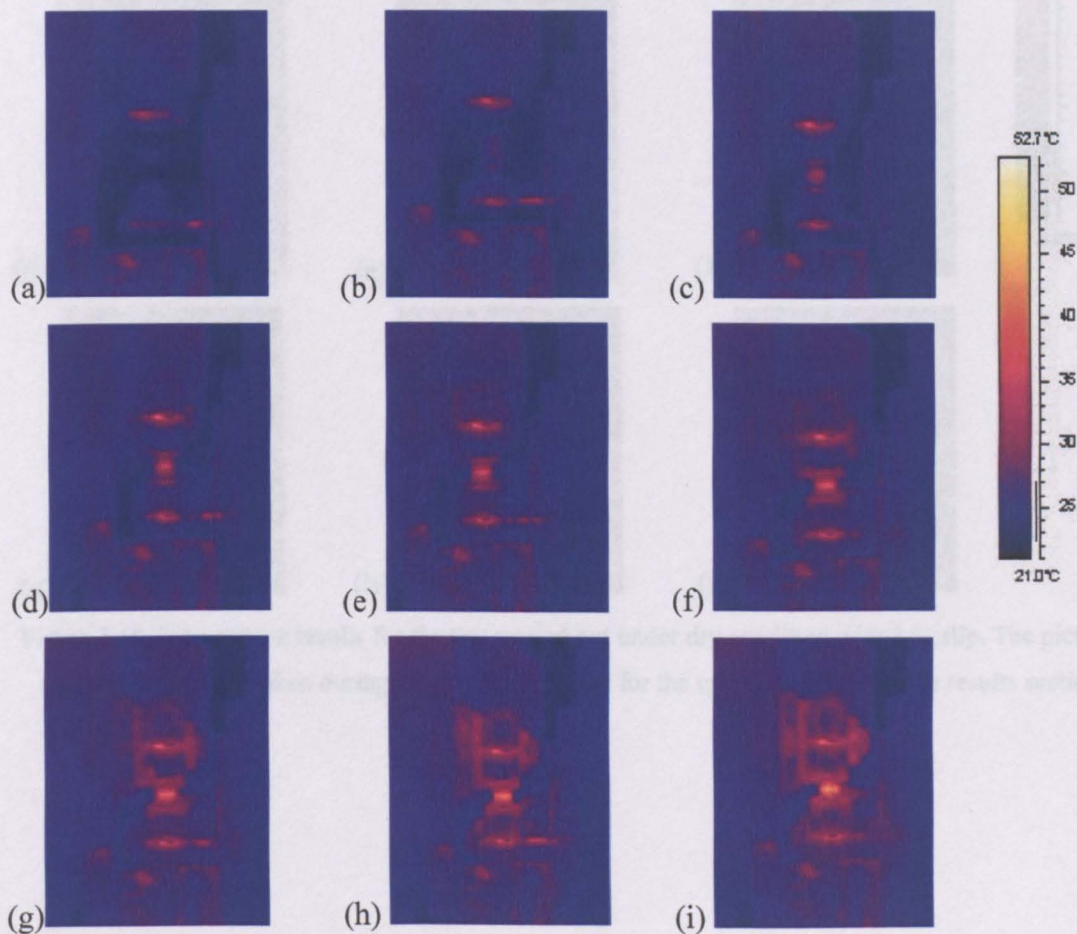

Figure 3.9 Temperature results for the test carried out under dry conditions at 0.5 % slip. The pictures show of the images taken during the test the progress for the cycles presented in the results section.
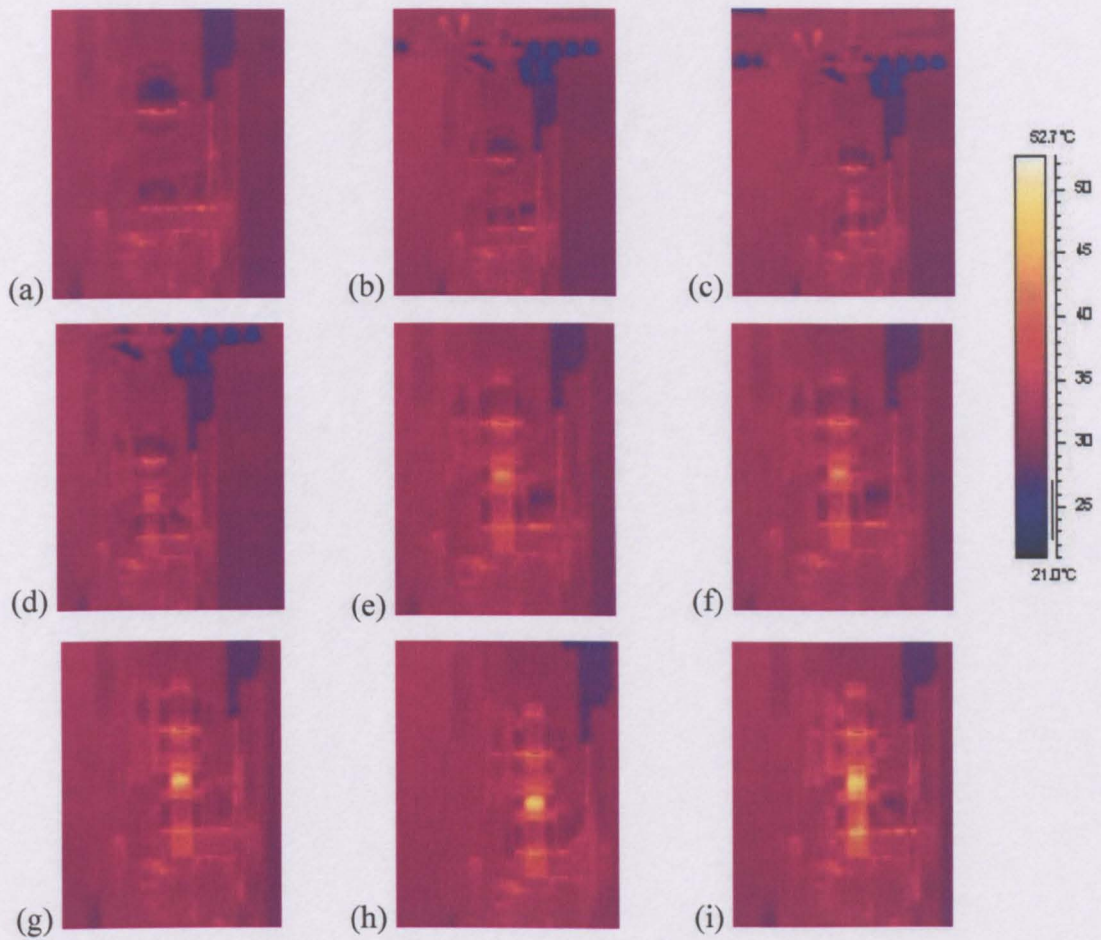
Figure 3.10 Temperature results for the test carried out under dry condition with 1 % slip. The pictures show of the images taken during the test the progress for the cycles presented in the results section.
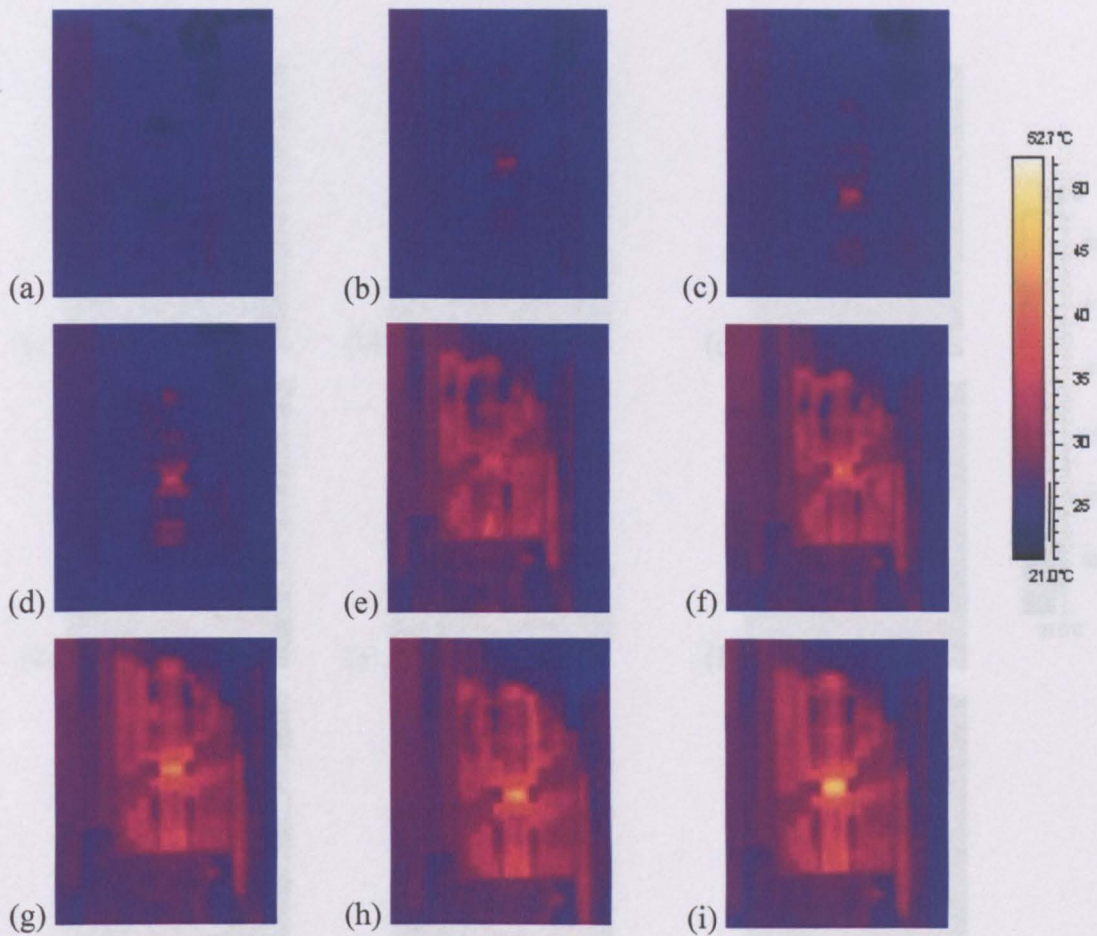
Figure 3.11 Temperature results for the test carried out under dry condition with 2 % Slip. The pictures show of the images taken during the test the progress for the cycles presented in the results section.
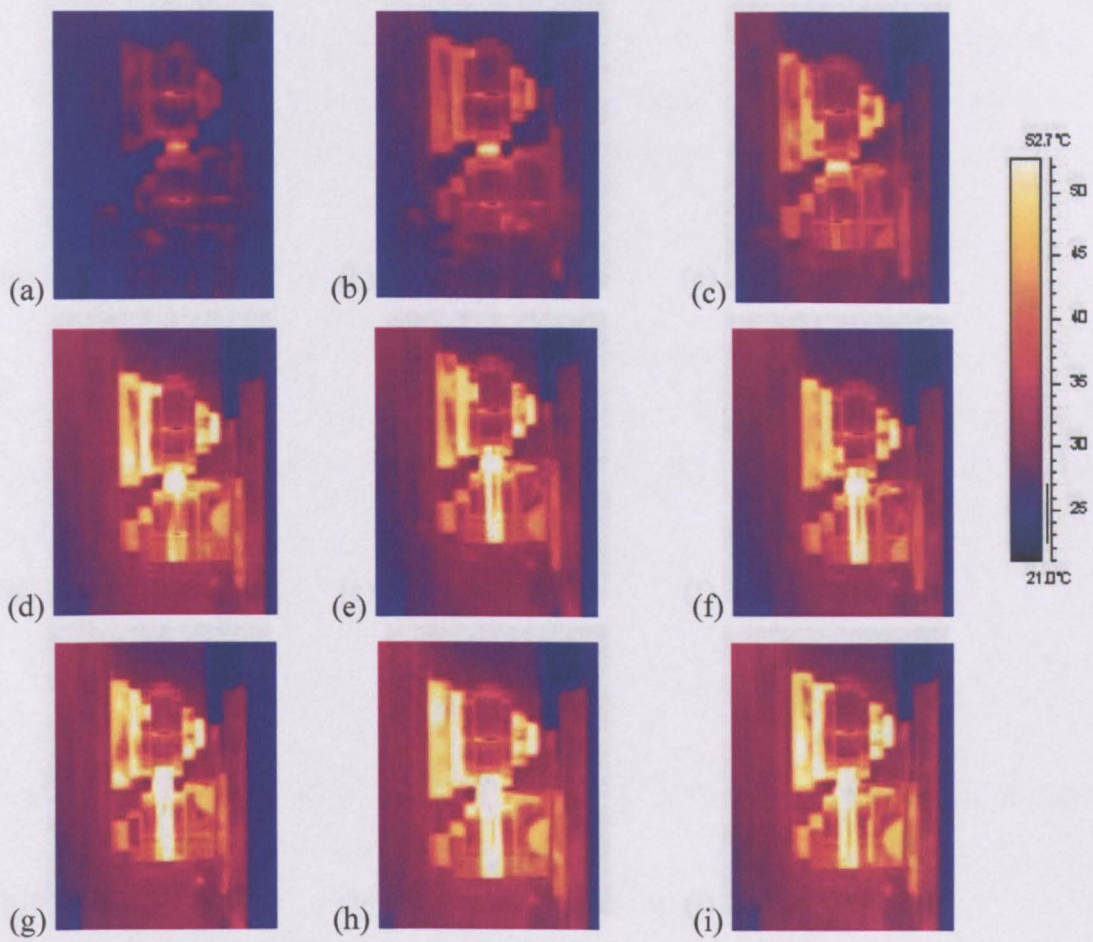
Figure 3.12 Temperature results for the test carried out under dry condition with 3 % slip. The pictures show of the images taken during the test the progress for the cycles presented in the results section.
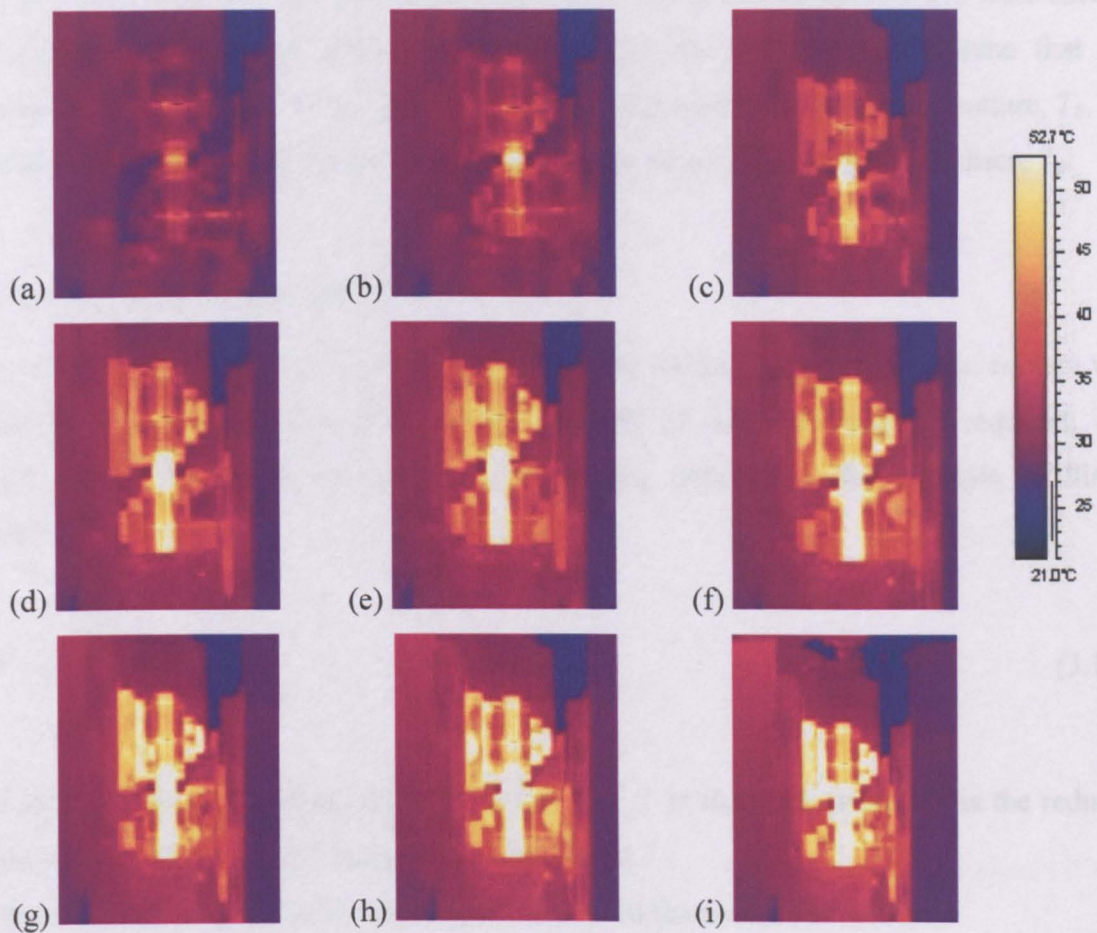
Figure 3.13 Temperature results for the test carried out under dry conditions at 5% slip. The pictures show of the images taken during the test the progress for the cycles presented in the results section.

3.3 Thermal Modelling

To provide a comparison with the measurements two analytical approaches were used to calculate the body and contact temperatures for the discs. These assume that the temperatures of the discs are made up of three components; the body temperature, T_b, the flash temperature in the contact T_f and the ambient temperature around the discs, T_a.

3.3.1 Hertzian Contact Analysis

In order to calculate disc temperature, the sliding distance in the twin disc contact was required. To calculate this distance the geometry of the line contact is required. The contact halfwidth, a, is given by (for calculation details see, for example, Williams (1994)):

$$a^2 = \frac{4WR'}{L\pi E^*} \tag{3.1}$$

where, a is the contact half width, W is the load, L is the track width, R' is the reduced radius of curvature and E^* is the reduced modulus.

First it is necessary to use the next equation to find the reduced modulus:

$$\frac{1}{E^*} = \left(\frac{1-v_1^2}{E_1} + \frac{1-v_2^2}{E_2} \right) \tag{3.2}$$

where E, is Young's modulus and v is Possion's ratio

For wheel and rail steels $E = 2.09 \times 10^{11}$ N/m^2 and $v = 0.3$, so:

$$\frac{1}{E^*} = \frac{1-(0.3)^2}{2.09 \times 10^{11}} + \frac{1-(0.3)^2}{2.09 \times 10^{11}} = \frac{1}{8.708 \times 10^{-12}}$$

$E^* = 1.148 \times 10^{11}$ N/m^2

The reduced radius of curvature, R, is given by Williams (1994):

$$\frac{1}{R} = \frac{1}{R_1} + \frac{1}{R_2}$$ (3.3)

R_1 and R_2, radius of curvature of both discs respectively.

Therefore for the twin disc simulation used in the testing:

$$\frac{1}{R} = \frac{1}{0.0235} + \frac{1}{0.0235} = 85.10$$

$R' = 0.01175$ m

Now, it is necessary to find the maximum contact pressure is given by Williams (1994):

$$p_0 = \sqrt{\frac{E^* W}{RL\pi}}$$ (3.4)

where load, W, is given by:

$$W = \frac{p_0^2 RL\pi}{E^*}$$ (3.5)

Substituting;

$W = 7307.17$ N

Using Equation (3.1):

$a = 0.000307$ m

The sliding speed at the disc interface will be given by:

$$u_s = (2 * 3.1416 * Slip\% * DiscRadius) * rpm \qquad (3.6)$$

Table 3.1 show the sliding speed in the contact for each slip value.

Table 3.1. Sliding speed.

Slip (%)	Sliding speed
0.5	0.00492 m/s
1	0.0098 m/s
2	0.019 m/s
3	0.029 m/s
5	0.049 m/s

3.3.2 Method 1

In order to calculate the body temperature of the two discs in contact, T_b, heat generated due to sliding friction in the contact is equated to heat loss due to convection, conduction and radiation giving:

$$\mu F_n u_s = 2(\dot{Q}_1 + \dot{Q}_2 + \dot{Q}_3) \qquad (3.7)$$

where μ is the coefficient of friction, F_n is the normal load applied to the discs, u_s is the sliding speed and $\dot{Q}_1$, $\dot{Q}_2$ and $\dot{Q}_3$ are heat loss due to convection, conduction and radiation respectively. The dissipated heat is multiplied by two as there are two discs.

3.3.3 Heat Generated by Convection

In this case the heat loss due to convection is obtained by assuming that a laminar thermal boundary layer exists at the disc surface. As the layer reaches the disc interface it is removed (to then reform on the subsequent disc rotation). The rate of heat loss as the thermal layer is removed gives the heat loss due to convection and can be expressed as (Young, 1989):

$$\dot{Q}_1 = 0.331 b k_a (T_b - T_a) \sqrt[3]{\frac{\eta_a C_p}{k_a}} \sqrt{\frac{u_r L_d \rho_a}{\eta_a}} \qquad (3.8)$$

where, b is the contact width of the discs (10 *mm*), K_a is the thermal conductivity of air (0.025 *W/m/K*), η_a is the dynamic viscosity of air (2 x 10^{-5} *kg/m/s*), C_p is the specific heat capacity of air (1 *kJ/kg/K*), u_r is the air velocity relative to the disc (equal to the disc surface speed), L_d is the disc circumference, T_a is the ambient air temperature and T_b is the disc body temperature.

3.3.4 Heat Generated by Conduction

Conduction is the mode of heat transfer in solid material and occurs by virtue of a temperature difference between different parts of the material. Conduction within a solid is a transfer of internal energy; this energy is, in fact, energy of motion of the constituent molecules, atoms, and particles of which the material consists. The kinetic energy is proportional to the absolute temperature; molecular collision lead to energy transfer to regions of lowers kinetic energy. Under steady conditions a molecule will pass on the same amount of energy that it receives. Under non-steady conditions the flow of energy is governed by the changing energy levels. The heat conduction is given by (Simons, 1975):

$$\dot{Q}_2 = \frac{2 \pi r k_s}{\ln\left(\frac{r_0}{r_i}\right)} (T_b - T_i) \qquad (3.9)$$

where, K_s is the thermal conductivity of the wheel and rail material, T_b is the body temperature, T_i the disc inner radius (shaft temperature), r_0 is the disc outer radius and r_i is the disc inner radius.

3.3.5 Heat Generated by Radiation

Radiation is an energy transfer which is transmitted most freely in a vacuum. It occurs between all material phases. All matter at temperatures above absolute zero emits an electro-magnetic spectrum. The mechanism by which radiation is propagated is not of various wave-lengths. Radiation is energy emitted by vibrating electrons in the molecules of material at the surface of a body, and the amount emitted depends on the absolute temperature of the body. The radiation heat loss is given by (Holman, 2002):

$$\dot{Q}_3 = \sigma A_d \varepsilon_{rad} (T_b^4 - T_a^4) \tag{3.10}$$

where, σ is the Stefan-Boltzman constant ($5.669 \times 10^{-8} W/m^2/K$), ε_{rad} is the emissivity of the disc steel and A_d is given by $5\pi r_0 b/6$.

In calculating the area A_d it was assumed that 300° of each disc is radiating heat to surrounding air and 60° on each is radiating heat to the other disc, as shown in Figure 3.1
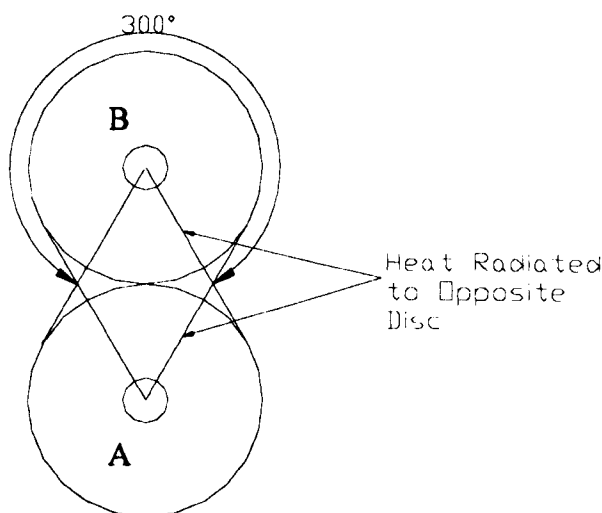
$$A_d = 6.15 \times 10^{-4}$$

Figure 3.14 Radiation from discs in contact.

The heat loss by conduction, convection and radiation is in Table 3.2

Table 3.2 Heat generated in the twin-disc contact and heat losses due to convection, conduction and radiation.

Slip (%)	$\dot{Q}_1$ (W)	$\dot{Q}_2$ (W)	$\dot{Q}_3$ (W)	$2(\dot{Q}_1+\dot{Q}_2+\dot{Q}_3)$
0.5	0.0883	4.1	0.0049	8.2
1	0.153	16.6	0.05	33.6
2	0.271	43.85	0.07	88.3
3	0.382	59.3	0.143	119.6
5	0.841	87.11	0.22	176.3

3.3.6 Analysis of the Flash Temperature

Expressions for flash temperature in line contacts for several ranges of velocity are summarised by Jaeger (1943). The formula to be used varies with the Peclet number, L, given by:

$$L = \frac{Ua}{2\chi} \tag{3.11}$$

where, U is the velocity, of either contacting solid (0.98 m/s), a is the contact half width (equal to 307 μm) and χ is the thermal diffusivity given by:

$$\chi = \frac{k_s}{\rho C_{ps}} \tag{3.12}$$

where ρ is the density of the wheel/rail (8000 kg/m^3), C_{ps} is the specific heat capacity of the wheel and rail steel (500 $J/kg/K$) and k_s is the thermal conductivity of the wheel and rail material(60 $W/m/K$); Therefore:

$$\chi = 15\times10^{-6}\ m^2/s$$

and

$$L = 10.02$$

For $L>5$, average flash temperature for a line contact is given by (Jaeger, 1943):

$$\bar{T}_f = 1.064 \frac{\dot{q}}{K_s} \left(\frac{\chi a}{U} \right)^{0.5} \tag{3.13}$$

where, $\dot{q}$ is the rate of heat supply per unit area given by:

$$\dot{q} = \frac{Q}{2ab} \tag{3.14}$$

where, Q is the heat generated $(\mu F_n u_s)$, b is the contact length, μ is the friction coefficient, F_n is the normal force in the contact and u_s is the sliding speed. The results of calculation are shown in Table 3.3. The heat generated calculated here is relatively equal to those presented in the Table 3.3 where the heat generated is due to conduction, convection and radiation.

Table 3.3 Heat generated in the twin-disc contact.

Slip	Sliding speed	Heat Generated
%	(m/s)	(W)
0.5	0.00492	8.2
1	0.0098	30.9
2	0.0196	86.2
3	0.0295	127.3
5	0.0492	172.6

The average flash temperature for each value of slip is shown in table 3.4, and also the maximum flash temperature, which is given by:

$$\hat{T}_f = \frac{2\,\dot{q}}{k_s}\left(\frac{2\chi a}{\pi U}\right)$$

(3.15)

Table 3.4 Flash temperatures.

Slip %	Average Flash Temperature (°C)	Maximum Flash Temperature (°C)
0.5	1.63	2.45
1	6.12	9.18
2	17.08	25.61
3	25.20	37.80
5	38.44	57.65

The heat generated in frictional contacts is split between the contacting solids. The proportion of the total heat flowing to each body is determined on the basis that the average surface temperature is the same for both bodies. To estimate the true temperature rise is to assume that all the heat generated is supplied to body A, T_{fa}. It should then also be carried out assuming that all the heat is supplied to body B to obtain T_{fB}. The true flash temperature rise must be the same for both solids in contact and is given by Jaeger (1943):

$$\frac{1}{T_f} = \frac{1}{T_{fA}} + \frac{1}{T_{fB}}$$

(3.16)

For the twin disc contact, the true average and maximum flash temperature at the disc conjunction, T_{fc} and T_{fc} are given by expressions:

$$\frac{1}{\bar{T}_{fC}} = \frac{1}{\bar{T}_{fA}} + \frac{1}{\bar{T}_{fB}} \qquad (3.17)$$

and

$$\frac{1}{\hat{T}_{fC}} = \frac{1}{\hat{T}_{fA}} + \frac{1}{\hat{T}_{fB}} \qquad (3.18)$$

The total surface temperature T_{TOT} is given by:

$$T_{TOT} = T_b + T_f \qquad (3.19)$$

Table 3.5 shows the last results of average, maximum and total temperature obtained by the equations shown before.

Table 3.5 Analytical results of temperature in the contact and body.

Slip (%)	T_b (°C)	$\bar{T}_{fC}$ (°C)	$\hat{T}_{fC}$ (°C)	$\bar{T}_{totC}$ (°C)	$\hat{T}_{totC}$ (°C)
0.5	13	0.81	1.22	13.8	14.2
1	21.0	3.06	4.59	24.4	25.9
2	35.5	8.54	12.8	44	48.3
3	49.3	12.6	18.9	61.9	68.2
5	89	19.22	28.8	108.2	117.2

3.3.7 Method 2

The second analysis approach used was that proposed by Olver (1991). This method is for calculating the temperatures of body and contact, T_B and T_C, for a pair of contact discs. This is based on the flash temperature approach of Block (1999) combined with a linear conduction and convection model and is not limited to the discs at the same skin temperature. Both discs are subject to the same ambient temperature T_A. Thus, the contact temperature is given by

$$T_C = T_A + \Delta T_B + \Delta T_C \tag{3.20}$$

where

$$\Delta T_B = T_B - T_A \tag{3.21}$$

For this method the total heat generated by sliding in the contact is.

$$Q = \mu W \Delta u \tag{3.22}$$

Being W the load applied, μ is the friction coefficient and $\Delta u = U_1 - U_2$ is the sliding speed.

Now the bulk temperature rise is directly proportional to the heat input to each disc:

$$(\Delta T_B)_1 = \alpha Q M_1 \qquad \text{for the disc 1} \tag{3.23}$$

$$(\Delta T_B)_2 = (1 - \alpha) Q M_2 \qquad \text{for the disc 2.} \tag{3.24}$$

α, is the proportion of the heat entering disc 1 and M_1 and M_2 are functions of the disc geometry, the conductivity (k_1 and k_2) and heat transfer coefficients (h_1 and h_2); α is

determined in the usual way by assuming that the average contact temperature rise above ambient is the same for both bodies, using the results of Jager (1943):

$$(\Delta T_f)_{av} = \frac{1.06\alpha Q}{Ak_1}\left(\frac{X_1 b}{U_1}\right)^{1/2} + (\Delta T_B)_1 \qquad (3.25)$$

$$(\Delta T_f)_{av} = \frac{1.06\alpha Q}{Ak_2}\left(\frac{X_2 b}{U_2}\right)^{1/2} + (\Delta T_B)_2 \qquad (3.26)$$

A is the contact area which is defined as; *2bl*. *l* is the contact half width and *b* the track width.

To calculate the thermal responsivity of moving hotspot (°C/W) the next equation is proposed.

$$B_i = \frac{1}{2bl}\frac{1}{k_i}\left(\frac{\chi_i b}{u_i}\right)^{1/2}, \quad i = 1,2 \qquad (3.27)$$

To solve α which is given by;

$$\alpha = \frac{1.06 B_2 + M_2}{1.06(B_1 + B_2) + M_1 + M_2} \qquad (3.28)$$

$$\alpha = (W\mu\Delta u)\left\{\frac{1.06 B_2 + M_2}{1.06(B_1 + B_2) + M_1 + M_2}\right\} \times (1.06 B_1 + M_1) + T_A \qquad (3.29)$$

And the maximum contact temperature is determined by Jaeger (1943):

$$(T_C)_1 = T_A + (\Delta T_B)_1 + (\Delta T_C) \qquad (3.30)$$

Here the term in the first bracket is the heat generated and that of the second bracket the heat partition, α. The terms in third bracket represent the temperature rise due to flash and skin response respectively. T_A is the ambient air temperature. It has to be noticed that

B_1 and B_2 are functions only of the material and contact parameters but that M_1 and M_2 must be found from a thermal model of the whole assembly.

The second analytical approach was that proposed by Olver (1991), where further details of the equations outlined below can be found. This approach also involves equating heat loss to heat generated by frictional sliding in the contact. Each disc is considered independently, allowing for discs off different geometries to be analyzed. The maximum contact temperature, $\hat{T}_{tot}$, is given by:

$$\hat{T}_{tot} = (\mu F_n u_s)\left\{\frac{1.06B_2 + M_2}{1.06(B_1 + B_2) + M_1 + M_2}\right\}(1.60B_1 + M_1) + T_a \tag{3.31}$$

Here the term in the first bracket is the heat generated and that of the second bracket the heat partition, α, which represents the proportion of heat entering disc 1. The terms in the third bracket represent the temperature rise due to flash and skin response respectively. Subscripts *1* and *2* refers to discs 1 and 2 respectively. *M* is the thermal responsivity of the disc surface and is related to the disc geometry. *B* is given by:

$$B_i = \frac{1}{2ab}\frac{1}{k_s}\left(\frac{\chi a}{U_i}\right)^{1/2} , i=1,2 \tag{3.32}$$

The second analytical approach was that proposed by Olver (1991), where further details of the equations outlined below can be found. This approach also involves equating heat loss to heat generated by frictional sliding in the contact. Each disc is considered independently, allowing for discs off different geometries to be analyzed. The maximum contact temperature, $\hat{T}_{tot}$, is given by:

$$\hat{T}_{tot} = (\mu F_n u_s)\left\{\frac{1.06B_2 + M_2}{1.06(B_1 + B_2) + M_1 + M_2}\right\}(1.60B_1 + M_1) + T_a \tag{3.33}$$

Various ways of calculating M were presented by Olver (1991). Two simplified situations were taken for this work. Firstly that for thin discs ($r_s = 0$, $b \leftrightarrow r_o$, where r_s is the shaft diameter, b the axial width of the disc and r_o the disc outer radius) was used. l a is the contact half width. As shown in Figure 3.15a, the thermal gradient is entirely radial and in this model convection from the sides of the discs is considered. This situation is analogous to a circular cooling fan and the following one-dimensional solution is well known:

$$M_R = \left\{ 8.88(hk_a)^{1/2} b^{1/2} r_o \frac{I_1(nr_o)}{I_0(nr_o)} \right\}^{-1} \tag{3.34}$$

where $n = (2h/k_a b)^{1/2}$ and h is the convective heat transfer coefficient and I_1 and I_0 are appropriate Bessel functions (for a derivation see Chapman (1974)).
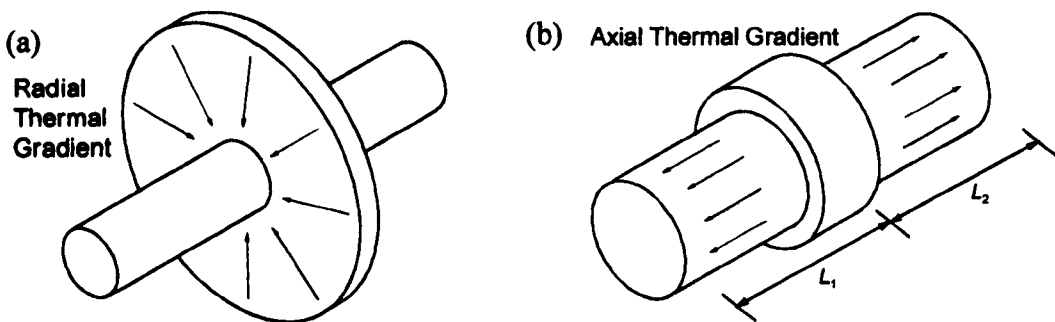
Figure 3.15 (a) The thin disc model and (b) the small disc model.

The second situation considered was that of a small disc with a thick shaft ($r_s \approx r_o$, $b \leftrightarrow r_o \leftrightarrow L_s$, where L_s is the shaft length). Heat conduction and temperature gradient is primarily axial as shown in Figure 3.15b. Again the relevant solution is well known, being one-dimensional in nature (Chapman, 1974):

$$M_A = \left\{ 4.44(hk_a)^{1/2} r_o^{3/2} (\tanh mL_1 + \tanh mL_2) \right\}^{-1} \tag{3.35}$$

where L_1 and L_2 are the stub shaft lengths (see Figure 16b) and $m = \left(2h/k_a r_o\right)^{1/2}$.

The convective heat transfer coefficient is given by:

$$h = 0.265 r_o^{-1/2} u_r^{1/2} \rho_a^{1/3} C_p^{1/3} k_a^{2/3} v^{-1/6} \qquad (3.36)$$

where v is the dynamic viscosity of air, given by η/ρ_a. The value of every literal has been mentioned before due to those constant are used for the other thermal model as well.

These two solutions were evaluated using the disc and shaft geometries and load and slip conditions used in the twin-disc tests and the resulting friction coefficients. Table 3.6 outlines the disc body and contact temperatures calculated.

Table 3.6 Thin disc and small disc solution temperature predictions.

Slip (%)	Thin Disc		Small Disc	
	T_b (°C)	$\hat{T}_{tot}$ (°C)	T_b (°C)	$\hat{T}_{tot}$ (°C)
0.5	1.6	21.3	3.2	12.9
1	6.3	34.2	12.0	40
2	17.7	90.2	33.7	106.3
3	26.1	131.6	49.8	155.2
5	39.9	199.2	75.9	235.3

3.3.8 Comparison of Analytical and Experimental Results

Figure 3.16 shows a comparison of the total analytical temperatures results, with T_A incorporated and the experimental results from the thermal camera for the disc body temperatures. Emissivity values used for the thermal camera data were those obtained in the calibration test (0.67 for the wheel disc and 0.22 for the rail disc). As can be seen a good correlation exists between the first analytical approach used and the thin disc model and the experimental results for the wheel and rail bodies, with the small disc model giving slightly lower temperatures.

Figure 3.17 shows how the temperatures varied if other values of emissivity were used with the thermal camera data. The range of spread is different in each case as different as slightly different spot positions on the discs were used for each calculation and roughness varies over the disc surfaces and this will heavily influence apparent temperature values.
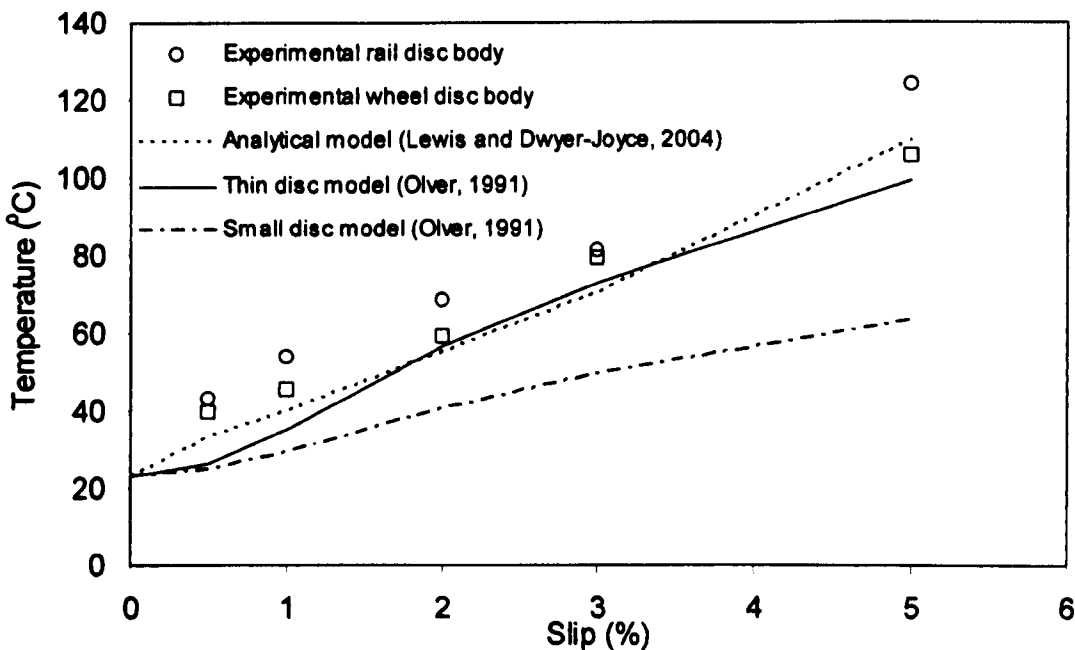
Figure 3.16 Thermal camera disc body temperature data (ε_{rail}=0.22; ε_{wheel}=0.67) compared with analytical models from Lewis & Dwyer-Joyce (2004) and Olver (1991).
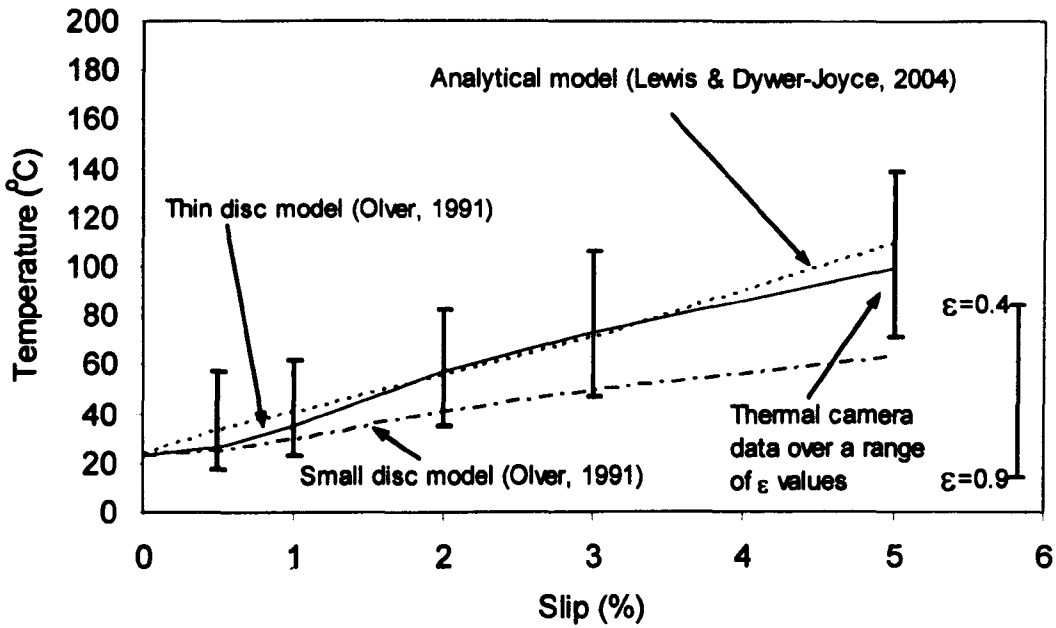
Figure 3.17 Thermal camera and analytical temperatures for the disc bodies for a range of ε values.

Figure 3.18 shows a similar plot for the contact temperatures. A value of emissivity would not be determined experimentally, but over the range of camera temperature using values from 0.12 to 0.67 good correlation is seen between the first analytical approach and the experimental result although it is likely that the actual value will change continuously as the contact surface conditions throughout a test. Thin disc and small disc approximations were slightly higher in this case.
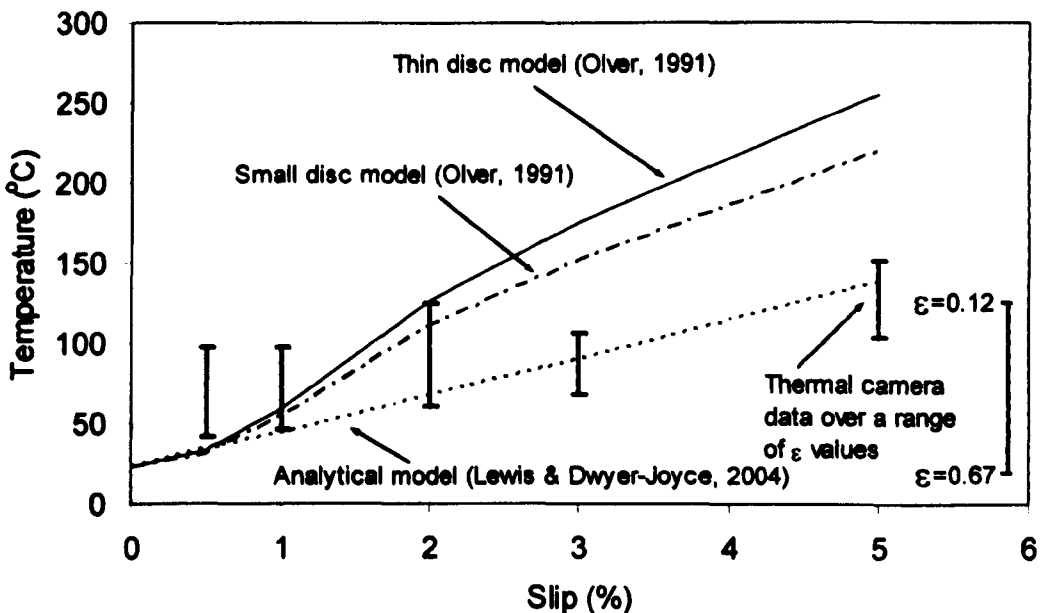
Figure 3.18 Thermal camera and analytical disc contact temperatures for a range of emissivity values.

Chapter 4. Wheel and Rail Adhesion

4.1 Introduction

Friction (or adhesion) loss has a large impact on safety and performance of railway networks. Poor adhesion in braking is a safety issue as it leads to extended stopping distances. If a train experiences poor adhesion in traction when pulling away from a station and a delay is enforced the train operator will incur costs. Similar delays will occur if a train passes over areas of poor adhesion while in service.

There is no standard testing approach for assessing adhesion loss. Tests methods used have ranged from specimen testing through to full-scale testing and field measurements. Specimen testing techniques have included pin-on-disc (Olofsson et al., 2004), disc on flat (Beagley et al., 1975) and twin disc testing (with a line contact) (Beagley et al., 1975, Beagley, 1976), (Chen et al., 2001). Twin disc testing has also been carried out with scaled wheel and rail profiles (Kumar et al., 1986). Full scale testing was used by Jin et al. (2004) to study the effect on adhesion of wet, dry and oil contaminated conditions using a range of axle loads and rolling speeds. Field measurements have been taken using track mounted tribometers (Broster et al., 1974; Harrison et al., 2002) and instrumented trains (Nagase et al., 1989).

As the testing techniques become more complex, the accuracy of the representation of the contact geometry and loading and environmental conditions increases. However, at the same time the level of control of operating parameters decreases. The twin disc approach perhaps gives the best compromise and has been used extensively for testing fatigue and wear properties of wheel and rail materials.

4.2 Test Apparatus and Specimens

The twin disc test machine used to carry out the testing is shown schematically in Chapter 3. The disc specimens were cut from UIC60 900A rail steel R8T wheel steel sections. They had a diameter of 47 mm with a contact width of 10mm (see Chapter 3). The discs were cleaned and weighed to then be mounted on the machine shafts. When the stability has been reached the test was stopped and the discs were taken out from the shafts. They were cleaned and once again the weight and the roughness were measured. The contact surfaces were ground to a roughness of 1 μm.

For wet conditions simple distilled water was used. The oil used was a standard 15W40 engine oil. The leaves used in testing were a mixture of varieties typically found trackside in the UK. They were dead leaves collected during autumn. They were partially broken down prior to testing.

The sand used was standard commercial grade railway silica sand complying to the guidelines issued by Railway Safety, UK, for fitting of sanding equipment to multiple units. In its raw form the sand has an average particle size of around 1.5 mm. In previous twin disc testing with this sand entrainment was a problem, (Lewis et al., 2003; Lewis et al., 2006) so for this work the sand was pre-crushed. The grains were then passed through sieves (see B.S. 1377:1975) to ascertain the size distribution. Figure 4.1 shows the percentage retained at each sieve.
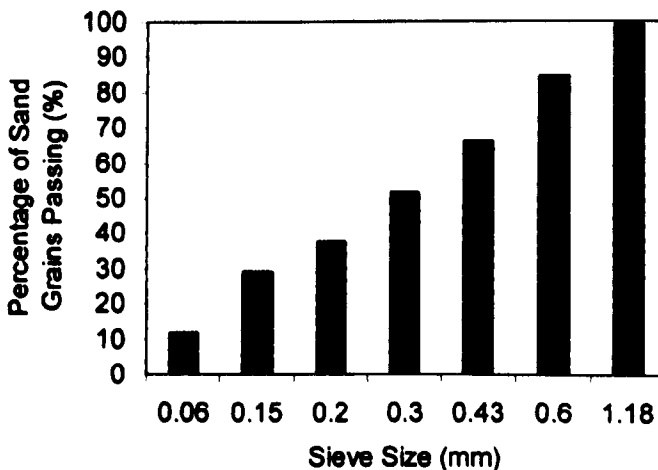

Figure 4.1 Sand grain distribution for every percentage retained.

4.3 Test Procedure

The tests were run on the twin disc machine described in section 3.2.1. The tests were carried out using the wheel disc as the driving disc and the rail disc as the braking disc, as shown in Figure 4.2. An environment chamber enclosed the discs. The inlet at the top was used to drip in the water and oil. A nominal disc rotational velocity of 400 rpm was used and a contact pressure of 1500MPa. The tests were carried out at slips of 0.5%, 1%, 2%, 3% and 5% representing values typical of tread and flange contacts.
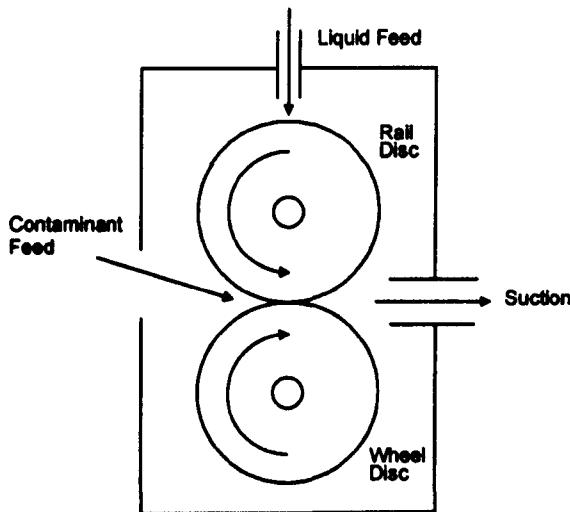
Figure 4.2 Schematic diagram of the disc environment chamber

Tests were initially run dry with no contamination and then with:

- water at two drops per second (enough to keep the discs completely wetted)
- oil at two drops per second
- leaves (dry and with water)
- leaves and sand

For tests with water and oil the supply of liquid was started prior to loading the discs together so the whole test was run lubricated. Water and oil were applied at two drops per second. For tests with leaves, the discs were run dry or wet until the friction stabilised and then the leaves were added suction was applied to draw the leaves through the contact and prevent then clogging the environment chamber. The sanding tests were run in a similar manner, except that after a certain period crushed sand was added with the leaves. This was not in a way representative of that which occurs in reality, where

sand is mixed with compressed air and project towards the wheel/rail contact via a nozzle placed a few centimetres away. Sand was applied at a rate of 7 g/s, most of which entered the contact.

Chutes were added to the test set-up to allow the leaves and sand to be added, as shown in Figure 4.3. Leaves were fed down the chute at a rate sufficient to ensure a continuous supply to the contact.
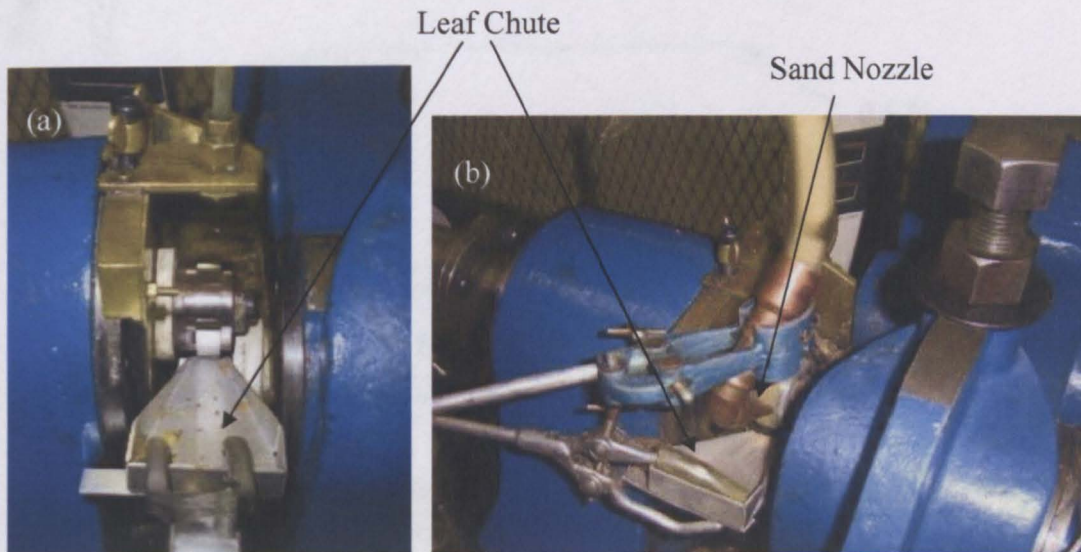
Leaf Chute

Sand Nozzle

(a)

(b)

Figure 4.3 Feeding arrangement for (a) leaves and (b) leaves and sand.

4.4 Results

4.4.1 Friction Data

Figures 4.4, 4.6 and 4.8 show examples of the data collected during the testing. Traction coefficient against time is displayed. Traction coefficient increases as slip increases. In wet conditions a sharp increase was observed between 1 and 2%. Tests run dry and wet actually showed a slight decrease in friction at higher slip values. In oil conditions a sharp increase was also seen between 0.5 and 1% and then a slower rise up to 5%. This was a typical of the behaviour seen with other contaminants. In the Figure 4.6 the data for 0.5% slip looks smooth, it is due to during the traction coefficient recorded at a lower rate than the other tests by accident.

Roughness post test was Ra 2.43 µm for the wheel disc and Ra 1.65 µm the rail disc on average for dry conditions. Figure 4.5 shows the characteristics of the discs post test.
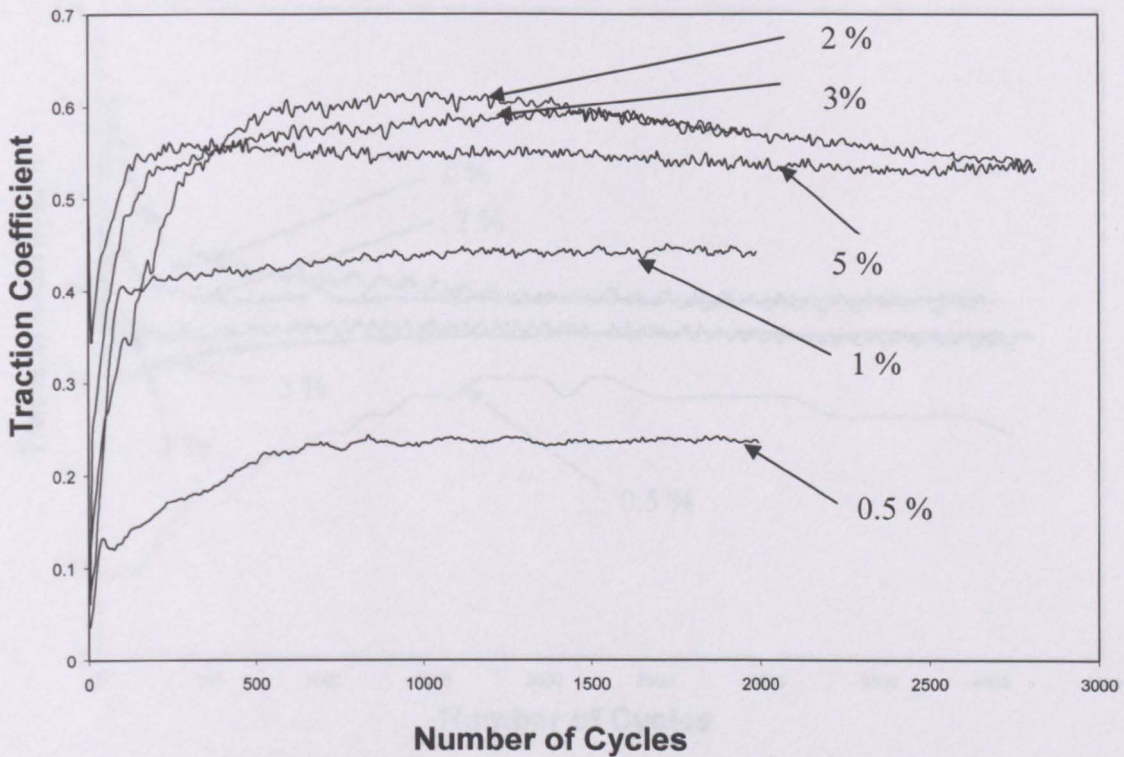
Figure 4.4 Traction coefficient against number of cycles for different values of slip in dry conditions.

(a) Wheel disc   **(b) Rail disc**

Figure 4.5 Rail and wheel discs after dry test.

Post test, the roughness was measured as Ra 0.89 μm for the wheel and Ra 1.15 μm for the rail on average with wet conditions and Figure 4.7 shows the characteristics of discs after they had been tested.
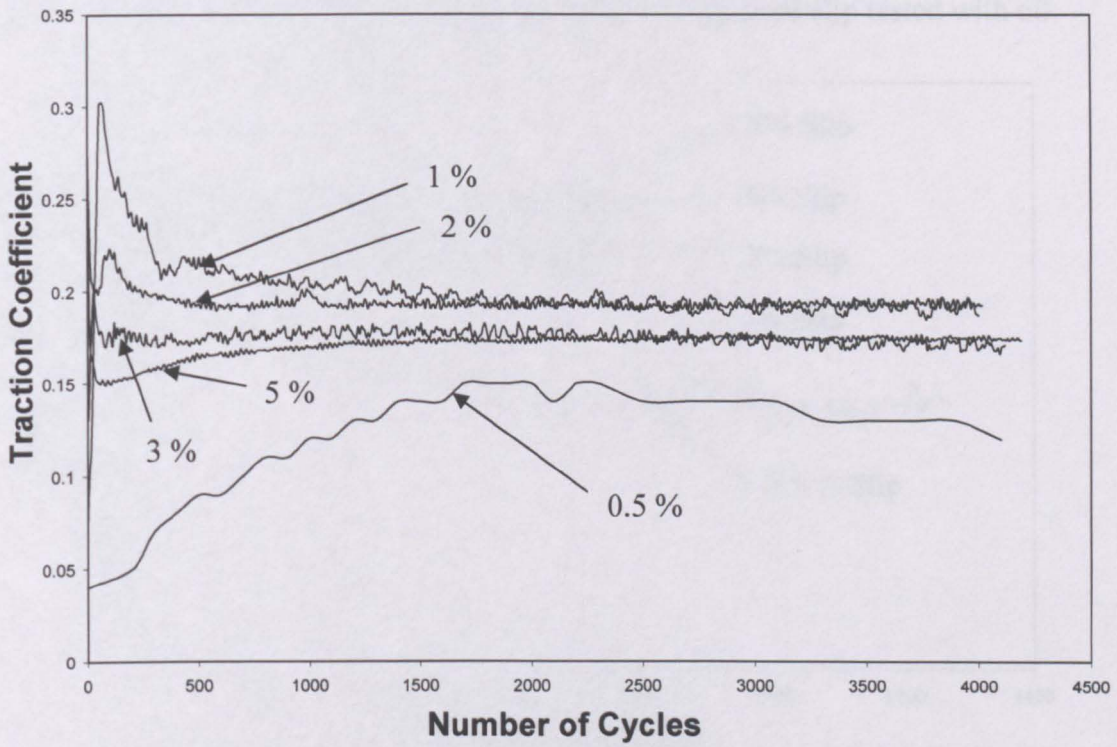
Figure 4.6 Traction coefficient progression in wet tests for different values of slip.

(a) Wheel disc   (b) Rail disc

Figure 4.7 Wet test discs after test.

Traction data is shown in Figure 4.8 for the different values of slip tested with oil.
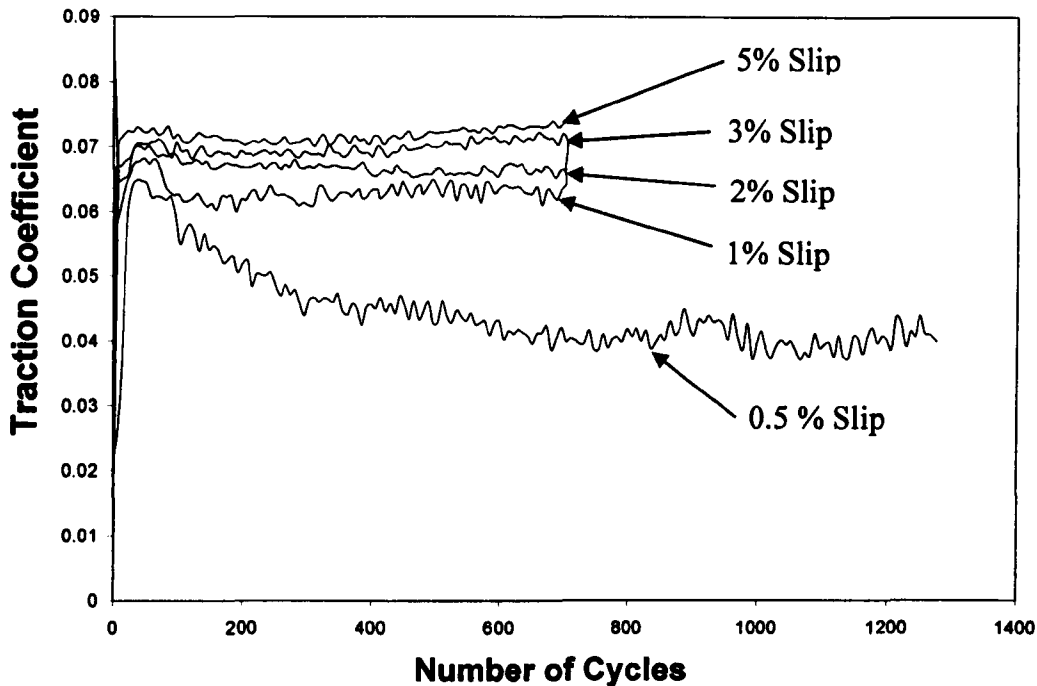
Figure 4.8 Traction coefficient against number of cycles for different values of slip with oil.

Figures 4.9 to 4.13 shown the data generated from the dry leaf tests carried out. They are plotted individually so it is easier to observe the behaviour of the friction for every value of slip after leaves have been added.

Note: As can be seen some graphs are smooth (Figure 4.6, 0.5% slip, Figure 4.11 and Figure 4.12). It is because during the tests was not selected high rate acquisition data at 60 values per minute. However, data was collected manually directly from the screen and lower rate acquisition data was also used.
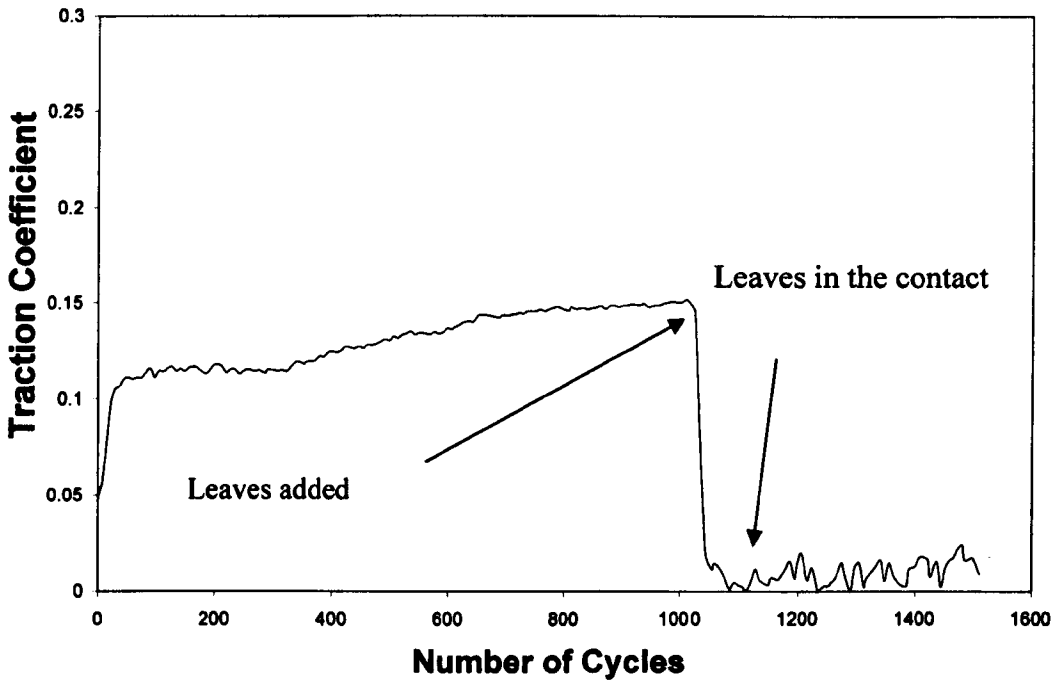
Figure 4.9 Traction coefficient against number of cycles for dry leaf tests at 0.5% slip.
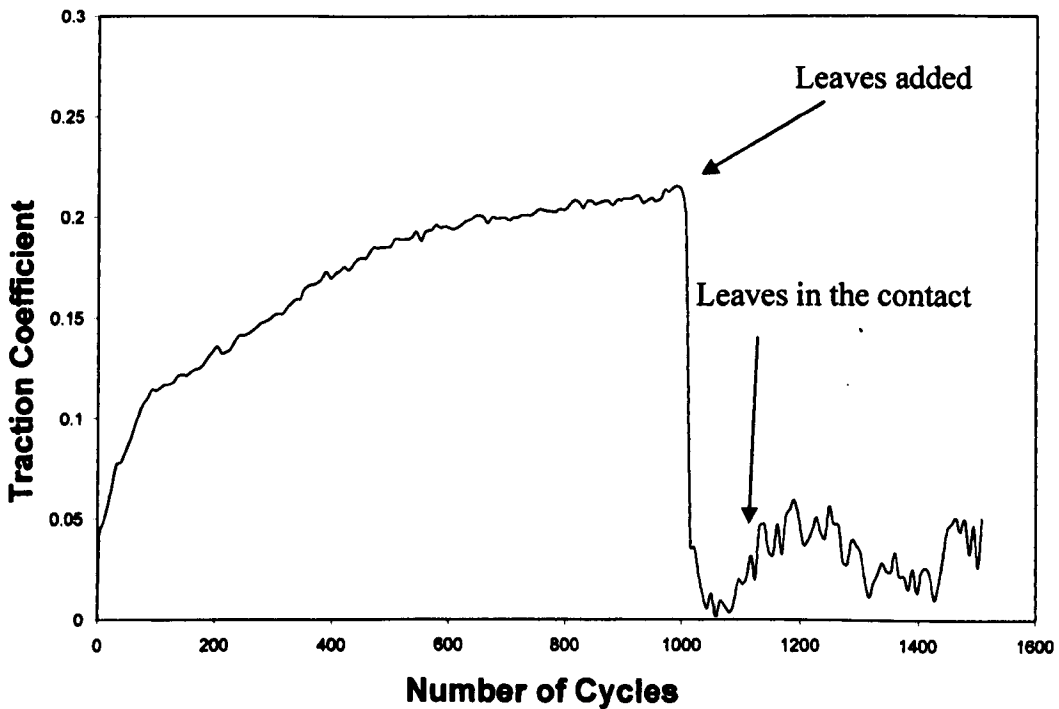

Figure 4.10 Traction coefficient against number of cycles for dry leaf tests at 1% slip.
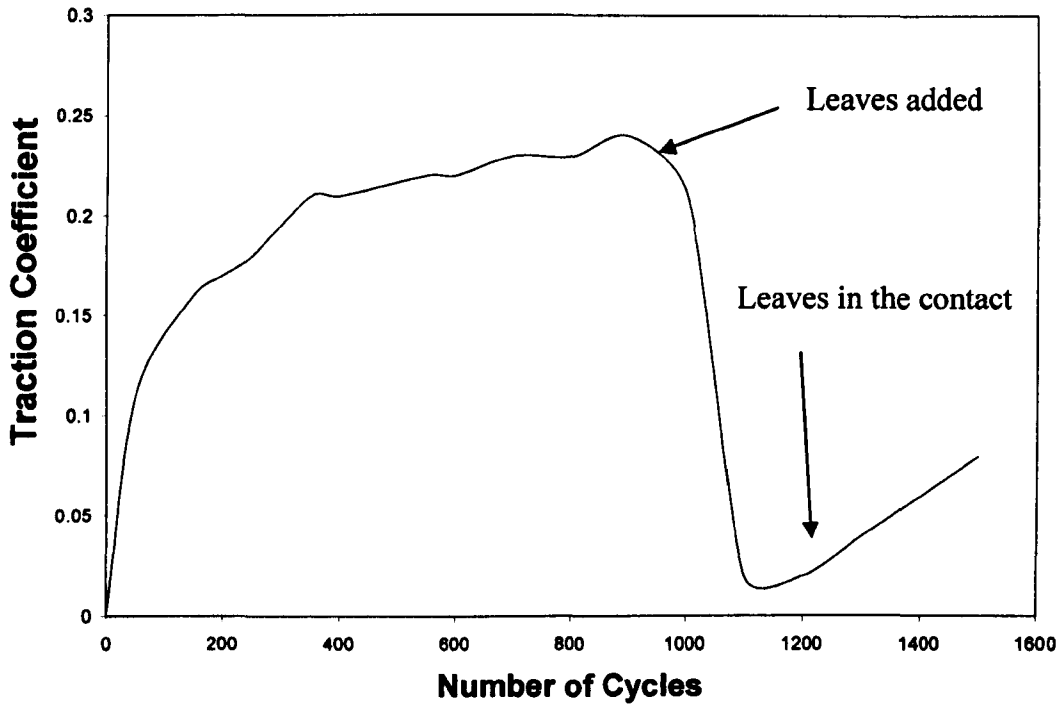
Figure 4.11 Traction coefficient against number of cycles for dry leaf tests at 2% slip.
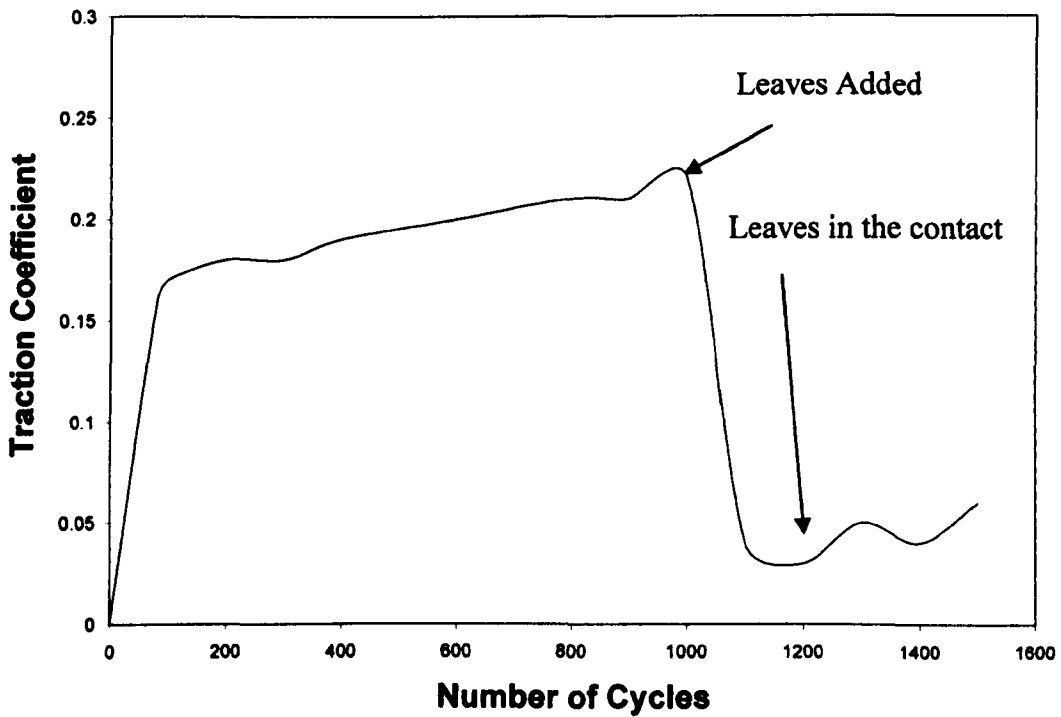

Figure 4.12 Traction coefficient against number of cycles for wet leaf tests at 3% slip.
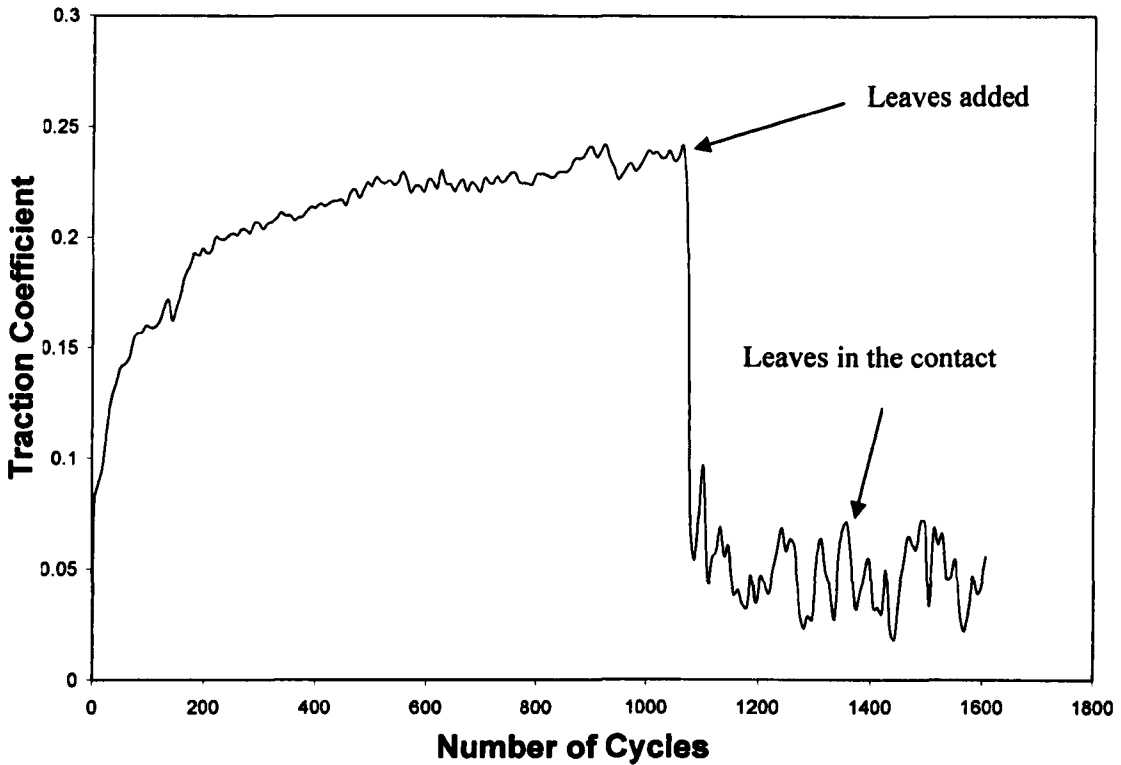
Figure 4.13 Traction coefficient against number of cycles for dry leaf tests at 5% slip.

During wet leaf tests they were fed down the chute at a rate sufficient to ensure a continuous supply to the contact and water was applied at 2 drips per seconds. Traction coefficient data are presented in Figures 4.14 to 4.18. The plots show the traction coefficient before and after leaves have been applied. In the figures is possible to observe when leaves were applied as the friction coefficient dropped dramatically.
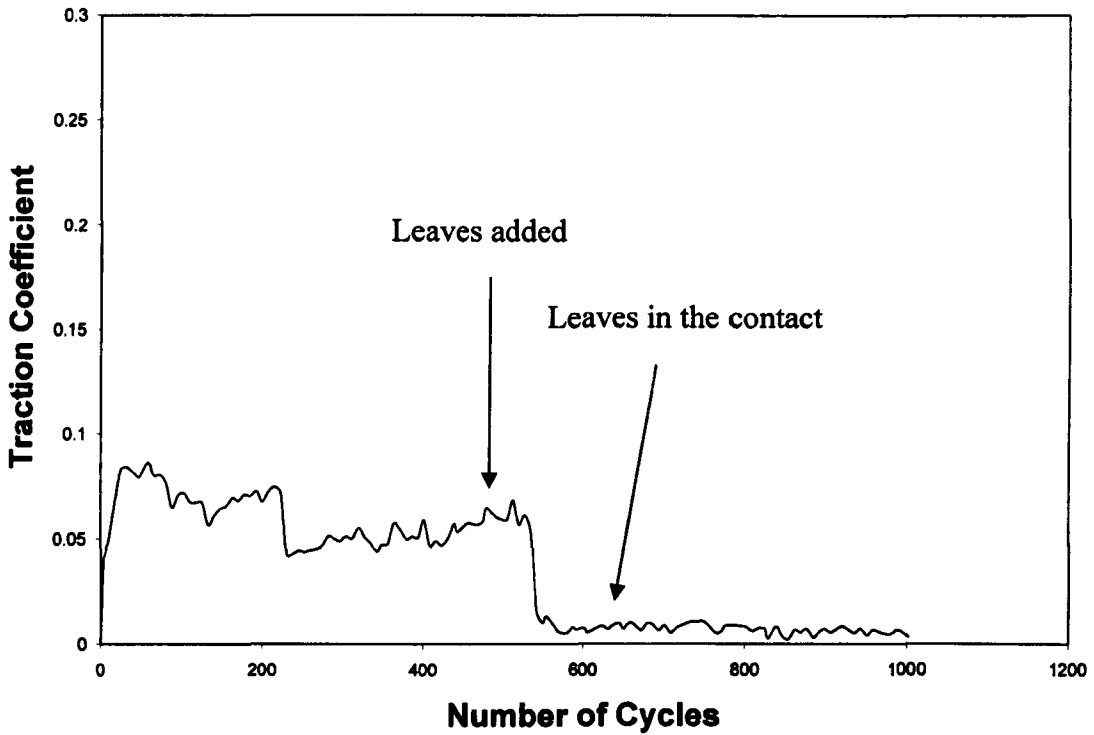
Figure 4.14 Traction Coefficient against number of cycles for wet leaf tests at 0.5% slip.
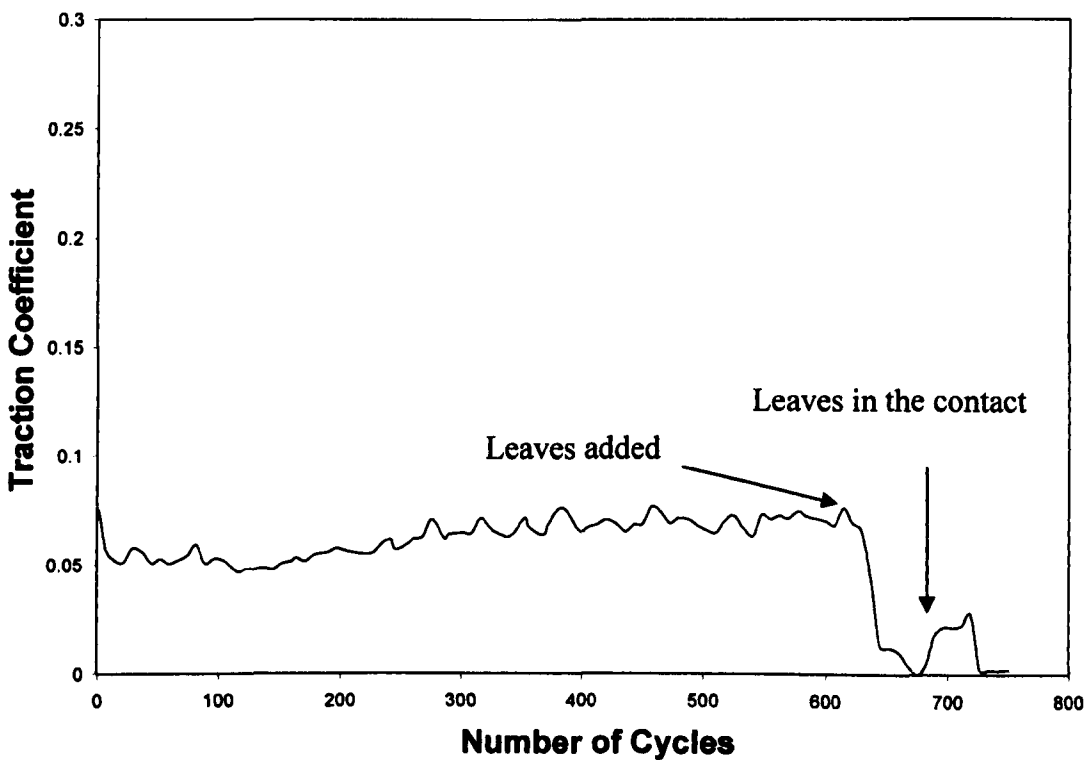

Figure 4.15 Traction coefficient against number of cycles for wet leaf tests at 1% slip.
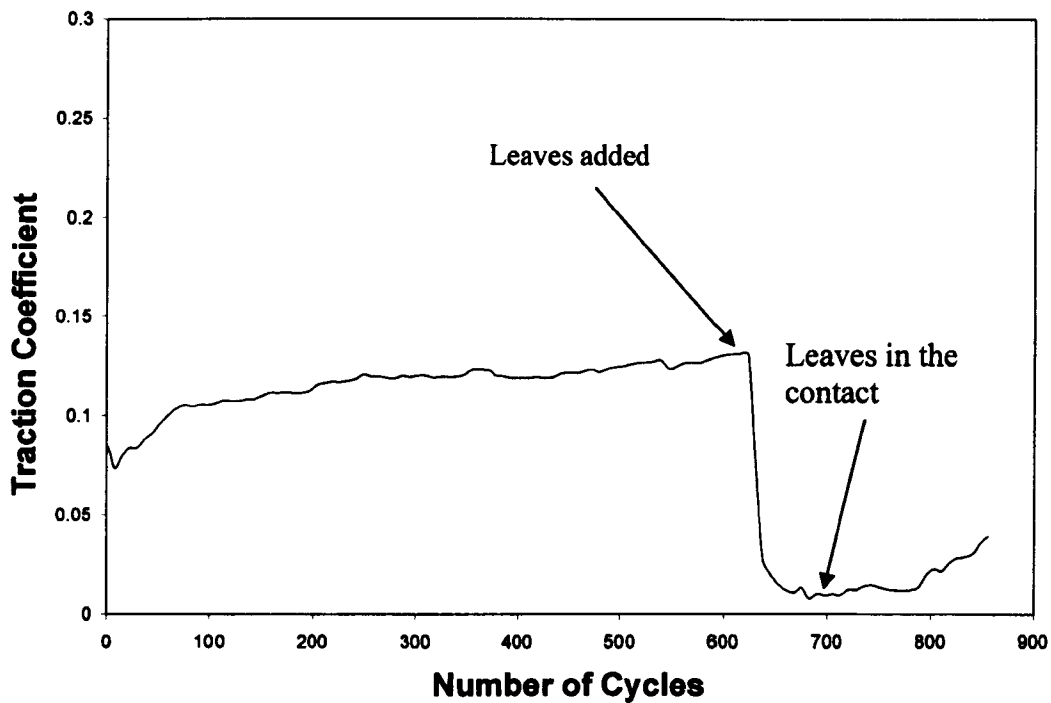
Figure 4.16 Traction coefficient against Number of Cycles for Wet Leaf Tests at 2% Slip.
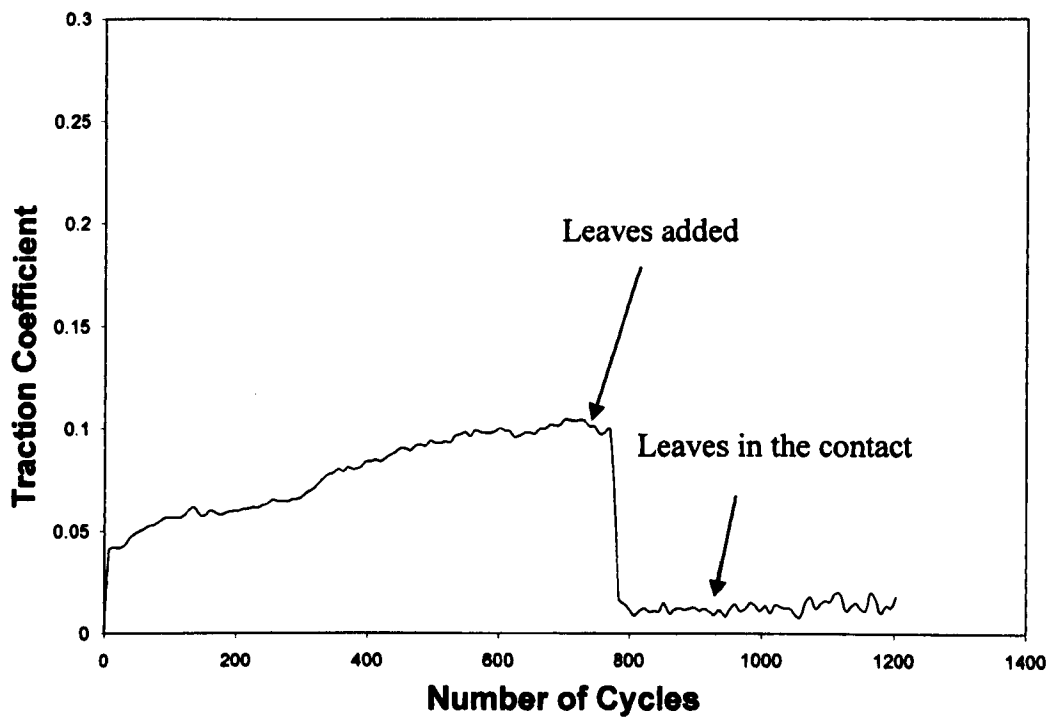

Figure 4.17 Friction coefficient against number of cycles for wet leaf tests at 3% slip.
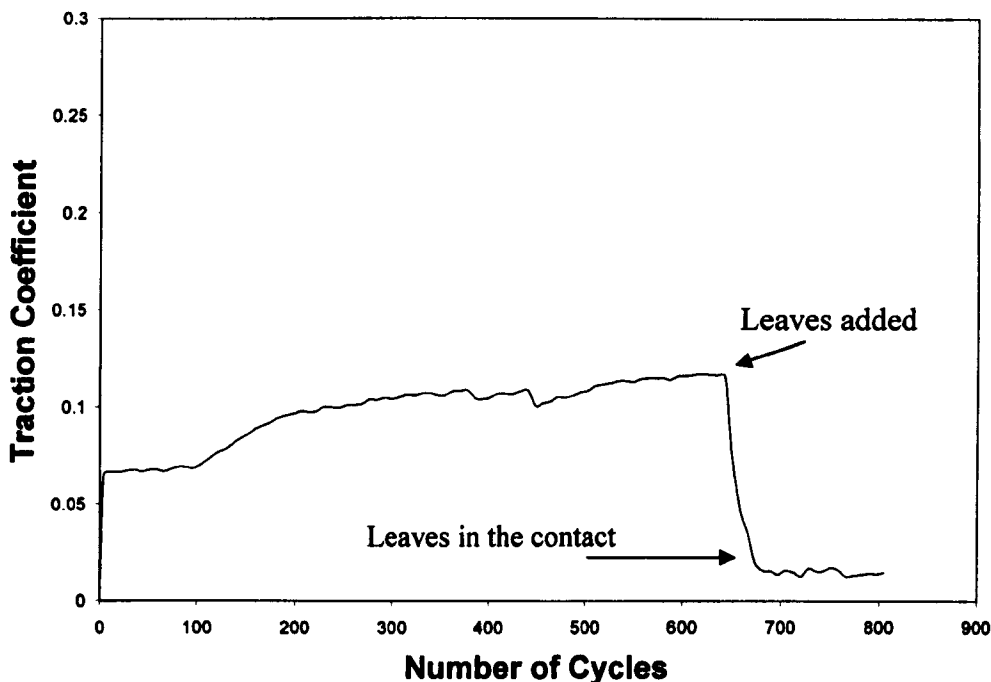
Figure 4.18 Traction coefficient against number of cycles for wet leaf tests at 5% slip.

Figures 4.19 and 4.20 show the traction coefficient when leaves and sand were added. In some cases the traction coefficients have reached the values obtained without leaves and sand only with water. The sand was put throughout after leaves were applied, which was about 400 cycles later.
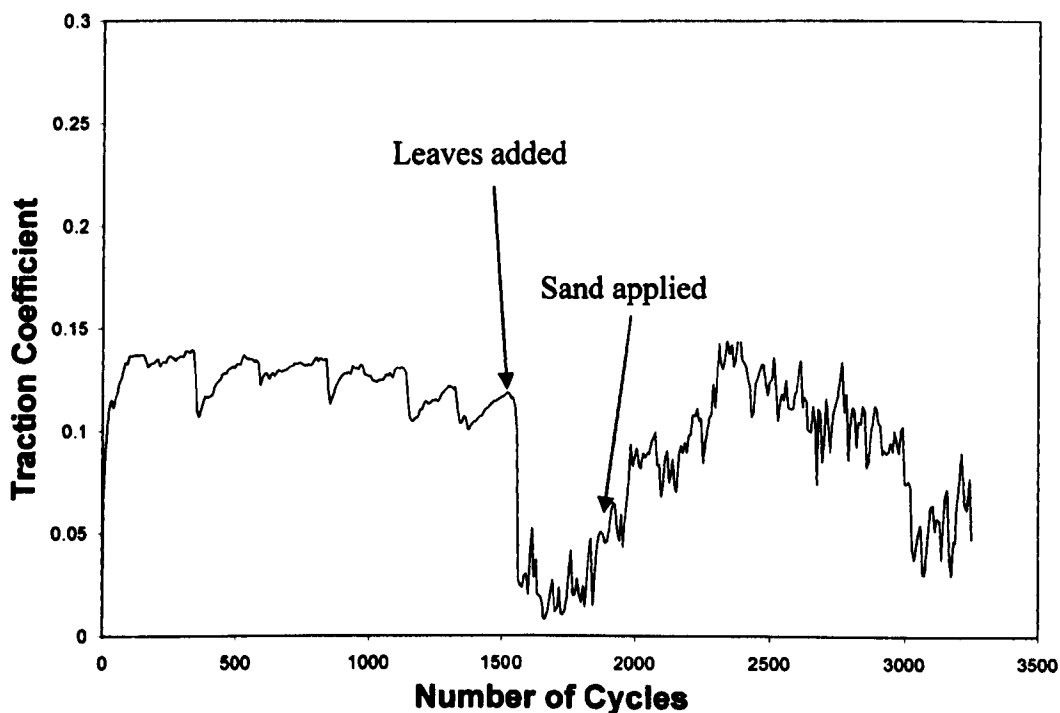

Figure 4.19 Traction Coefficient against Number of Cycles for a Test run with Leaves, Sand and Water at 1% slip.
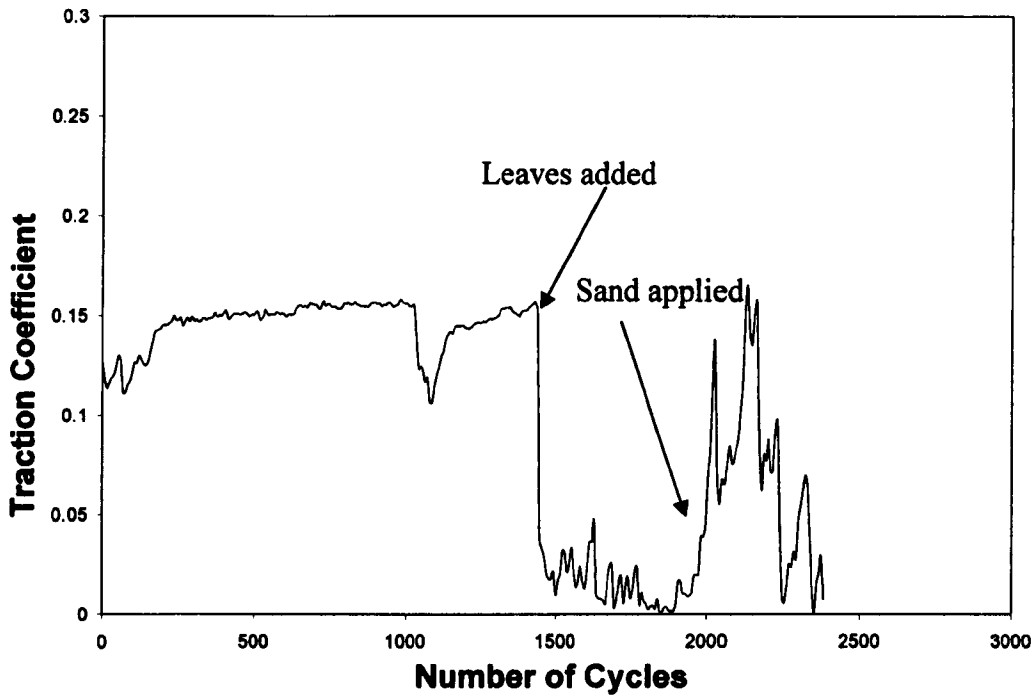
Figure 4.20 Friction Coefficient against number of cycles for a test run with leaves, sand and water at 2 % slip.

For each slip value for all the tests, an average traction coefficient was determined for the established region. These were then compiled to create creep curves for the different conditions, as shown in Figure 4.21. It is clear from these results that leaves are a very good lubricant. They give lower friction than oil, even when dry.

Figure 4.21 Creep curves for the various test conditions.

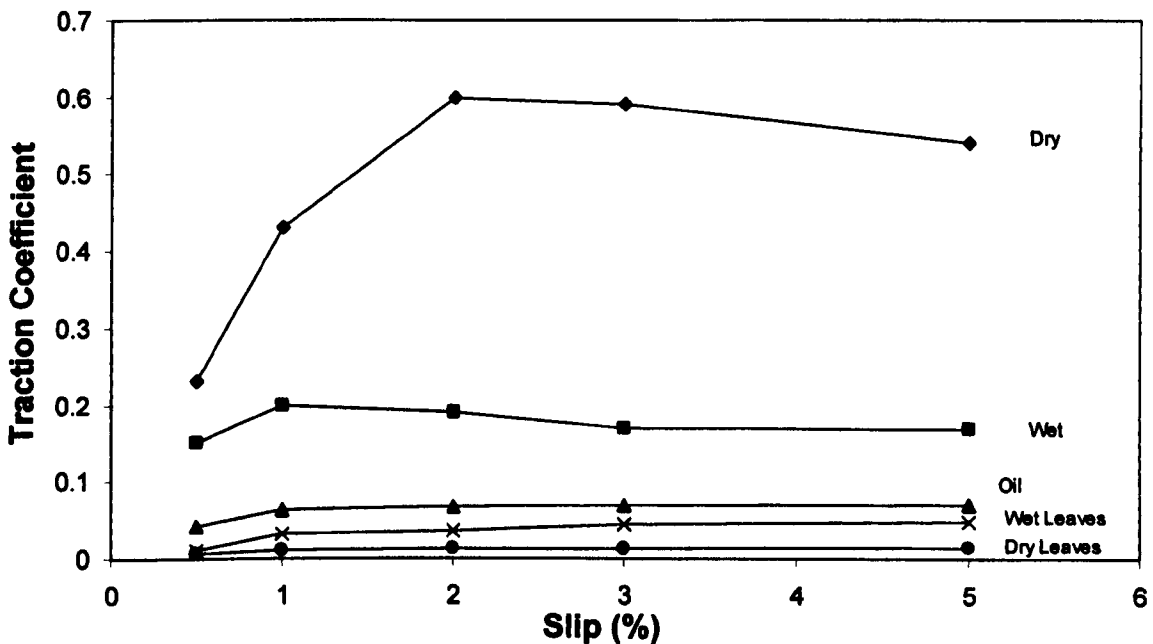The oil used during the tests was SAE 10W40 engine oil. A different grade of oil will offer a different traction coefficient. The viscosity of oil is important because it is directly related to its load-carrying capabilities. The greater a viscosity of the fluid, the greater the load it can withstand. The viscosity of a fluid must be adequate to separate moving parts and offer low traction coefficient under normal operating conditions (temperature and speed).

4.4.2 Leaf Layers

During the dry tests, a thick hard layer of compressed leaf material formed on the disc surfaces at every slip value, as shown in Figure 4.22a. The hardness of the layer was measured using a micro-hardness tester. Different zones in the layer had different hardness depending on the level of compaction that had occurred. Average hardness in the more compacted areas was 40 HV_{1gr}, while the average value in other zones was 14 HV_{1gr}. During wet leaf tests a soft dark layer was apparent on the disc surfaces immediately after the tests, as shown in Figure 4.22b. This was relatively easy to remove, but underneath was a much harder compacted layer that was extremely difficult to remove (see Figure 4.22c). Micro-hardness tests on this layer gave values of 59 HV_{1gr}. The hardness was also taken for the steel where the layer was presented, being 295 HV_{10kg}.

Figure 4.22 Leaf layers after (a) a dry test and (b) a wet test and (c) the hard layer left after a wet test.

Figure 4.23 shows the indentations produced during the hardness test on the leaf layer. Some times during the hardness testing cracks appeared. It is because the layer areas are fragile. When the load was applied, cracking was generated in the axial direction.
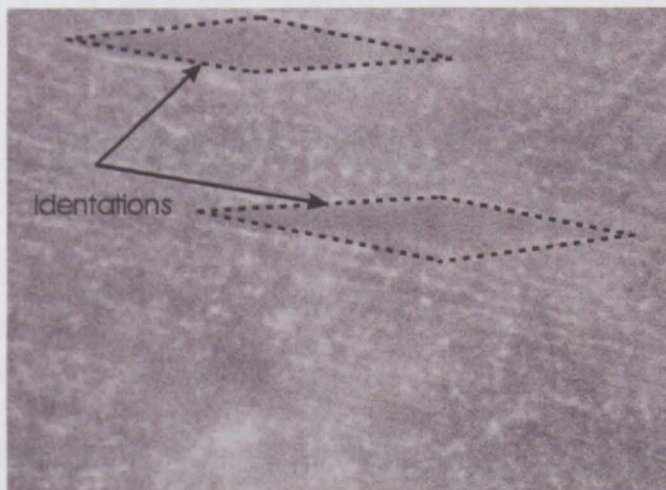

Figure 4.23 Indentation on leaf layers.

After the dry tests, separate tests at different slip values were run to see how long it would take to remove the layers. The number of cycles to remove the layers can be seen in Figure 4.24. As would be expected the number of cycles reduced with the amount of sliding in the contact, but the values shown represent many wheel passes.
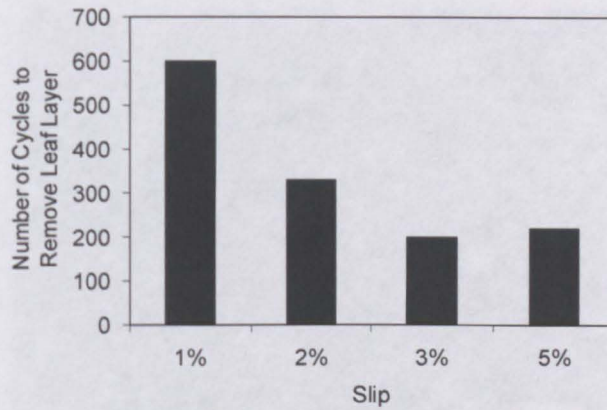
Figure 4.24 Number of cycles to remove hard leaf layer at different slip values.

4.4.3 Surface Morphology

After the tests the disc surfaces were examined using optical microscopy and roughness measurements were taken. The disc surfaces after the oil tests were smoother than they had been before the test (the wheel and rail discs Ra values of 0.57 µm and 0.65 µm post test, compared with 1µm before) and exhibited characteristics of mild lubricated wear (see Figure 4.25).

The discs surfaces showed relatively high damage after the tests carried out with dry leaves. Some deep indents and scratches could be seen (see Figure 4.26). These were probably due to stalks being entrained into the contact. The wheel and rail discs had Ra values of 3.94 µm and 1.3 µm respectively.

Figure 4.25 (a) Rail and (b) Wheel Surfaces after Oil Tests.

Figure 4.26 Wheel disc surface damage due to the interaction with dry leaves.

Severe surface damage was seen in the discs after sand application, as shown in Figure 4.27. Deep indentations were visible on the wheel disc surface and indentations and some scratches were seen on the rail disc surfaces. This is in line with observations made after previous sand testing (Lewis et al., 2004). The sand particles had indented into the softer wheel material and then abraded the harder rail material and it was clear something similar had occurred in this work. Post test Ra values for the wheel and rail discs were 13.9 μm 5.54 μm respectively.

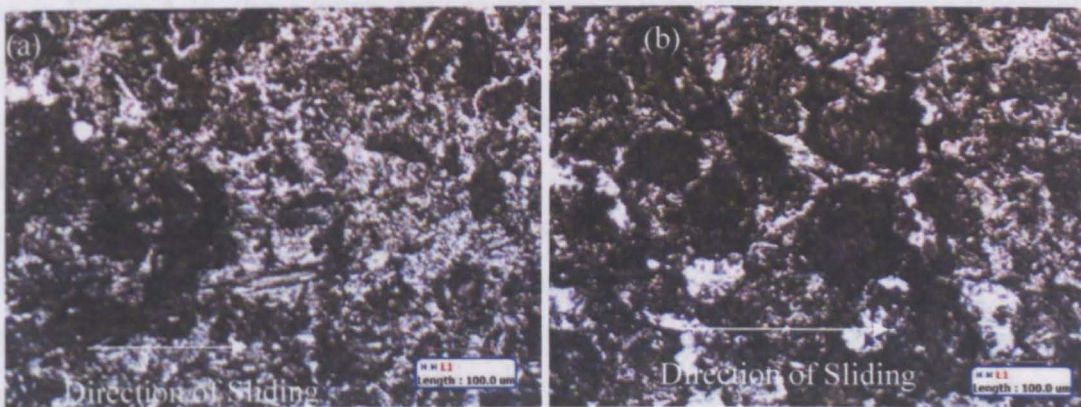
Figure 4.27 (a) Rail and (b) Wheel disc surface features after leaves, water and sand were applied.

4.5 Comparison with other Data

The twin disc test approach has been used to produce creep curves for a number of different contact conditions. This method, while not having the scale or geometry of the actual contact, provides a good simulation of the rolling-sliding motion and allows close

control of operating parameters not available in more complex test methods.

The data shown in Table 4.1 was collected from the literature and was determined using a variety of full-scale techniques using a bogie on a roller-rig, a rail tribometer and an instrumented train. The roller-rig tests were carried out under closely controlled conditions so load, velocity and slip are known. It was shown in this work, as mentioned previously, that varying load and rolling speed affects friction. This is something that needs exploring further with the twin disc technique. Clearly in the actual track testing a range of loading and slip conditions will have occurred.

The shape of the creep curves derived from the roller-rig tests is similar to those seen in this work. This is significant as the initial slope of the curve is important and this as well as the initial peak and then slight decline seen with some conditions differs from results achieved using analytical modelling techniques (as noted previously (Bucher et al., 2006).

The techniques used to apply contaminants worked well. The data recorded for leaves further indicates what a good lubricant they are, even in dry conditions. The test method allows for testing of potential friction modifiers to increase adhesion when leaves are present as seen with the sand tests. An added benefit was the generation of a relatively hard leaf layer on the discs, which has not been achieved experimentally before. As was seen in Figure 4.35, these layers took some time to wear away. If one cycle represents a wheel pass then it would be sometime in the real situation before the layer is removed by wear alone and this does not allow for further leaves falling. This may allow testing of leaf removal solutions.

As shown in Table 1, the twin disc results with leaves are similar to those seen with an instrumented train run over leaves. In that work (Nagase K., 1989), different leaves gave different results, with oily needle leaves from pine trees giving the highest friction. The leaves in this work were mixed, so further work may be appropriate to identify which leaves may be worst.

It was interesting to note that even leaves can cause damage to the disc surfaces. It was expected that sand would, and this could potentially be an issue if sand is applied regularly to a stretch of track that suffers from poor adhesion.

Table 4.1 Data collected from the literature and determined using variety techniques.

Author	Test Apparatus	Load/Contact Pressure	Rolling Speed (km/h)	Test Conds.	Peak μ	Slip at Peak μ (%)	Stable μ (5% slip)
Zhang et al., 2002	Full-scale roller rig (using an actual bogie)	44 kN	10-70	Dry	0.57-0.5	2	0.57-0.5
		67 kN	10-70	Dry	0.55-0.44	1-2	0.52-0.44
		44 kN	120-240	Wet	0.13-0.07	0.5-1	0.12-0.065
		67 kN	80-240	Wet	0.11-0.05	0.5-1	0.105-0.05
Jin et al., 2004		67 kN	140-300	Oil	0.055-0.045	1	0.052-0.044
		135 kN	140-300	Oil	0.05-0.04	1	0.048-0.037
Harrison et al., 2002	Triborailer (used on actual track)			Dry	0.52	1	0.5
	Push Tribo-meter			Dry	0.7	2-5	0.7
Nagese, 1989	Instrumented bogie on test vehicle (run on test track and actual routes)	Variable	Variable	"Dry"	Range of μ: 0.2-0.4		
				Wet	Range of μ: 0.05-0.2		
				Oil	Range of μ: 0.05-0.07		
				Leaves	Range of μ: 0.025-0.10		
Present study	Twin Disc	1500 MPa/ 7.7kN	3.54	Dry	0.6	2	0.54
			3.54	Wet	0.2	1	0.17
			3.54	Oil	0.07	1	0.06

Chapter 5. **Isolation Test**

5.1 Introduction

This chapter describes the testing carried out to duplicate the conditions where an interfacial solid stick friction modifier HPF has been applied onto the wheel and rail contact for a simulated 8 Hz track circuit, using the twin disc technique described in Chapter 2.

Friction modifiers have been developed to contribute to the wheel (tread and flange) and rail traction control.

Contaminants on the rail tracks such as dust, rust, oil or leaves, and also some substances to improve train operation (Friction modifiers or sand) may cause the contact between the wheel and the track to be compromised, inhibiting train detection. The designed friction modifiers can be used either in liquid or solid form depending on the requirements application. Thus, friction modifiers are used to minimize curve noise, lateral forces, corrugation, and wear (Eadie et al., 2005; Eadie et al., 2006). Friction modifiers form a third body applied to the rail head provides a thin dry film putting in risk the train detection. Trains present on the track section the rails will be short-circuited and the detector will no longer be able to sense the electrical energy from transmitter. It can be seen that any short-circuit, caused by a train or otherwise, or a break in the circuit will fail the tracks circuit and inform the signalling system that the track is occupied, so a good degree of a fail-safe is incorporated. The system, however, relies on good wheel/rail electrical contact to work. Thus, in order to investigate the effect of the friction modifiers on the train detection using the twin disc method, some baseline tests were run at typical loads and slips without and with friction modifiers to then later carry out dynamic tests to measure the contact impedance in presence of HPF. Static tests were also carried out using disc pre-conditioned with a friction modifier film.

5.2 Test Apparatus Set-up

The SUROS Machine was modified to electrically isolate the disc with an 8 kHz circuit. All the data were logged in an acquisition system for monitoring the friction coefficient and track circuit. Figure 5.1 shows the points electrically insolated.
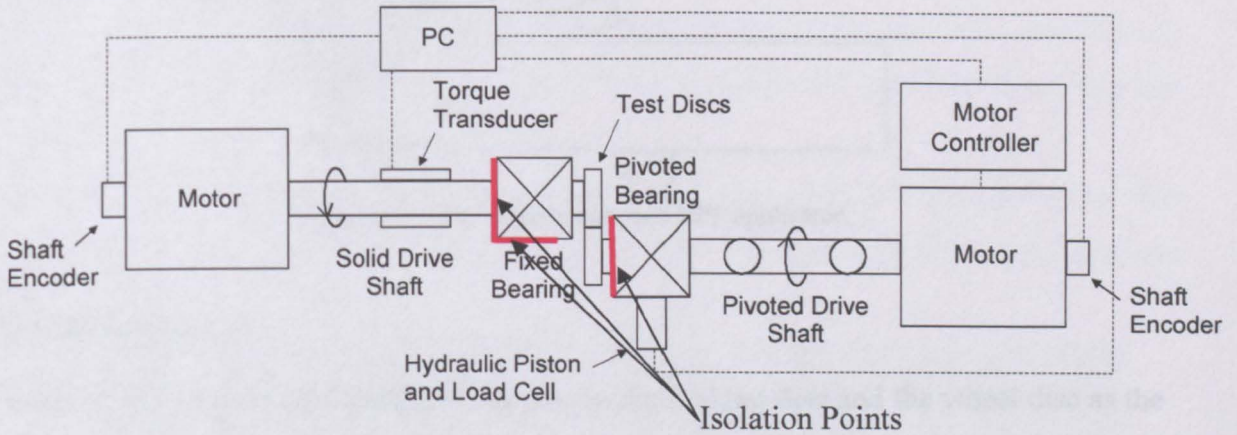

Figure 5.1 Twin disc rig for an isolation test.

In order to duplicate the transfer mechanisms of HPF film on the wheel disc as is found in the field (see Figure 5.2a), an arm applicator was designed to apply the stick (which is 10 mm diameter) as show in Figure 5.2b.
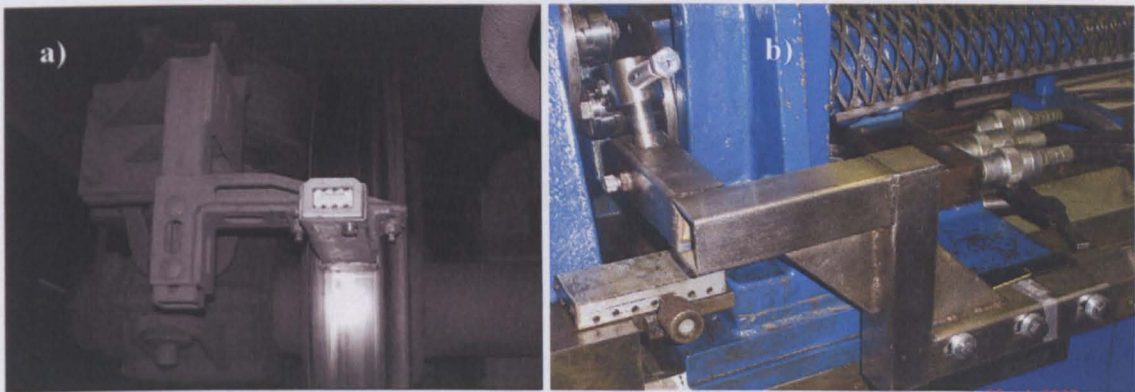

Figure 5.2 a)Friction modifier applicator on field b)Friction modifier arm applicator for the SUROS machine.

The HPF was designed to ensure the whole area of the wheel disc was covered. It was applied under a spring load onto the moving wheel disc. The spring was capable of applying the same pressure as is the field with a 1.01 kPa spring. Figure 5.3 shows a schematic view of how HPF was applied.
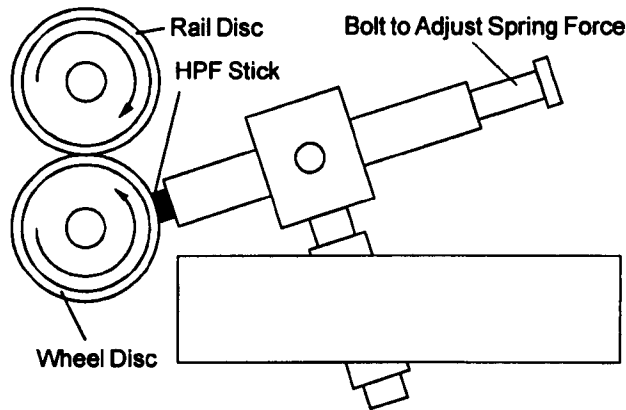
Figure 5.3 Disc arrangement and HPF applicator.

5.3 Test Procedure

The tests were performed using the rail disc as the braking disc and the wheel disc as the driving disc as shown in Figure 5.3. The solid friction modifier was directly applied on the wheel disc (see Figure 5.3). The selected values of slip are those ones corresponding to the track conditions in curves (high creep) and tangent track (low creep).

5.3.1 Outline of the Tests

1. Baseline tests. Test with no HPF and with HPF in order to establish friction reference values for the impedance. The tests were carried out at 0.1%, 1% and 3% slip.

3. Dynamic tests. The objective of these tests was to investigate disc contact impedance under rolling sliding conditions. The slip values used in these tests were 0.1%, 1% and 3% at 900MPa.

2. Static tests. The aim of these tests was to asses the impact of the friction modifier on the disc contact impedance under static conditions. The tests were carried out at 900 MPa contact pressure.

A nominal disc rotational velocity of 400 rpm was used for all tests.

5.4 Test Specimens

For this testing the disc and the solid friction modifiers were supplied by Kelsan Technologies. The wheel and rail were manufactured from actual sections of the wheel and rail sourced from North America.

The traction coefficient was monitored during the course of the interfacial conditioning until once the coefficient of the friction has been observed stable to then stop the machine.

Disc surfaces were examined to ensure that the complete surface was cover by an HPF film. Figure 5.4 shows the discs before and after HPF has been applied to form a uniform film.
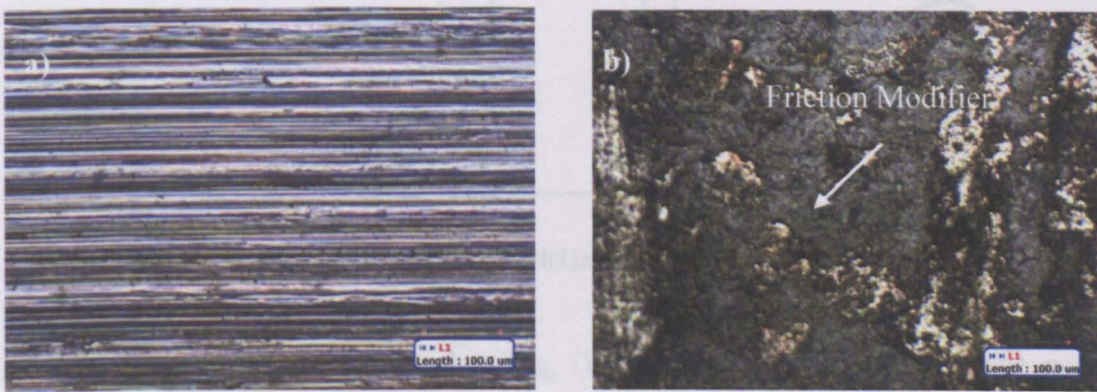

Figure 5.4 a) Wheel and b) rail disc with friction modifier on.

5.5 Track Circuit

A signal generator was used to provide an 8 kHz signal; a power amplifier was used to boost the signal current to 1 amp. The circuit design was modified based on recommendations provided by MTRC (Mass Transit Railway Corporation in Hong Kong) and is shown in the Figure 5.5. The primary change was to reduce the first resistor in series to 1 ohm to better reflect the transmitter impedance of MTRC's audio frequency track circuits.

Figure 5.5 8KHz track circuit.

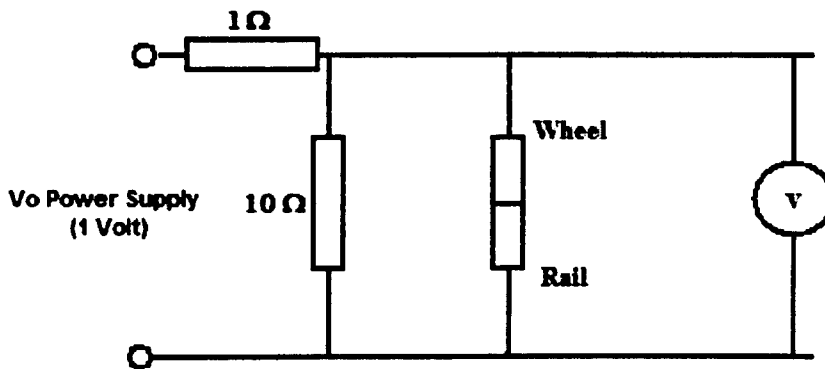Data acquisition system was used to log, i) input voltage, ii) (rms) voltage potential across the isolate wheel/rail discs and iii) (rms) current. Data was logged every tenth of a second. The measured impedance of the circuit when the wheel-rail discs were not in contact was approximately 9000 milli-Ω. Circuit impedance measurements were taken continuously during wheel/rail disc rolling contact.

5.6 Traction Coefficient Data Results

5.6.1 Baseline tests

Initial baseline tests are shown in Figure 5.6 for dry conditions to establish reference values of impedance testing. It can be observed that the traction coefficient is 0.07, 0.4 and 0.6 for 0.1%, 1% and 3% respectively.
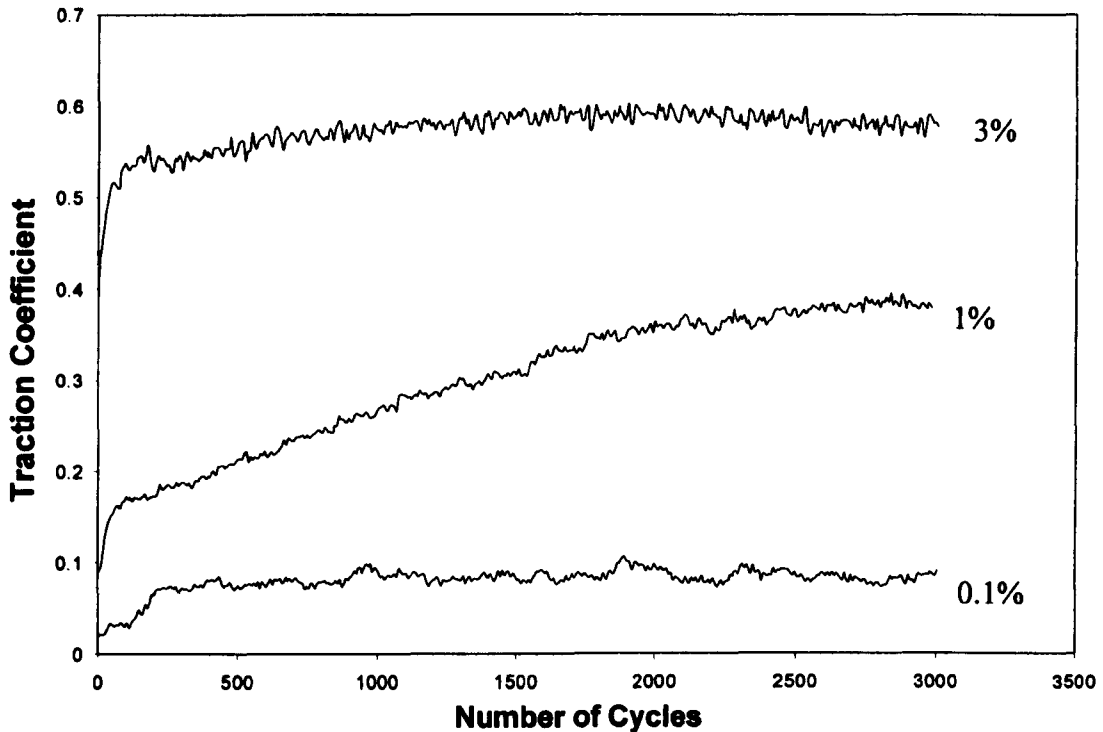

Figure 5.6 Baseline traction values for dry conditions at 900 and 400 rpm speed.

In Figure 5.7 data from a test with 3% slip is shown. The dry value can be seen, as well as the moment when the friction was applied. With HPF, traction coefficient dropped to approximately 0.28. During the impedance measurement tests the discs were run dry to condition the surface, until seen the baseline friction values to then afterwards HPF was applied. Impedance values were recorded throughout the test. The tests were repeated three times. Figure 5.8 shows traction coefficient data for all slip values without and with HPF and the moment when HPF has been applied. For 0.1% slip, there was no change in traction coefficient with HPF application. This was due to the almost pure rolling conditions.
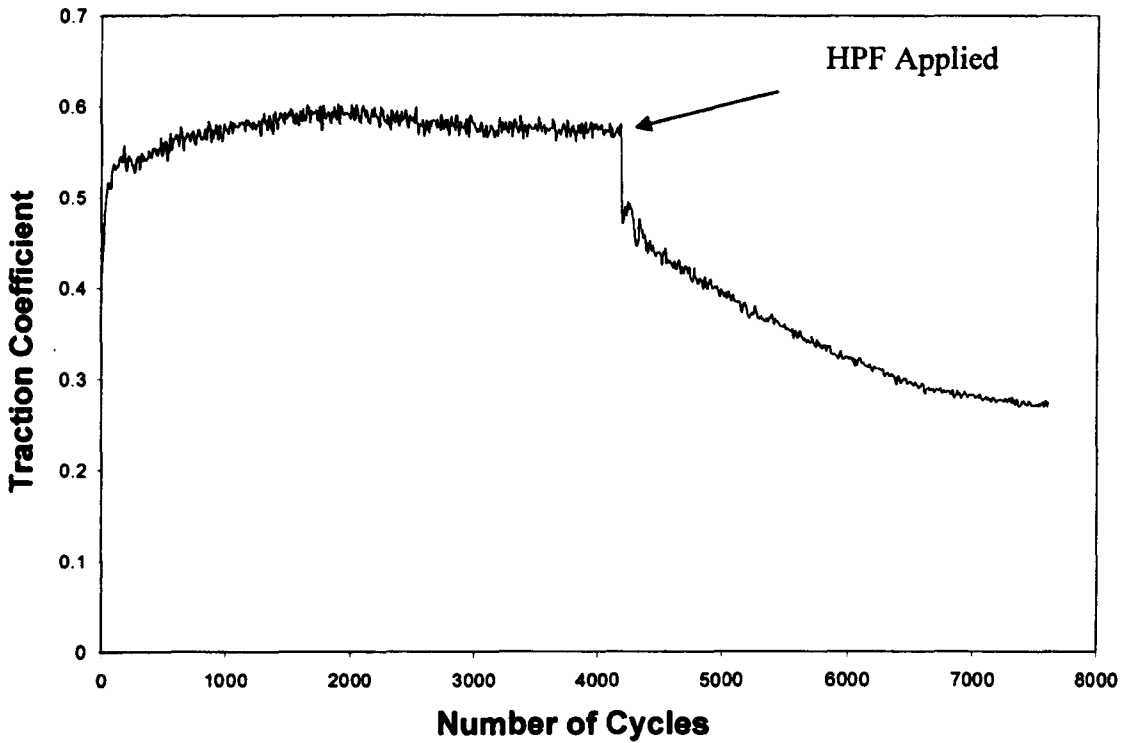
Figure 5.7 Baseline traction values for HPF application at 3% slip and 900MPa.
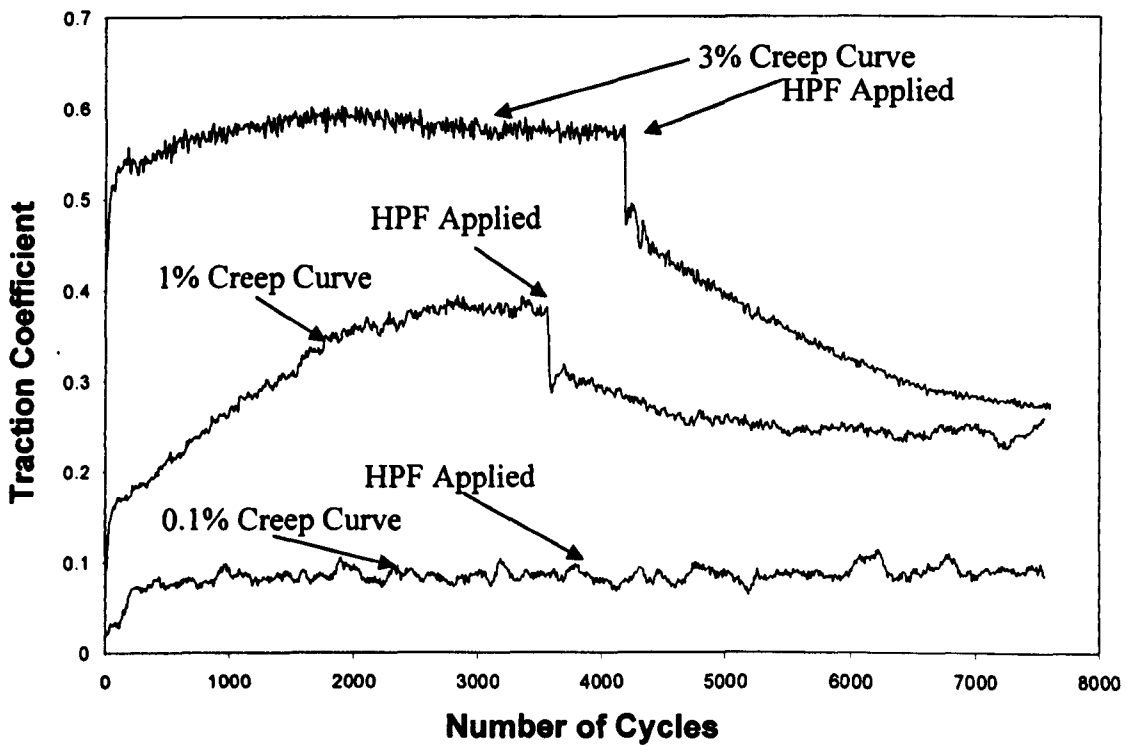
Figure 5.8 Traction coefficients versus number of cycles for 0.1, 1 and 3%.

5.6.2 Dynamic Test

The methodology used had some limitations due to the fact slip at 0.1% test conditions it was impossible to monitor the change in coefficient of traction under almost pure rolling conditions. For these tests the no HPF and HPF applied section were segregated by time rather than traction coefficient (as shown in Figure 5.9, 5.10 and 5.11). For 0.1%, 1% and 3% tests, data was segregated using the change in traction coefficient seen on HPF application.
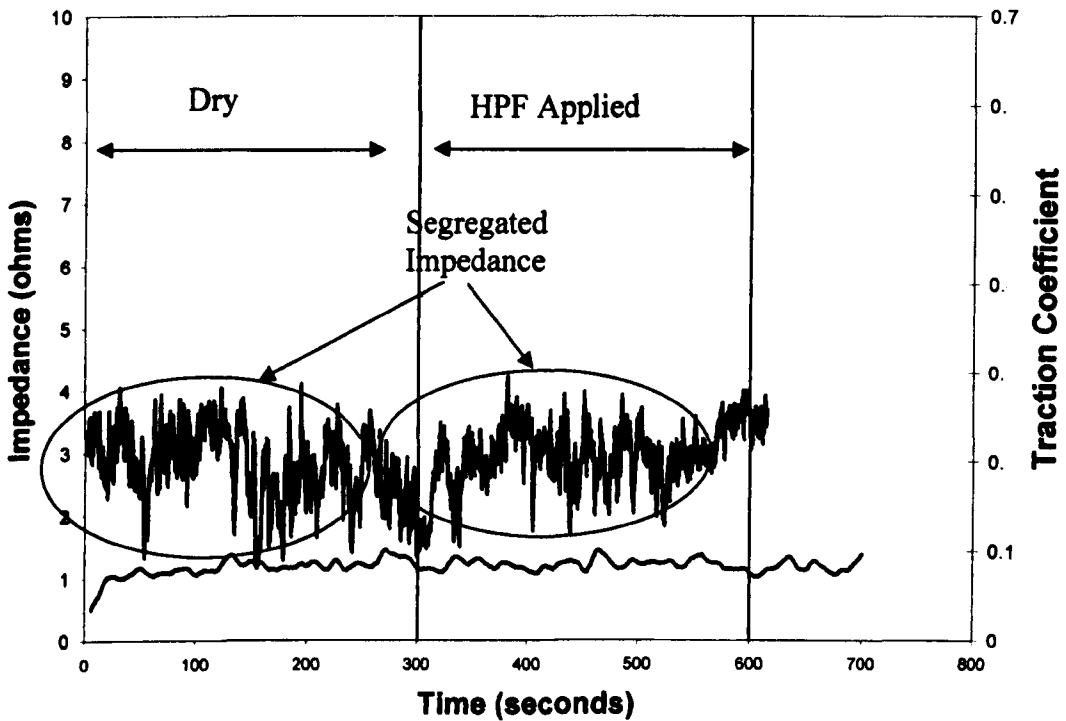
Figure 5.9 Impedance segregation for 0.1% slip.
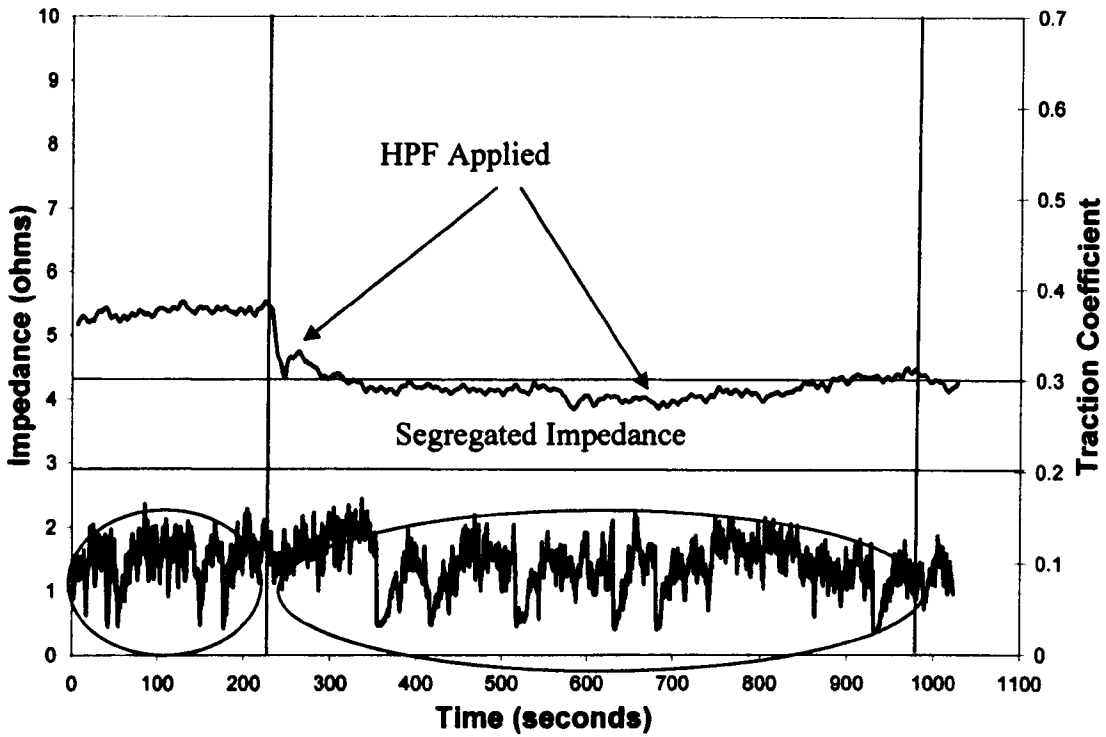
Figure 5.10 Impedance segregation for 1% slip.
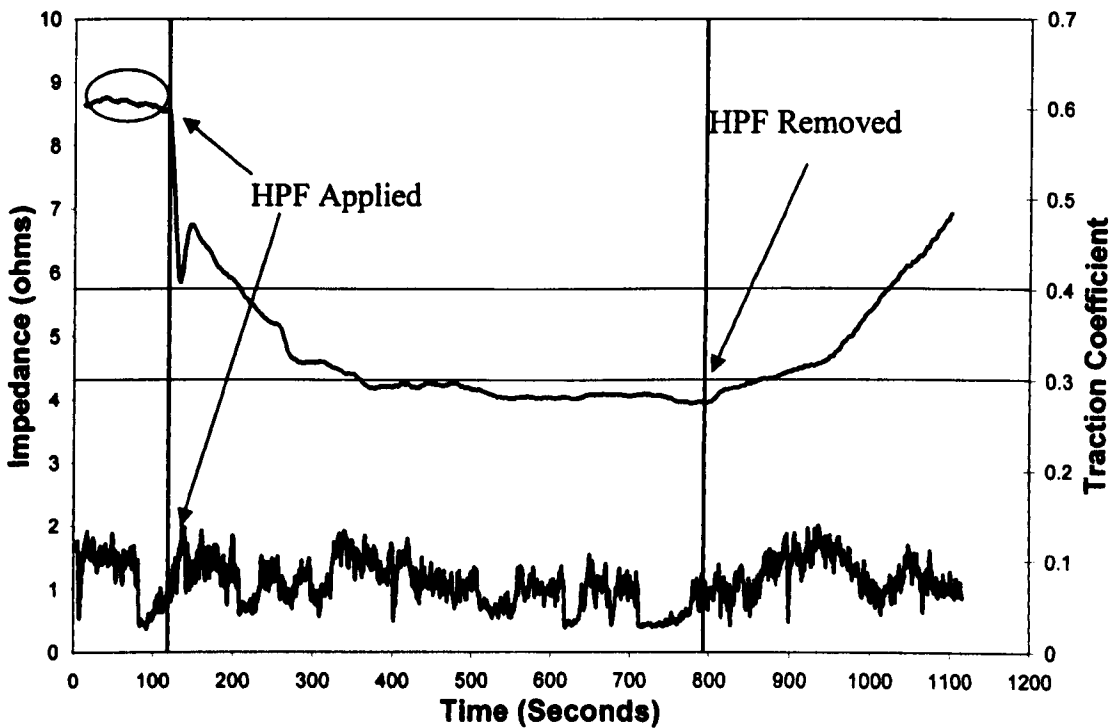
Figure 5.11 Impedance segregation for 3% slip.

5.6.3 Static Tests

The static circuit impedance measurements were taken around the circumference of the wheel/rail discs. Apart from slightly higher measured impedance values for the dry conditions, probably due to the presence of debris, the measured impedance values (HPF and Dry) appear to be similar. Under these test conditions, the introduction of HPF friction modifier technology does not appear to have resulted in an increase in impedance for the 8 kHz circuit. Figure 5.12 shows the results from the six contact points.

Figure 5.12 Measured static impedance values for dry and HPF conditions wheel/rail disc.

Chapter 6. Effect of the Water and Oil on Friction

6.1 Introduction

This chapter is focused on the effect of water/oil oil/water mixtures on adhesion. Oil has been found on tracks in small amounts however this can led to a significant reduction in adhesion levels. Oil from the rail head can be easily spread to the by the passage of trains forming a very thin layer over the continue rail head. Previous work has shown that the presence of wear debris at the interface can result in very low adhesion conditions while drying in the presence of water. Water jetting systems are used on the UK network to remove autumn contamination and anecdotal evidence suggests that low adhesion, greater than expected from the presence of water alone, can be experienced immediately after the passage of a treatment train. There has been researched or proved case of this phenomenon (Beagley and Pritchard, 1975), (Beagley et al., 1975), (Chen et al., 2008).

6.2 Test Apparatus

The Rolling Sliding Twin Disc Machine has been used to carry out the testing which has been shown and describe previously in Chapter 3.

The arrangement used to mix water and oil is shown which consists of two funnel glasses connected to a "Y" pipe which is also connected to the inlet disc environment chamber box. The percentages water and oil can be controlled by the funnels valves. The arrangement is shown in the Figure 6.1.
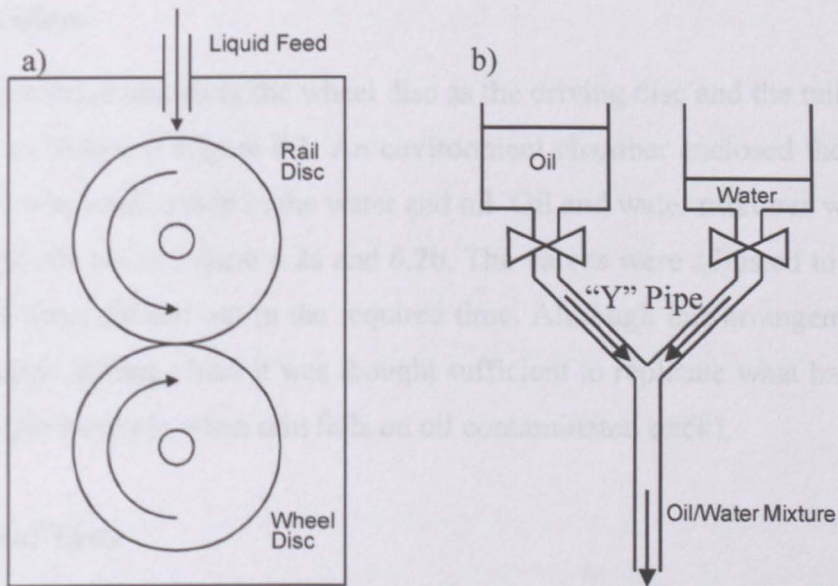
Figure 6.1 a) Disc environment chamber and b) Mixture feed method

6.3 Specimens

The disc specimens were cut from UIC60 900A rail steel and R8T wheel steel sections. They are also described in chapter 3. Wheel and rail disc contact surfaces were ground to a roughness of Ra 1 μm. A textured rail disc (see Figure 6.2) with a roughness of Ra 9.89 μm was produced to investigate the effect of roughness on adhesion.

Figure 6.2 Textured disc (Ra 9.89 μm).

6.4 Test Procedure

The tests were carried out using the wheel disc as the driving disc and the rail disc as the braking disc, as shown in Figure 6.1. An environment chamber enclosed the discs. The inlet at the top was used to drip in the water and oil. Oil and water mixtures were applied using the set-up shown in Figure 6.2a and 6.2b. The valves were adjusted to ensure that all the oil and water flowed out in the required time. Although this arrangement did not provide a through mixing effect it was thought sufficient to replicate what has been seen on actual rail (for example when rain falls on oil contaminated track).

6.4.1 Outline of Tests

The aims of the tests carried out in this chapter are shown listen below:

1. Some baseline adhesion values to compare results from the subsequent tests. Tests were run at 1500 MPa in dry, wet (2 drips/sec) and oily (2 drips/sec) conditions. The slips used for these tests are; 05%, 1%, 2%, 3% and 5%.

2. The aim of these tests was to establish which had the dominant effect (if either), when applied to a rolling/sliding contact. Tests were again carried out at 1500 MPa for slip values of 0.5%, 1%, 2%, 3% and 5%. Mixtures of 50% oil/50% water and 20% oil/80% water were applied.

3. Contact Pressure. The aim of these tests was to investigate the effect of contact pressure on adhesion. Tests were run at 900 MPa in dry, wet (2 drips/sec) and oily (2 drips/sec) conditions.

4. Roughness. The aim of this test was to study how increased roughness affected adhesion. A rail disc was machined, as illustrated in Figure 3, to increase its roughness to Ra 9.89 μm. The test was run at 1500 MPa and 0.1% slip. Oily (2 drips/sec) were used to try and reduce wear and subsequent roughness evolution.

5. Low Oil Test. The aim of this test was to establish if friction was as low with a small amount of oil as it was in the previous tests with the oil reference tests (2 drips/second

applied throughout test). Static and dynamic oil deposition tests were carried out to establish what the minimum amount of oil was that could be deposited (in its raw form). Oil was applied to discs and then left for varying periods of time. Residual amounts were weighed and the coverage calculated. Tests were also carried out while rotating the discs to see how much could be "flung" off. For the actual tests, 5 drops of oil were applied to the top rail disc and left for 5 minutes. The rail disc was then rotated at 400 rpm for 40 seconds before the load was applied and the rolling/sliding test was started. The test was repeated.

6. Low Oil with Water Test. The aim of this test was to see if the addition of water influenced friction. Five drops of oil were applied to the top rail disc and left for 5 minutes. The rail disc was then rotated at 400 rpm for 40 seconds before the rolling/sliding test was started. The discs were run for 1500 cycles before water was added at 2 drips/second. The test was repeated.

7. Drying Test. The aim of this test was to see if a drop in friction was seen as the drying started, as was observed with tests carried out previously (Beagley and Pritchard, 1975). The discs were run dry for approximately 1000 cycles (or until stable friction was reached) before water was added for 1000 cycles at 2 drips per second. The water was then stopped and a hot air drier started immediately, which was focused on the disc contact. The test was repeated.

A nominal disc rotational velocity of 400 rpm was used for all tests.

6.5 Results
6.5.1 Dry, Wet and Oily Tests

Figure 6.3 to 6.5 show the data from tests carried out using dry, oily only and water only tests over the range of slips mentioned previously and Figure 6.6 illustrates the corresponding creep curves for the same conditions. The tests were carried out at 400 rpm and 1500 MPa contact pressure.
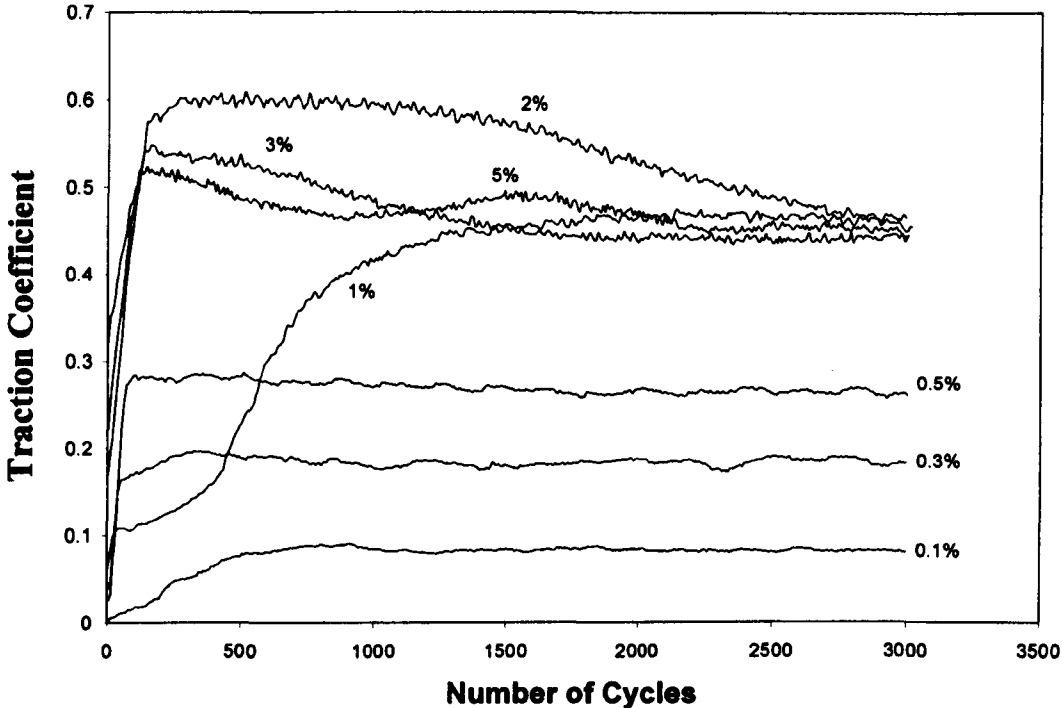
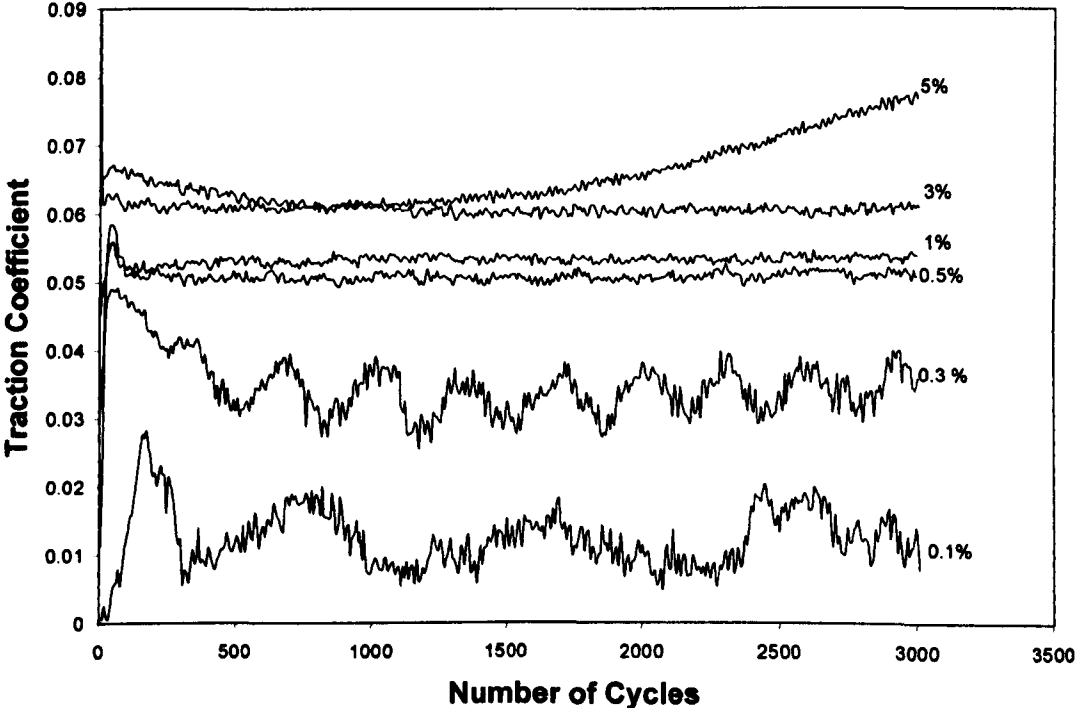Figure 6.3 Traction coefficient data for dry tests.

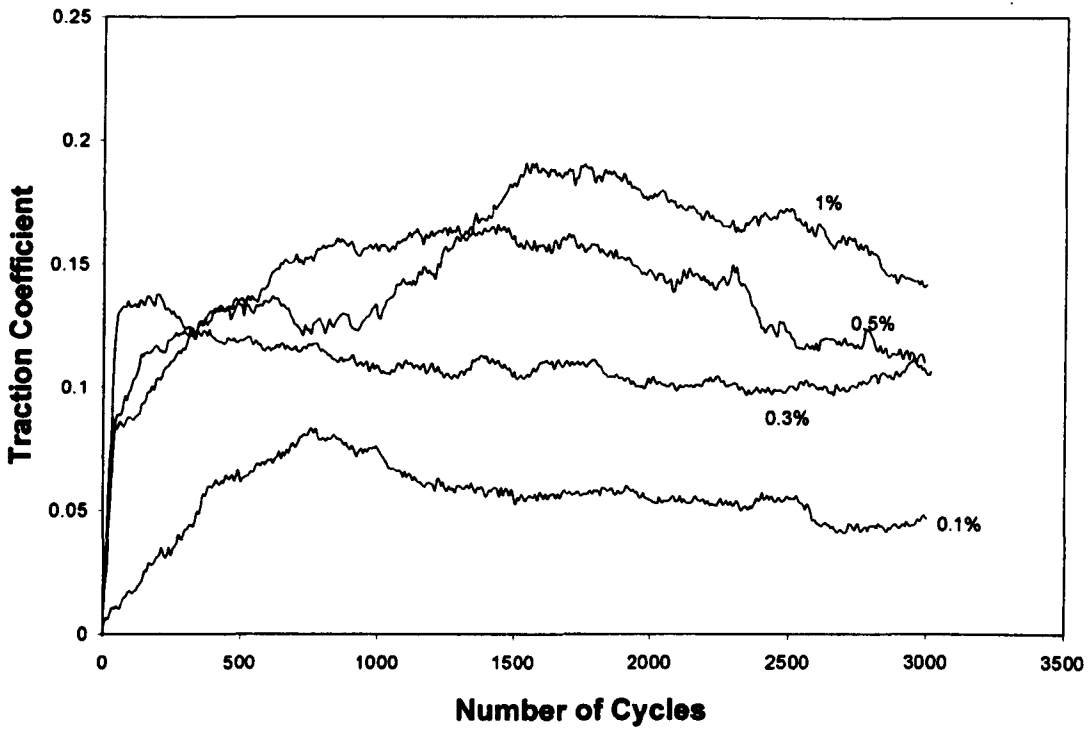Figure 6.4 Traction coefficient data for oil tests.

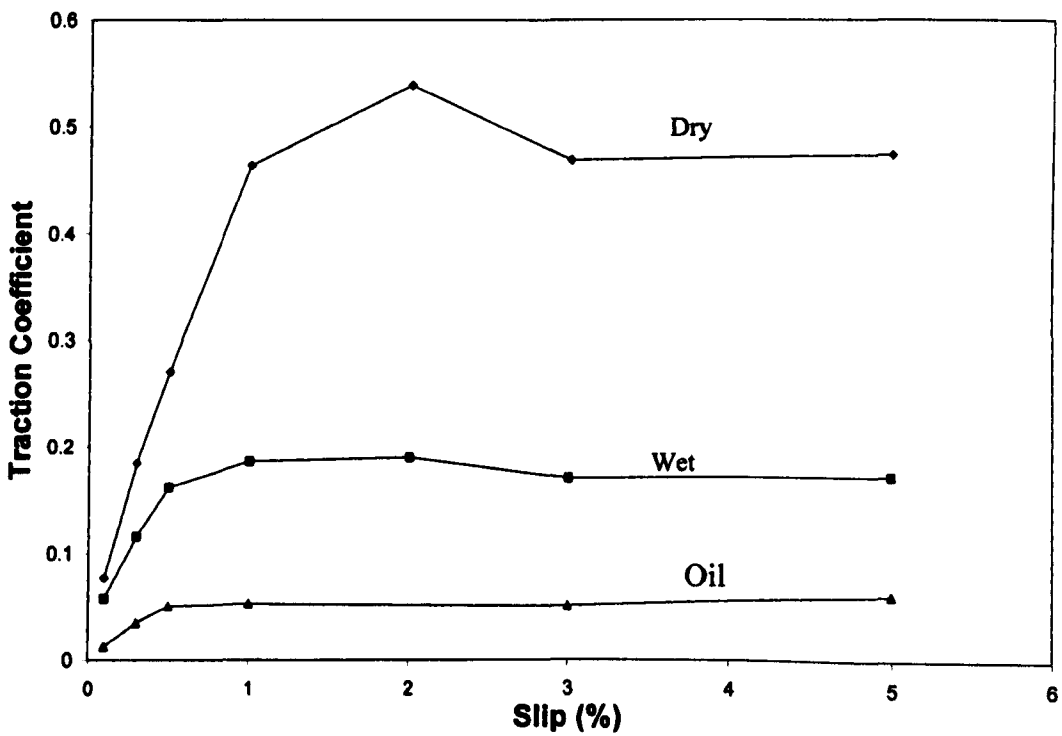Figure 6.5 Traction coefficient data for water tests.

Figure 6.6 Creep curves for dry, water and oil tests.

6.5.2 Oil/Water Mixtures

Figure 6.7 and 6.8 show data from 50% oil/50% water and 20% oil/80% water tests. (where incomplete data is shown, data was not collected at the highest rate on the test-rig). The tests were run at 400 rpm and 1500 MPa contact pressure. As can be seen the data is very similar to that for the oil only tests (Figure 6.4) as emphasized in Figure 6.9 which shows the creep curves. It is clear that oil is having the overriding effect. During the water/oil mixture tests it was possible to see globules of liquid around the contact entrance as shown schematically in Figure 6.10. These were seen to be expelled sideways for the contact region or actually back along the disc surface against the disc motion. It is thought that these globules were made up largely of water, which was being squeezed from the contact. This effect has been seen in previous work using a ball-on-flat configuration (Yang et al., 2004) where at low speed, oil and water/oil emulsions gave similar friction coefficients for a range of slip values. It was also found, however, that at higher rolling speeds this behaviour changed. This may also be an issue with the twin disc contact.
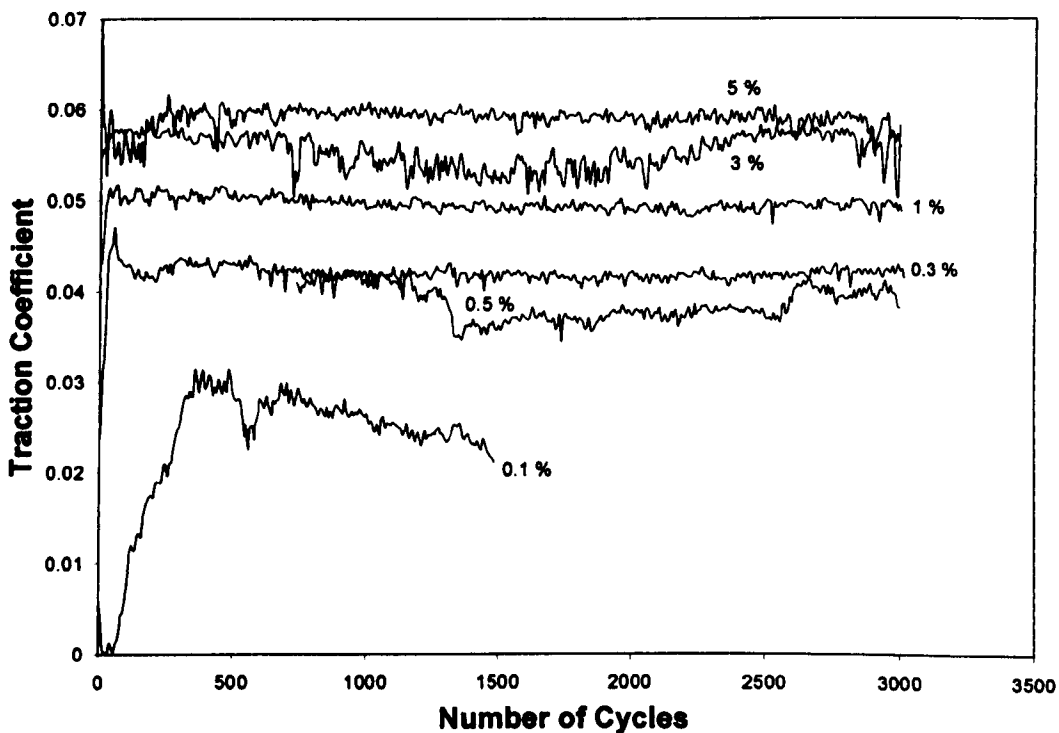
Figure 6.7 Traction coefficient data for 50% oil/50% water tests.
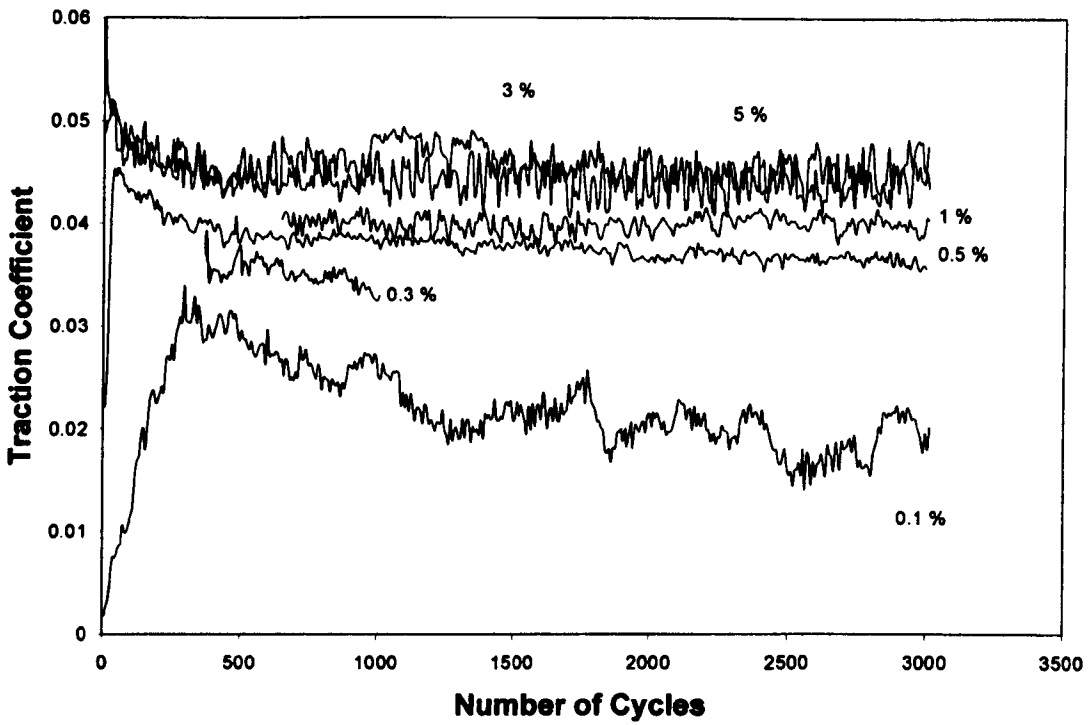
Figure 6.8 Traction coefficient data for 20% oil/80% water tests.
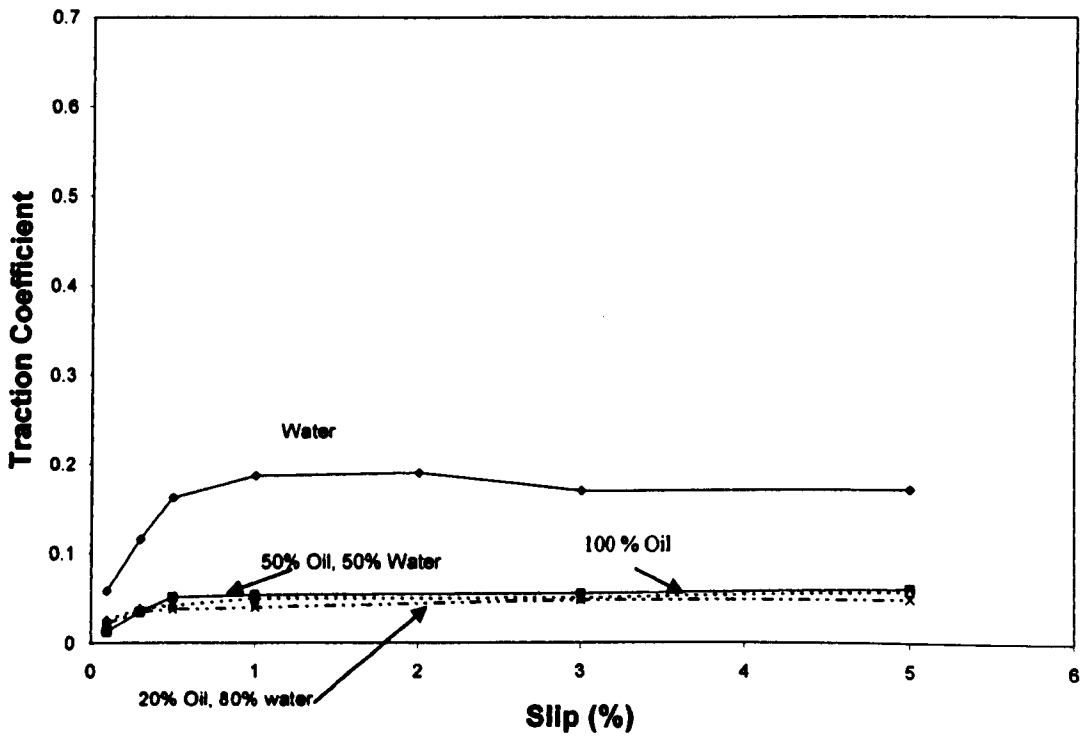
Figure 6.9 Creep curve for oil and water tests.
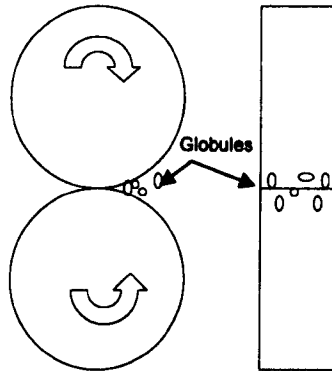
Figure 6.10 Globules forming around the contact.

6.5.3. Effect of Contact Pressure

Figure 6.11 shows the effect of the contact pressure on traction coefficient. The tests were carried out at 400 rpm. In dry conditions, it can be seen that when 1500 MPa contact pressure is applied, traction coefficient is relatively close to 900 MPa. However in wet conditions traction coefficient for 1500 MPa and 900 MPa is seen between the range in wet conditions. With oil traction coefficient seems to present the same behaviour in the two different contact pressure. Work carried out by Baek et al., 2007 has demonstrated that changing contact pressure the traction coefficient increases linearly and reaches to a peak and then decreases a little and becomes steady.
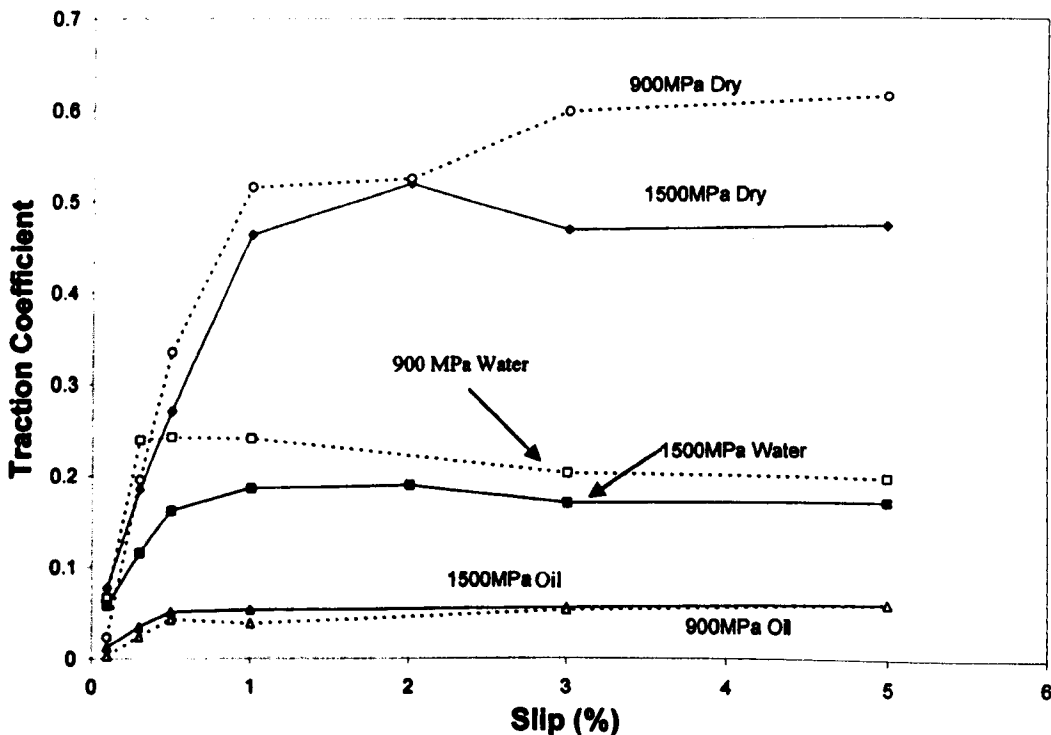
6.11 Creep curves comparing tests with different contact pressure.

6.5.4 Effect of Roughness

Increasing roughness leads to higher friction as shown in Figure 6.12. Rail disc roughness at the end of the test had reduced from the initial 9.89 μm to 1.12 μm. This explains the gradual decrease in traction coefficient as the disc smoothed during the test. The final surface is shown in Figure 6.13 and 6.14. It has been shown by Baek et al., 2007 that after starting the test, surface roughness decreases a little until the traction coefficient reaches the peak. This could explain that after starting the test the surface is conditioning to then after a while the disc roughness surfaces change.
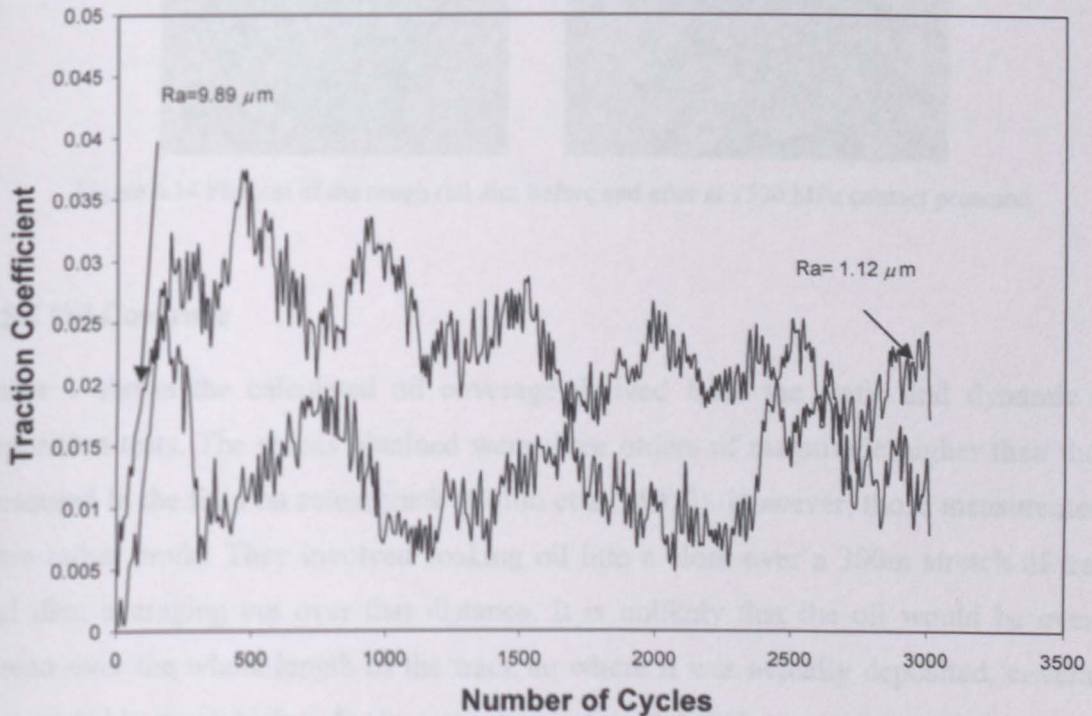
6.12 Traction coefficient versus time for the rough and standard disc.
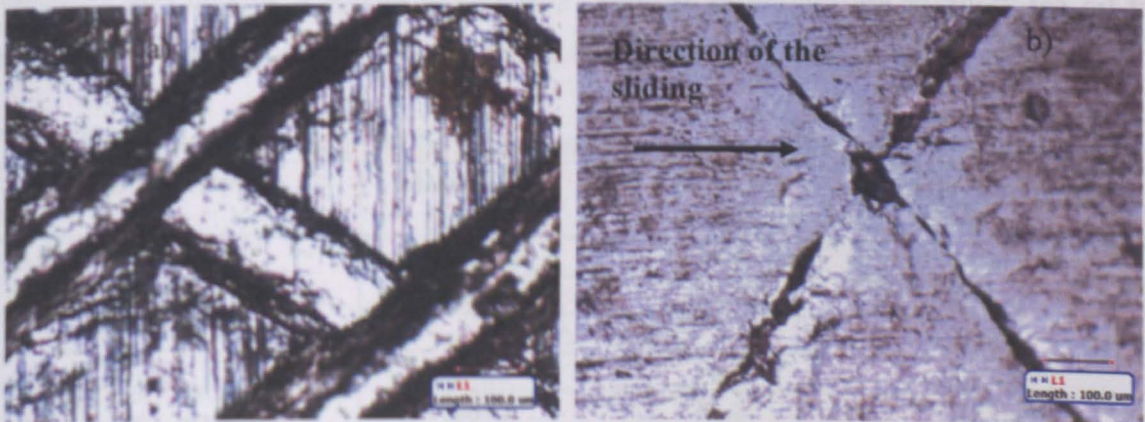
Figure 6.13 Pictures of the rail disc taken in the optical microscope.

95

Figure 6.14 Pictures of the rough rail disc before and after at 1500 MPa contact pressure.

6.5.5 Oil Coverage

Table 1 shows the calculated oil coverage derived from the static and dynamic oil deposition tests. The values obtained were three orders of magnitude higher than those measured in the field on actual track (Collin et al., 1972). However, those measurements were rather crude. They involved soaking oil into a cloth over a 300m stretch of track and then averaging out over that distance. It is unlikely that the oil would be evenly spread over the whole length of the track so where it was actually deposited, coverage was probably much higher. In the same piece of work bench tests were carried out using these oil coverage values, achieved by mixing the oil with chloroform to change its viscosity and making it spread more easily. The use of chloroform to allow the oil to spread would have immediately changed its lubricating properties.

Table 1. Calculated average oil film thicknesses from deposition Tests.

Test Description	Mass of Oil (g)	Disc Area (cm^2)	Oil Coverage (g/cm^2)
5 drips oil/5 minutes	0.0808	14.8	0.00547
	0.090	14.8	0.00610
	Average		0.00479
5 drips oil/5 minutes/disc rotated for 40 seconds	0.0705	14.8	0.00477
	0.0692	14.8	0.00469
	Average		0.00473

6.5.6 Friction with a Low Amount of Oil

As shown in Figures 6.15 and 6.16, the friction stabilized at just over 0.05 for the tests run with a small amount of oil. This value is very close to that seen with 2 drops per second of oil at the same test conditions (Broster, 1974). Tests in previous work (Broster, 1974) using oil film thicknesses of the order of 0.5×10^{-6} g/cm^2 showed that as the oil film thickness reduced the friction went up. This makes sense as more and more metal to metal contact would apparent as the thickness reduces. A transition was observed at a thickness of 1×10^{-6} g/cm^2, so in this work tests were run above the transition, where friction is independent of the amount of oil. It is arguable whether these coverages actually exist in reality, however, and those used in the present study could be deemed to be more realistic, i.e. dropping on oil and letting it spread. If oil drops onto track during train operation this is what would happen.
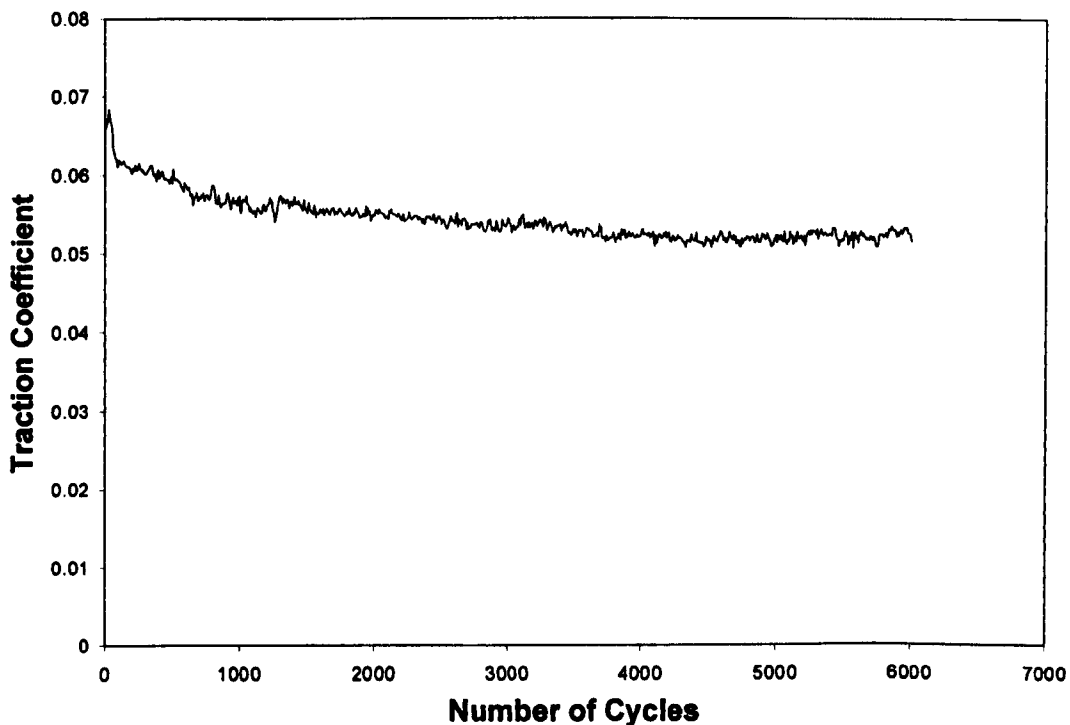
Figure 6.15 Traction coefficient data for test run with small amount of oil.
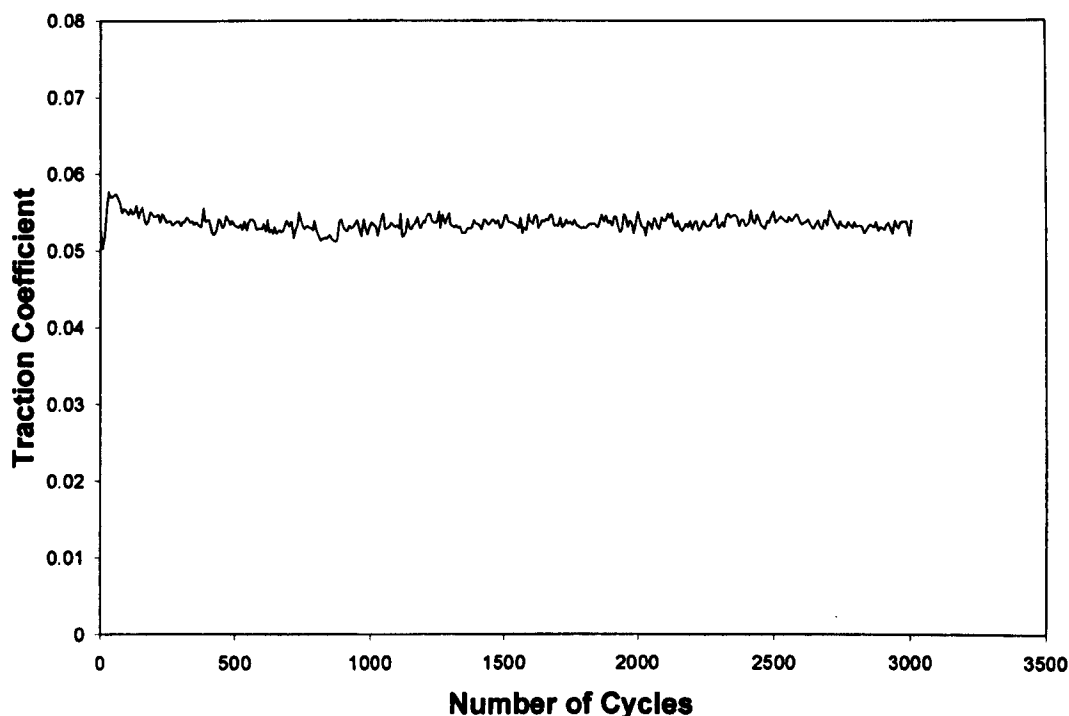
Figure 6.16 Traction coefficient data for test run with small amount of oil.

6.5.7 Friction with Oil and Water

As shown in Figures 6.17 and 6.18, the friction stabilized at just over 0.05 for the tests run with a small amount of oil. This value is very close to that seen with 2 drops per second of oil at the same test conditions (Broster et al., 1974). Tests in previous work (Broster et al., 1974) using oil film thicknesses of the order of 0.5×10^{-6} g/cm^2 showed that as the oil film thickness reduced the friction went up. This makes sense as more and more metal to metal contact would apparent as the thickness reduces. A transition was observed at a thickness of 1×10^{-6} g/cm^2, so in this work tests were run above the transition, where friction is independent of the amount of oil. It is arguable whether these coverage actually exist in reality, however, and those used in the present study could be deemed to be more realistic, i.e. dropping on oil and letting it spread. If oil drops onto track during train operation this is what would happen.
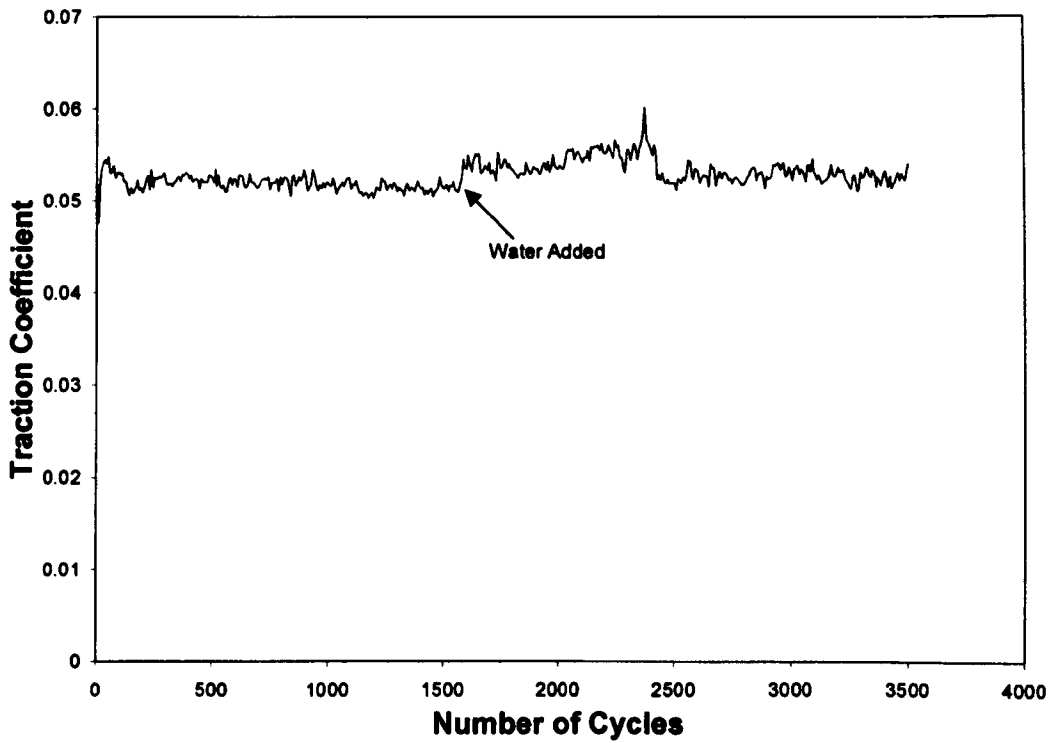
Figure 6.17 Traction coefficient data for test run with small amount of oil before the addition of water.
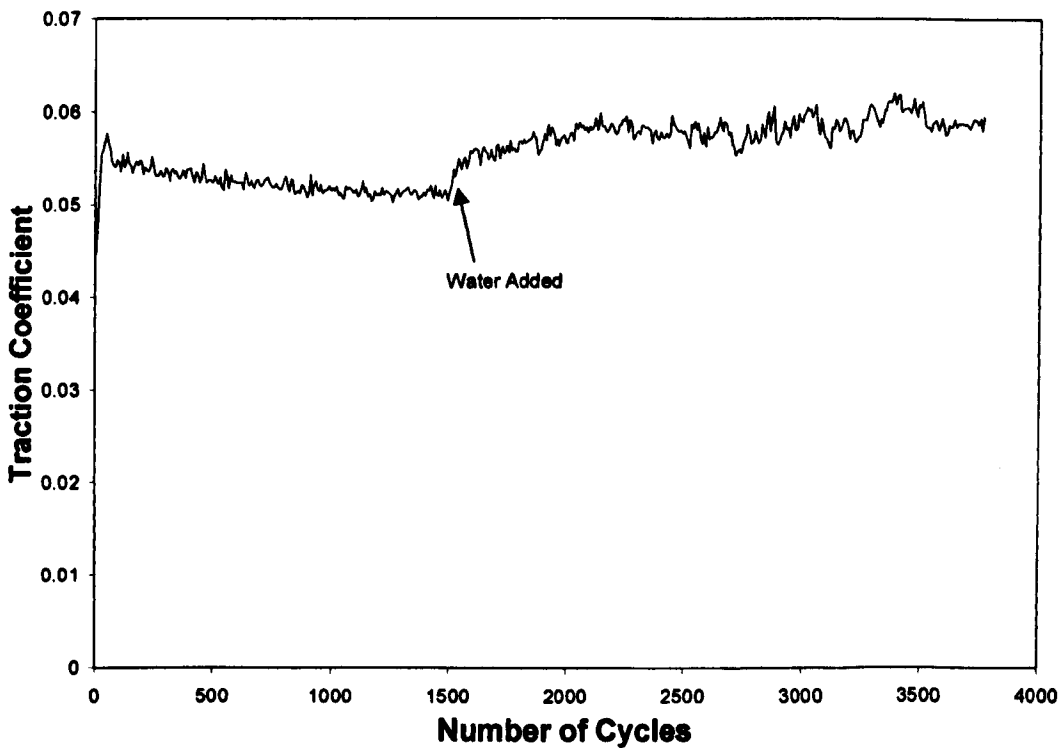
Figure 6.18 Traction coefficient data for test run with small amount of oil before the addition of water.

6.5.8 Friction in a Drying Test

Figures 6.19 and 6.20 show the results of the drying tests. A slight decrease in friction was observed on the on-set of drying (about 0.04-0.05). In this work the drying process has been accelerated. In the previous work carried out the drying was done naturally (Broster et al., 1974). The absolute coefficient values for wet conditions are similar for both pieces of work however the pronounced drop in adhesion levels of $\mu\approx0.1$ previously seen were not witnessed in the latest tests.
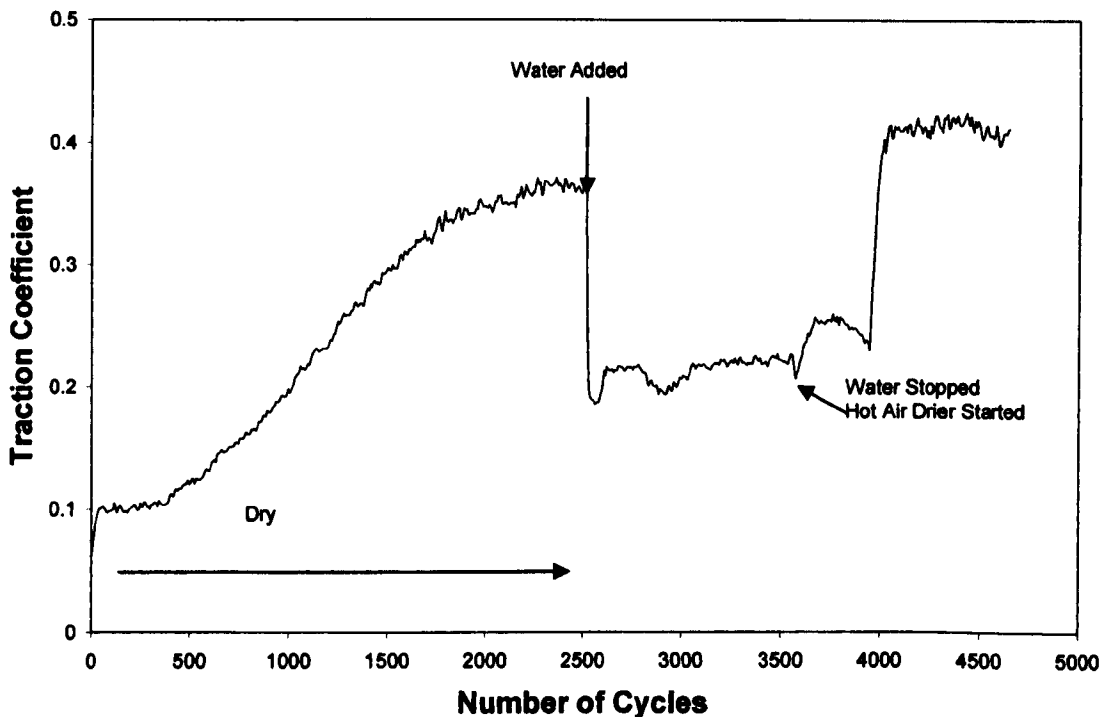
6.19 Traction coefficient data for drying test run dry.
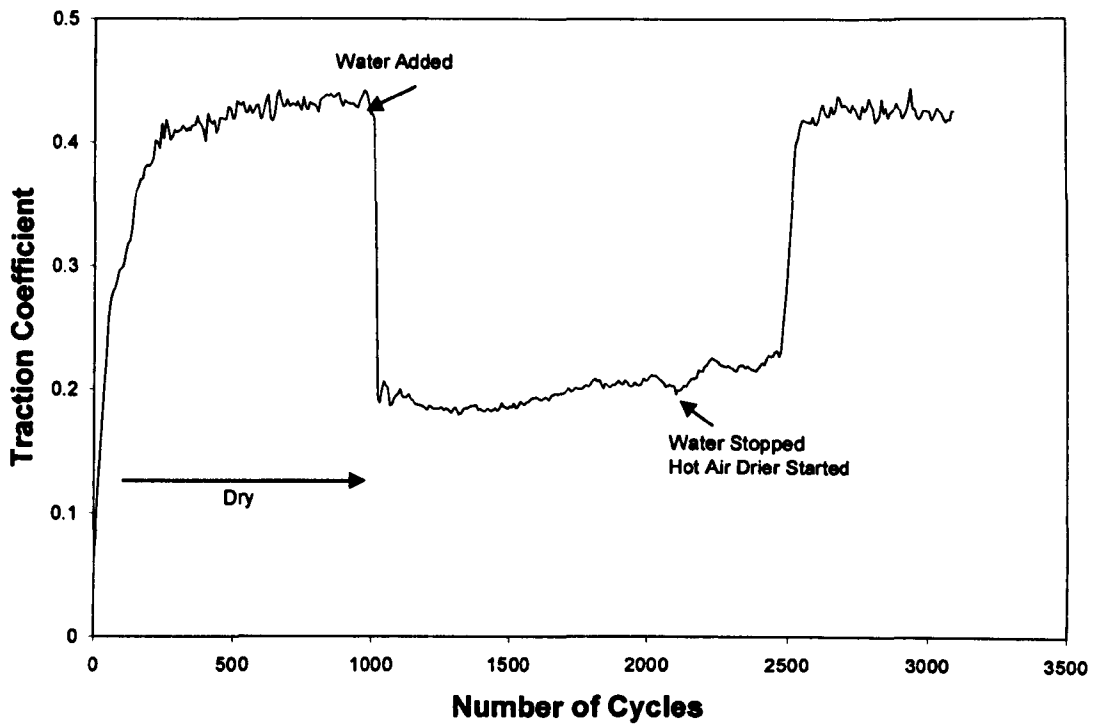
Figure 6.20 Traction coefficient data for drying test run dry.

Chapter 7. Discussion

7.1 Introduction

The wheel/rail contact is a crucial factor in ensuring good performance of railway systems. The wheel/rail contact, however, has many factors affecting its performance. These included the fact it is an open system affected by environmental conditions, third bodies (from the environment and applied) are present which affect adhesion. Also the contact over a small area at high load which drives a number of damage mechanisms, such as wear and RCF. In this work a number of wheel/rail contact issues have been investigated using a twin disc simulation of the wheel/rail contact:

1. Contact temperature. Analytical models have been compared with thermal camera measurements.
2. Adhesion. The effect of contaminants, such as leaves, sand, oil and water have been investigated.
3. Isolation. The effect of solid stick friction modifier has been studied.

There are discussed in the following sections:

7.2 Temperature Measurements

In this thesis one of the aims was to establish the temperatures in the bodies and contact between the wheel and rail discs using two analytical methods and to compare them with measurements carried out by a thermal camera. The thermal camera measurements and calculations using the analytical approach proposed by Lewis & Dwyer-Joyce (2004) compare well for the body temperature of the discs in a rolling-sliding test set up compare well. This is despite the number of assumptions in the analytical modelling and the deficiencies in the thermal camera measurements. This provides a measure of validation for the analytical approach. Temperatures from this twin disc approach and the "small disc" approach (Olver, 1991) also give reasonable agreement. There are some significant differences between the two analytical approaches though. The most important is related to how the heat losses are assumed to occur. Heat loss due to

conduction is significant and much higher from the contact with convection and radiation having smaller effect on the contact temperature using the Lewis & Dwyer-Joyce method. This is similar to the "small disc" method, however, in the "small disc" model heat flow is considered to be in axial direction and in the Lewis & Dwyer-Joyce model it is entirely radial.

In the "thin disc model" also proposed by Olver (1991), convective heat loss dominates. It was found that for the same change in convective heat transfer coefficient the change in contact temperature was greater in the "thin disc" model than the small disc model.

Determining the correct emissivity value to use is possibly the biggest source of discrepancy in the thermal camera measurements. The values found in the calibration test were for the disc after they had been tested at 5% slip. The range of values recorded was large and varied considerably with the disc surface condition. After the tests at other slip values the surface characteristics were different and as a result the emissivity values would be different.

Validation of the analytical approaches provides support for the hypothesis that temperature effect causes the second transition seen in wheel and rail material wear rates during twin-disc testing. Figure 2.7 shows the results of wear tests on UIC60 900A rail steel and R8T wheel steel carried out during previous twin-disc testing as well as temperatures calculated using the first analytical method (Lewis & Dwyer-Joyce, 2004). The second wear transition occurs at around 200-250°C which coincides with the temperature at which the mechanical properties of these steels start to decline (British Steel Makers Creep Committee, 1973).

A fully validated thermal model will be useful in carrying out further investigations on wear transitions and the influence of contact geometry and sliding in the interface.

Temperatures in the actual wheel/rail contact have been analyzed analytically and numerically (Ertz and Knothe, 2002; Gupta et al., 1996). Temperatures ranged from 280 to 700°C for slips from 8 to 20%. These slips represent those likely in the rail gauge corner/wheel flange contact as those in the tread are very much lower. Clearly the situation is very different from that considered in the twin-disc testing as there is a much larger volume of material in which to dissipate heat and the wheel is rolling over cold

rail. The temperatures are similar, however, because the wheel velocity is much higher than that of the discs so there is much higher heat generation. This adds some support to the twin-disc test method as it is likely that wear transitions are occurring where they would in an actual wheel/rail contact for the same contact conditions. Results from twin-disc testing, though, could only be translated where the actual wheel/rail contact conditions have been fully defined.

7.3 Adhesion Experiments

The results derived for dry wet and oily conditions compare well with previous testing and actual track measurements as the data in Table 4.1 in Chapter 4 shows.

The data shown in Table 4.1 in Chapter 4 was collected from the literature and was determined using a variety of full-scale techniques using a bogie on a roller-rig, a rail tribometer and an instrumented train. The roller-rig tests were carried out under closely controlled conditions so load, velocity and slip are known. As was seen previously, that varying load and rolling speed affects friction. This is something that needs exploring further with the twin disc technique. Clearly in the actual track testing a range of loading and slip conditions will have occurred.

The shape of the creep curves derived from the roller-rig tests is similar to those seen in this work. This is significant as the initial slope of the curve is important and this as well as the initial peak and then slight decline seen with some conditions differs from results achieved using analytical modelling techniques (as noted previously (Bucher, 2006)).

The techniques used to apply contaminants worked well. The data recorded for leaves further indicates what a good lubricant they are, even in dry conditions. The test method allows for testing of potential friction modifiers to increase adhesion when leaves are present as seen with the sand tests. An added benefit was the generation of a relatively hard leaf layer on the discs, which has not been achieved experimentally before. As was seen in Figure 4.24, these layers took some time to wear away. If one cycle represents a wheel pass then it would be sometime in the real situation before the layer is removed by wear alone and this does not allow for further leaves falling. This may allow testing of leaf removal solutions.

As shown in Table 1 Chapter 4, the twin disc results with leaves are similar to those seen with an instrumented train run over leaves. In that work (Nagase, 1989), different leaves gave different results, with oily needle leaves from pine trees giving the highest friction. The leaves in this work were mixed, so further work may be appropriate to identify which leaves may be worst.

It was interesting to note that even leaves can cause damage to the disc surfaces. It was expected that sand would, and this could potentially be an issue if sand is applied regularly to a stretch of track that suffers from poor adhesion.

7.4 Isolation

Isolation experiments were carried out with a solid stick friction modifier (High Positive Friction (HPF)) which is most used on curves to reduce noise and wear. Three values of slip were used in order to simulate the contact conditions of the wheel and rail in curves and tangent tracks, they were 0.1%, 1% and 3%.

It was observed that at 0.1% of slip, traction coefficient had no significant change with HPF. However, the traction coefficient changed at slips of 1% and 3% when HPF was applied

With HPF traction coefficient was 0.28. A black layer built up on the disc on application of HPF.

Contact impedance was low at all slip levels and loss train identification in unlikely at these conditions.

The decrease in impedance seen with increasing slip was expected as the higher slip would make more metal-to metal occurred.

7.5 Adhesion with Oil / Water Mixtures

The set of tests carried out varying the percentage of water and oil at the same conditions (speed, load, and slip) have shown that even changing the percentage, traction coefficient stays as it did with pure oil involved. The superficial tension is much higher for the oil, and as a result the water is squeezed away as soon as it tries to enter into the contact and water may only flow around of the contact. One of the reasons why oil goes into the contact is the affinity of the solid to the oil phase (Benner, 2006).

Zhu et al. (1994) and Yang et al. (2004) found that the film thickness of emulsions behaved identically to pure oil at low speed. However when speed was increased the film thickness increased. They concluded that water was drawn into the contact zone at higher speeds because of this.

However, to carry out tests at higher speed with the twin disc machine is not possible as to it is necessary to change the gear box.

It is clear that from these tests oil remains an effective lubricator in the wheel/rail interface independent of the presence of water in any amount. These tests have also shown that a small quantity of oil, equivalent to a teaspoon (2.5 ml) of oil spread over 4m of running band provides a robust low adhesion surface that remains largely unaffected by the presence of a continuous stream of water applied to the wheel/rail interface.

Previous work has shown that the adhesion of an oil coated surface remains largely independent of oil quantity until a threshold level as low as 1×10^{-6} g/cm[1], or a teaspoon of oil distributed over 2 km of running band. This work used chloroform to thin oil to allow it to be spread evenly over the test surfaces, and while Chloroform is a volatile solvent, it is likely that it will have affected the lubricating properties of the oils used. The work also showed the effect that low quantities of oil had on reducing adhesion, increased with humidity, and in particular the humidity during application of the oil to the surface. Conceptually it is hard to imagine oil being spread into layers only a few molecules thick along the railhead over large distances (2 km) without its removal by wear debris as suggested by other work. Droplets of oil deposited onto the rail head will spread under the passage of trains and may be distributed to levels that are similar to those seen during these tests (Beagley et al., 1975). Given the low quantities of oil required to reduce adhesion, and the robustness of the layer in the presence of water it is

possible that small quantities of surface active organic compounds could build up over time, perhaps as a result of leaf contamination. Levels of semi-volatile organic compounds in the order of 5×10^{-6} g/cm^2 have been found on the UK at sites where low adhesion is considered to be an issue, Beagley et al. (1975).

The low amounts of oil required to cause reduced levels of adhesion could well explain the phenomenon of low adhesion experienced on apparently clean rail. It is not known whether high pressure water jetting, used on the UK network, is capable of removed such low levels of oil from the rail surface. Beagley et al. (1975), demonstrated using a rolling tribometer that small amounts of oil can reduce the adhesion coefficient. However water can mitigate the oily effect, washing some away depending on the original oil coverage applied on the disc surface. This can explain the slight effect of water added on the adhesion coefficient (see Figures 6.17 and 6.18 in Chapter 6).

Experimental results where the drying process was accelerated showed good correlations with results by Beagley (1975 & 1974). Adhesion in dry conditions came up to 0.45 and in presence of water, adhesion was lower, at around 0.2, with a slight decrease in the adhesion after the drier was started. It may be due to some debris forming a viscous paste for a few seconds before adhesion started recovering to that value previously seen in dry conditions. In the work carry out by Beagley (1975), using a rolling disc tribometer a paste of $FO_2\,O_3$ with water painted on the discs and a test with some water sprayed on the rail disc were carried out which showed the same decrease in the adhesion coefficient on the on-set of the drying.

Broster et al. (1974) found in the field that water reduces adhesion immediately (becoming less that 0.24) and adhesion regained its original level once the water had evaporated. Also it was found that a locomotive slipping is promoted in damp conditions where a larger amount of debris was observed on the rails heads. This can promote a low shear strength quasi-viscous paste of debris particles.

Chapter 8. Conclusions

8.1 Introduction

This thesis had initially four major objectives for the analysis of the wheel/rail contact.

- The first one was to experimentally measure the temperatures in a simulated wheel and rail contact compare then with analytical methods from Lewis & Dwyer-Joyce (2004) and Olver (1991).

- The second objective was to evaluate the effect on adhesion of a number of contaminants.

- The third objective was to find the effect of the friction modifier on the wheel and rail isolation.

- The fourth objective was to observe the effect of water and oil mixtures on adhesion.

In this regard, the problems treated in this thesis represent those ones commonly presented in the field. The twin disc rolling sliding method has shown a good simulation of the wheel/rail contact.

8.2 Temperature

Thermal camera measurements have been carried out to determine temperature values (body and contact) for a range of slip values in a twin disc contact.

To find the correct temperature values a calibration tests had to be carried out to determine emissivity values for the disc surfaces to use with the thermal camera data. The emissivity varies considerably with the condition of the surface. Average values of 0.67 for the wheel disc and 0.22 for the rail disc were measured.

Two analytical models were used to predict the temperatures in the twin-disc contact. The first model was developed for the twin disc contact, by Lewis & Dwyer-Joyce (2004) and the second model was derived by Olver (1991) for thin or small discs assuming radial and axial thermal gradients respectively.

Body and disc contact temperatures compare well with analytical models of the temperatures despite the assumptions in the models and deficiencies inherent in determining correct emissivity values for the thermal camera measurement. The camera gives a measure of validation for the models.

8.3 Adhesion

Adhesion of wheel and rail disc contact was assessed with some contaminants, such as water, oil and leaves in dry and wet conditions using the twin disc approach. Sand was added with leaves and was shown to be a good improver of traction, as it brought back the traction coefficient to values seen before the sand was applied.

During the leaf tests, leaf layers were generated that were between $14Hv_{1gr}$ and $58Hv1_{gr}$. These layers took between 200 and 600 cycles to remove in dry uncontaminated conditions, depending on the slip value.

Traction coefficient was reduced once leaves were applied, however, according to the data displayed in Figure 4.21, wet leaves reduced the adhesion more than leaves in dry conditions. Oil showed higher values of adhesion followed by pure water conditions. As was expected, tests in dry conditions yielded the higher traction coefficients.

Leaves caused some surface damage to the discs, particularly when stalks were passing through the contact, which resulted in long indentations. Sand also caused indents and scratches in the wheel and rail materials.

In this work the twin disc technique has been shown to be an effective means to study wheel/rail traction coefficients as greater control can be exerted over test parameters. At present no standard test has been developed for studying adhesion and the effect of friction modifiers, so this may be the direction to head in.

The results determined during the tests compare well with those from other tests and from the field, enhancing the credibility of the twin disc approach as a standard test for

assessing traction and friction coefficient, especially when trying to characterise the performance of friction modifiers.

8.4 Isolation

For twin disc tests at relative contact pressure and slips HPF did not cause isolation of the discs.

Static test have also shown that, even with no traction in the contact that would enhance metal-to-metal contact, the presence of HPF does not affect impedance.

Increasing slip reduce impedance as more metal-to-metal occurred.

8.5 Oil Water Mixtures

Applying oil and water at different percentage in the twin disc contact at same speeds has shown that the mixing oil/water behaves in a range as the pure oil condition.

The testing carried out to investigate the effect on adhesion of a number of contaminants has shown that if oil and water are present (regardless of amount), oil has the dominating effect and traction coefficients remain at similar levels to having oil alone. Even when spraying water at relatively high pressure the traction coefficient will only rise a very slight amount.

Results from this work have backed up previous tests using different approaches indicating that low amounts of oil are still able to reduce traction coefficient and that drying a wet contact can initially give a slight drop in traction coefficient. They have also confirmed that that roughness will increase traction coefficient and that reducing contact pressure also increases adhesion.

8.6 Future Work

This work has been carried out mainly on temperature, adhesion and isolation. Every area can be expanded. The necessity of understanding how the wheel/rail contact can be affected due by different issues involved can be explore of more using the twin disc machine approach in order to increase the knowledge of the wheel/rail contact. For this some complementary work is proposed.

- Carry out more experiments varying the load and the speed.
- Study the effect of the load and speed on the traction coefficient.
- Experiment with other contaminants, such as frost, wear debris, tyre rubber wear debris from automobiles and different kind of leaves.
- Test friction modifiers.
- Perform isolation experiments in terms of impedance with different friction modifiers.
- Carry out more experiments with oil/water mixtures at higher speeds.
- Make some experiments with high and low temperature water.
- Study possible solutions to remove leaf layers.

8.7 Publications

The following papers have arisen from this work:

Conference

Gallardo-Hernandez, E.A., Lewis R., Dwyer-Joyce, R. S., "Temperature in a Twin-Disc Wheel/Rail Contact Simulation", Proceedings 32nd Leeds-Lyon Symposium on Tribology. Lyon, France. 6-9 September 2005.

Gallardo-Hernandez, E.A., Lewis R., 2006, "Twin Disc Assessment of Wheel/Rail Adhesion", Proceedings of CM2006, 7th International Conference on Contact Mechanics and Wear of Rail/Wheel Systems, Brisbane Australia, 24-27 September 2006, Vol. 2, pp311-319.

Lewis, R., Gallardo-Hernandez, E.A., Hilton, T., Armitage, T., "Twin Disc Assessment of Wheel/Rail Adhesion", Proceedings of the DGM International Symposium on Friction, Wear and Wear Protection, Aachen, Germany, 9-11 April, 2007.

Lewis, R., Gallardo, E.A., Eadie, D.T., Cotter, J., 2008, "The Effect of Friction Modifiers on Wheel/Rail Isolation", Proceedings of the 2008 ASME/IEEE Joint Rail Conference, Wilmington, Delaware, 22-23 April 2008.

Journal Papers

Gallardo-Hernandez, E.A., Lewis, R., Dwyer-Joyce, R.S., 2006, "Temperature in a Twin-Disc Wheel/Rail Contact Simulation", Tribology International, Vol. 39, pp1653-1663.

Gallardo-Hernandez, E.A., Lewis, R., 2008, "Twin Disc Assessment of Wheel/Rail Adhesion", in press Wear.

Chapter 9. References

Adrievsky, S.M., 1961, "Side Wear of Rail Heads in the Curves", Proceedings of TZNII (VNIIGHT) (in Russian).

Ahlsotrom, J. and Karlsson, B., 1999, "Microstructural Evaluation and Interpretation of the Mechanically and Thermally Affected Zone Under Railway Wheel Flats", Wear, Vol. 232, pp1-14.

Arriva Trains Wales, 2006, "Leaves on the Line (Online)", Available: http://www.arrivatrainswales.co.uk, (Accessed in 2007)

Baek, K. S., Kyogoku, K., Nakahara T., 2007, "An Experimental Investigation of Transient Traction Characteristics in Rolling–Sliding Wheel/rail Contacts under Dry–Wet Conditions", Wear, Vol. 263, pp169-179.

Beagley, T.M., McEwen, I.J. Prithchard, C., 1975, "Wheel/Rail Adhesion Boundary Lubrication by Oily Fluids", Wear, Vol. 31, pp77-88.

Beagley, T.M., McEwen, I. J., Prithchard, C., 1975, "Wheel/rail Adhesion the Overriding Influence of Water", Wear, Vol. 35, pp295-313.

Beagley, T. M., 1976, "Severe Wear of Rolling/Sliding Contacts", Wear, Vol. 36, pp317-335.

Beagley, T.M.., Prithchard, C., 1975, "Wheel and Rail Adhesion the Overriding Influence of Water", Wear, Vol. 35, pp299-313.

Beagley, T.M., McEwen, I.J., Pritchard, C., 1975, "Wheel/Rail Adhesion — the Influence of Railhead Debris", Wear, Vol. 33, pp141-152.

Benner J.J., Sadeghi F., Hoeprich M. R., Frank M. C. 2006 "Lubricating Properties of Water in Oil Emulsions", ASME, Vol., 128, pp296-311.

Block, B., (1999), "Horse for your course", Proceedings of IHHA, STS Conference on the Wheel/Rail Interface.

Bower A.F. Johnson K.L., 1989, "The Influence of Strain Hardening on Cumulative Plastic Deformation in Rolling and Sliding Line Contact", J Mech, Phys Solids Vol. 37 No. 4, pp471-493.

British Steel Makers Creep Committee, 1973.

British Steel Makers Creep Committee, BSCC 1973, "High Temperature Data", London: The Iron and Steel Institute for the BSCC.

Broster, M., Pritchard, C., and Smith, D. A., 1974, "Wheel/Rail Adhesion: Its Relation to Rail Contamination on British Railways", Wear, Vol. 29, pp309-321.

Bugarcic, H., (1986), "The Influence of Contamination on Metallic Friction", Wear, Vol. 113, pp21-35.

Bucher, F., Dmitriev, A.I., Ertz, M., Knothe, K., Popov, V.L., Psakhie , Shilko, E. V., (2006), "Multiscale Simulation of Dry Friction in Wheel/Rail Contact", Wear, Vol. 261, pp874-884.

Catnip website, 1996-2007, "Track Pictures" (online), Available: www.catnip.co.uk (Accessed 03 September 2007).

Cann, P.M., 2006, "The leaves on the Line Problem a Study of Leaf Residue Film Formation and Lubricity under Laboratory Test Conditions", Tribology letters, Vol. 24(2), pp151-158.

Chapman, A.J., 1974, "Heat Transfer". 3rd Edition, Collier Mac-Millan.

Chen H., Ban T., Ishida M. Nakahara T., 2002, "Adhesion Between Rail/Wheel under Water Lubricated Contact", Wear, Vol. 253, pp75-81.

Chen, H., Ban, T., Ishida, M., 2001, "Adhesion between Rail/Wheel under Water Lubricated Contact", Proceedings of the 2nd World Tribology Congress, Vienna, Austria, 3-7 September.

Collins, A.H., and Pritchard, C., 1972, "Recent Research on Adhesion", Railway Engineering Journal, Vol. 1(1), pp19-29.

Eadie, D.T., Kalousec, J., Chiddick, K.C., 2000, "The Role of High Positive Friction (HPF) Modifier in the Control of Short Pitch Corrugation and Related Phenomena", Proceeding of the 5th international conference on Contact Mechanics and Wear of Rail/Wheel Systems, Tokyo, pp42-49.

Eadie, D.T., Santoro, M., Kalousek, J., 2005, "Railway Noise and the Effect of Top of Rail Liquid Friction Modifiers: Changes in Sound and Vibrations Spectral Distributions in Curves", Wear, Vol. 258, pp1148-115.

Eadie, D.T., Santoro, M., 2006, "Top of Rail Friction Control for Curves Mitigation and Corrugation Rate Reduction", Journal of Sound ad Vibration, Vol. 293, pp747-757.

Ertz, M., Knothe, K., (2002), "A Comparison of Analytical and Numerical Methods for the Calculation of Temperatures in Wheel/Rail Contact", Wear, Vol. 253, pp298-508.

Fichaux, H., Moore D.F., 1968, "Improvement in Rail-Wheel Adhesion by Spark Discharge", Wear, Vol. 11, pp51-67.

Fletcher, D. I., Beynon, J. H., 2000, "Development of a Machine for Closely Controlled Rolling Contact Fatigue and Wear Testing", Journal of Test and Evaluation, Vol. 28(4), pp267-275.

Garnham, J. E., Beynon, J.H., 1991, "The Early Detection of Rolling-Sliding Contact Fatigue Cracks", Wear, Vol. 144, pp103-116.

Ghonem, H., Kalousec, J., Stone, D., Dibble, D.W., 1982, "Observation of Rail Wear", Proceedings of Contact Mechanics and Wear of Rail-Wheel Systems, Vancouver, pp249-269.

Gupta, V, Hahn, G.T, Bastias, P.C., Rubin, C. A., 1996, "Calculations of the Frictional Heating of a Locomotive Wheel Attending Rolling Plus Sliding", Wear, Vol. 191, pp237-241.

Harrison H., McCanney T., Cotter J., 2002, "Recent Developments in Coefficient of Friction Measurements at the Rail/Wheel Interface", Wear, Vol. 253, pp114-123.

Holman, J. P., 2002, "Heat Transfer", New York, McGraw-Hill.

Hou K., Kalousek J., Magel E., 1997, "Rheological Model of Solid Layer in Rolling Contact", Wear, Vol. 211, pp134-140.

Iordanoff I., Berthier Y., Descartes S., Heshmat H., 2002 "A Review of Recent Approaches for Modeling Solid Third Bodies", Journal of Tribology, Vol. 124, pp725-735.

Jaeger, J. C., 1943, "Moving Sources of Heat and the Temperature at Sliding Contacts", Proceedings of the Royal Society, N.S.W., Vol. 76, pp203-224.

Jin, X.S., Zhang, W.H., Zeng, J., Zhou, Z.R., Liu, Q.Y., Wen Z.F, 2004, "Adhesion Experiment on a Wheel/rail System and its Numerical Analysis", Journal of Engineering Tribology, Proceedings of the IMechE Part J, Vol. 218, pp293-303.

Kalker, J.J., 1990, "Three-Dimensional Elastic Bodies in Rolling Contact", Kluwer, Dordrecht

Kalousek, J., Magel, E., 1997, "Optimising the Wheel/Rail System", Railway and Track Structure, January.

Kalousek, J., Magel, E. Grassie, S., 1999, "Perspective in Metallurgy and Contact Mechanics", Proceedings of IHHA, STS Conference on the Wheel/Rail Interface, pp175-186.

Kapoor, A., Johnson, K. L., 1995, "Plastic Ratchetting as a Mechanism of Erosive Wear", Wear, Vol.186-187, pp86-91.

Kapoor, A., Fletcher, D. I., Franklin, F. J., 2003, "The Role of Wear in Enhancing Rail Life", Tribological Research and Design for Engineering Systems, D. Dowson et al., (editors). Elsevier B. V.

Lewis, R., Dwyer-Joyce, R.S., 2004, "Wheel/Rail Wear and Surface Damage Caused by Adhesion Sanding", Proceedings of the 30th Leeds-Lyon Symposium on Tribology, Elsevier Tribology Series No. 43, pp731-741.

Lewis, R., Dwyer-Joyce, R.S., Lewis J., 2003, "Wheel/Rail Contact Isolation due to Track Contamination", 6th International Conference on Contact Mechanics and Wear of Rail/Wheel Systems, Gothenburg, Sweden, pp10-13.

Lewis, R, Olofsson, O. 2004, "Mapping Rail Wear Regimes and Transitions", Wear, Vol. 257, pp721-729.

Lewis, R., Dwyer-Joyce, R.S., 2004, "Wear Mechanisms and Transitions in Railway Wheel Steels", Journal of Engineering Tribology, Proceedings of the IMechE Part J, Vol. 218, pp467-478.

Lewis R., Dwyer-Joyce R.S., 2006, "Wear at the Wheel/rail Interface when Sanding is Used to Increase Adhesion", Journal of Rail and Rapid Transit, Proceedings of the IMechE Part F, Vol. 220, pp29-41.

Lewis, R., Masing, J., 2006, "Static Wheel/Rail Contact Isolation due to Track Contamination", Proceedings of the IMECH E Part F Journal of Rail and Rapid Transit, Vol. 220 (1), pp43-53.

Lewis, R., Dwyer-Joyce, R.S., Lewis, J., 2003, "Disc Machine Study of Contact Isolation During Railway Track Sanding", Journal of Rail and Rapid Transit, Proceedings of the IMechE Part F, Vol. 217, pp11-24.

Nagase, K., 1989, "A Study of Adhesion between the Rails and Running Wheels on Main Lines: Results of Investigations by Slipping Adhesion Test Bogie", Proceedings of the IMechE Part F, Journal of Rail and Rapid Transit, Vol. 203, pp33-43.

Nilsson, R., 2003, "Wheel and Rail Wear Measured Profile and Hardness Changes during 2.5 Years for Stockholm Commuter Traffic", Railway Technology Vehicle.

Ohyama, T., 1991, "Tribological Studies on Adhesion Phenomena between Wheel and Rail at High Speeds", Wear, Vol. 144, pp263-275.

Olofsson, U., Sundvall, K., (2004), "Influence of Leaf, Humidity and Applied Lubrication in Wheel-Rail Contact: Pin on Disc Experiments", Proceedings Institutuon of Mechanical Engineerings Vol. 218 Part F: Rail and Rapid Transit, pp235-42

Olver, A. V., 1991, "Testing Transmission Lubricants: the Importance of Thermal Response", Proceedings of the IMechE, Part G, Journal of Aerospace Engineering, Vol. 205, pp35-43.

Profillidis, V.A., 1995, "Railway Engineering", Avebury Technical, Ashgate Publish Limited, Gower House, Crofot Road., Aldershot, Hants GU11 3HR England.
Railway-Technical Web Pages 1998–2007, "Wheels and Bogies" (online), Available: www.railway-technical.com/whlbog.shtml (Accessed 03 September 2007).

Rail Safety and Standards Board, 2004.

Schmid, F., 2003, "Mechanical Aspects of Railway Systems", MSc Programme in Railway Systems Engineering, University of Sheffield.

Seireg, A.A., 1998, "Friction and Lubrication in Mechanical Design", Marcel Dekker Inc.

Sinclair, J., 2004, "Friction Modifiers", in "Vehicle Track Interaction: Identifying and Implementing Solutions", IMechE Seminar, February 17th.

Simons, J.R., 1975, "Engineering Heat Transfer", MacMillian Press, Hong Kong.

The Tramway Museum Society of Victoria Inc, Railway-Technical Web Pages 1998–2007, "Tracks", (Online), Available: website: www.tmsv.org.au, (Accessed 03 September 2007).

Tomeoka, M, Kabe, N., Tanimoto, M., Miyauchi, E., Nakata, M., 2002, "Friction Control between Wheel and Rail by Means of on-Board Lubrication", Wear, Vol. 253, pp124-129.

Tournay, H., 1999, "Rail/Wheel Interaction from a Track and Vehicle Design Perspective", Proceedings of IHHA, STS Conference on the Wheel/Rail Interface.

Tournay, H., 2001, "Supporting Technologies Vehicle Track Interaction", in Guidelines to Best Practice for Heavy Haul Railway Operations: Wheel and Rail Interface Issues, International Heavy Haul Association, Virginia, USA.

Williams, J. A., 1994, "Engineering Tribology", Oxford Science Publications.

Williams, J., Harris, J., 2001, Guidelines to Best practice for Heavy Haul Railway Operations: Wheel and Rail Interface Issues", Virginia, USA: International Heavy Haul Association.

Xie, Y., Williams, J. A., 1993. "The Prediction of Friction and Wear when a Soft Surface Slides against a Harder Rough Surface", Wear, Vol. 196, pp21-34.

Yang, H., Schmid S. R., Kasun. T. J., Reich, R. A., 2004, "Elastohydrodynamic Film Thickness and Tractions for Oil-in-Water Emulsions", Tribology Transactions, Vol. 47(1), pp123–129.

Young, A. D., 1989, "Boundary layers". Oxford, Blackwells.

Zakharov, S., 2001, "Wheel/Rail Performance", in Guidelines to Best Practice for Heavy Haul Railway Operations: Wheel and Rail Interface Issues, International Heavy Haul Association, Virginia, USA.

Zhang W., Chen J., Wu X., Jin X., 2002, "Wheel/Rail Adhesion and Analysis by Using Full Scale Roller Rig", Wear, Vol. 25, pp. 82-88.

Zhu, D., Biresaw, G., Clark, S. J. Kasun, T., J., Schmid, S. R., Wilson, W. R. D., (1994), "Elastohydrodynamic Lubrication with O/W Emulsions", Journal of Tribology, Vol. 116(2), pp. 310-320.